



Instituto Carlos I de Física Teórica y Computacional
y Depto. de Electromagnetismo y Física de la Materia
Universidad de Granada

Langevin Equations for Nonequilibrium Phase Transitions

Omar Al Hammal

Ph.D. THESIS

Advisor: Dr. Miguel Angel Muñoz
Granada, February 16th, 2007

Fué un placer para mí compartir estos 4 años con los miembros del grupo de Física de la Materia Condensada. El buen humor y el ambiente de trabajo no han faltado nunca, siendo siempre fuente de motivación. Así en particular, agradezco a Joaquín Marro y a Pedro Garrido por haberme iniciado a la labor de investigador y a Antonio Lacomba por su ayuda logística. Jesús y Pablo por haberme aconsejado con experiencia. Especialmente, a Manolo y Juan Antonio por su constante compañerismo y por la amistad. Los privilegiados momentos del almuerzo fueron la ocasión para hablar de física y compartir las ilusiones y desilusiones del día a día, sin la compañía de Luca Donetti, Joaquín Torres, Francisco Ramos y David Navidad habrían sido distintos.

Agradezco a Hugues Chaté por haberme acogido en Saclay y haber hecho que mis estancias allí fuesen muy provechosas, su ayuda, consejo y a veces dirección a lo largo de mi tesis. De la misma forma, soy reconocido a Ivan Dornic por lo que me enseñó. Finalmente, quiero dar las gracias a Francisco de los Santos por su ayudax y todo lo que me enseñó siempre con su paciencia y su buen humor.

De manera personal, quiero agradecer muy calorosamente a Miguel Ángel Muñoz por su dirección acertada. Sin duda, estos 4 años han sido más fructíferos y agradables gracias a sus calidades científicas y personales excepcionales. Le estoy especialmente agradecido por todo lo que me enseñó de física y de la vida en general durante este período.

Agradezco a todos mis amigos por la ayuda y la atención que me aportaron, y por las tertulias con ellos que me permitieron superar mis problemas mejorandome. A Jesuús, Israel, Cristina y Raquel.

Je remercie Irène pour son aide précieuse durant la rédaction, et pour être comme elle est, si aimante des gens qui l'entourent. Je ne serai jamais assez reconnaissant envers ceux qui m'ont façonné comme personne, toute ma famille, mon père, ma mère et Khaled pour tout l'amour qu'ils m'ont donné dans les moments heureux et ceux plus difficiles.

Contents

1	Introduction	1
2	Phase Transitions with Two Competing Absorbing States	5
2.1	Motivation	5
2.1.1	Generic Absorbing Phase Transition: Directed Percolation	6
2.1.2	Generalized voter	8
2.2	From microscopic to Langevin equation: two symmetric absorbing states	12
2.2.1	The form of the Langevin equation	12
2.3	Results for Langevin equation with two symmetric absorbing states	13
2.3.1	Mean-field	14
2.3.2	Algorithms for Langevin equations	16
2.3.3	Numerical results in $D = 2$	17
2.3.4	Numerics in $D = 1$: Compact directed percolation, Parity conserving	18
2.4	Symmetry breaking in Generalized Voter	20
2.4.1	Relevant ingredients: coarsening without surface tension	22
2.4.2	Microscopic non-integrable model	22
2.4.3	Asymmetric generalized voter	26
2.4.4	Non-integrable and asymmetric Langevin	29
2.5	Counter-example	29
2.6	Conclusion	30
3	Nonequilibrium wetting phenomena	33
3.1	Introduction and motivation	33
3.2	Free interface: microscopic description	37

3.2.1	Equilibrium	37
3.3	Bounded interface microscopic description	40
3.3.1	Equilibrium $p = 1$	41
3.3.2	Nonequilibrium $p \neq 1$	43
3.4	Free interface Langevin description	44
3.4.1	Equilibrium: Edwards-Wilkinson	44
3.4.2	Nonequilibrium: Kardar-Parisi-Zhang	45
3.5	Langevin description of nonequilibrium interface depinning	47
3.5.1	Multiplicative Noise 1	48
3.5.2	Multiplicative Noise 2	49
3.5.3	Mean-field results	52
3.5.4	Numerics for MN2	54
3.5.5	Quenched noise for MN1 and MN2	56
3.6	Experimental realizations	56
3.7	Conclusion	57
4	Long ranged nonequilibrium wetting	59
4.1	Motivation	59
4.2	Introduction	60
4.3	Non-equilibrium long-ranged unbinding: the model	63
4.4	Brief review of equilibrium wetting	65
4.5	Brief review of non-equilibrium short-ranged unbinding	67
4.6	Non-equilibrium long-ranged unbinding: results	69
4.6.1	Analytic results	70
4.6.2	Numerical Results	72
4.6.3	Discrete Model	82
4.7	Discussion and Conclusions	83
5	Disordered substrates: Stochastic DNA models	87
5.1	Introduction	87
5.2	Continuous Langevin equation with disordered substrate	88
5.2.1	Quenched disorder for Reggeon-Field-Theory	88
5.2.2	Quenched disorder for Multiplicative noise Langevin equation	89
5.3	Peyrard-Bishop-Dauxois: a Langevin equation	89
5.3.1	An equilibrium model	90
5.4	Melting: critical wetting	90
5.4.1	Numerical study of the transition	91

5.5	Localized effect of mutation : bubbles statistics	92
5.5.1	DNA tanscription start site	93
5.6	Conclusion	93
6	Non-accessible absorbing state in reaction-diffusion systems	95
6.1	Introduction	95
6.2	Field theory analysis of $A \leftrightarrow 2A$	98
6.3	Extension to non-reversible reactions	104
6.4	Monte-Carlo simulations	107
6.5	Conclusion	108
7	Resumen	111
7.1	Introducción	111
7.2	Capítulo 2: Transiciones con dos Estados Absorbentes que compiten	113
7.3	Capítulo 3 : Fenómenos de mojado fuera del equilibrio	116
7.4	Capítulo 4 : Fenómenos de Mojado con potenciales de largo alcance	118
7.5	Capítulo 5 : Substratos desordenados y modelos de ADN es- tocásticos	121
7.6	Capítulo 6 : Sistemas de reacción-difusión y ecuaciones de Langevin	123
7.7	Conclusiones	125

List of Figures

2.1	Directed bond percolation in 1+1 dimensions	9
2.2	Voter coarsening experiments	9
2.3	The density of active sites ρ (+), the inverse of the variance of magnetization s (\times) and magnetization m (\square) as a function of temperature.	11
2.4	Potentials for two separate phase transitions, Ising and DP. . .	13
2.5	Potentials for a single generalized voter phase transition. . . .	13
2.6	Mean-field self-consistent result.	15
2.7	Numerical simulations in two space dimensions	19
2.8	Mapping linking parity-conseving and DP2 in $D = 1$	20
2.9	Generalized voter in $D = 1$	20
2.10	Spreading experiment for generalized voter in $D = 1$	21
2.11	Phase diagram for microscopic model with two absorbing states.	23
2.12	Coarsening experiment for system size in $D = 2$	25
2.13	Conservation of magnetization at the critical point.	25
2.14	The three vertices of the theory.	26
2.15	Symmetric modification in perturbation theory.	26
2.16	Generalized voter behavior for asymmetric equation.	28
2.17	Ordering time.	28
3.1	Droplet in contact with a wall	34
3.2	Random deposition with surface relaxation.	39
3.3	Detailed balance condition	40
3.4	Phase diagram for the equilibrium wetting transition.	42
3.5	Effective potentials for the pinned and depinned phases	48
3.6	Representative sketches of the “solid-vapor” interface for repulsive interaction and a lower wall	50
3.7	Order-parameter and finite-size measurements.	55

3.8	Decay experiment for distinct q and β measurement.	56
4.1	Effective potentials	62
4.2	Phase diagrams for positive and negative KPZ nonlinearities .	69
4.3	Effective potentials in terms of n	70
4.4	Features common to all simulations	75
4.5	Time evolution at the critical point	76
4.6	Time evolution at the critical point	77
4.7	Transients illustration	78
4.8	For $p = 2$ exponents are compatible with MN1	79
4.9	For an attracting barrier results are compatible with DP . . .	81
4.10	Results for the discrete model	83
5.1	Time evolution of quenched disorder fixed point	88
5.2	First order transition in PBD model	92
5.3	Continuous transition in PB model	93
6.1	Schematic zero-energy manifolds	100
6.2	Results of Monte-Carlo simulations in $D = 1$	107
6.3	Results of Monte-Carlo simulations in $D = 2$	108

List of Tables

4.1	Summary of the critical exponents	84
-----	---	----

Chapter 1

Introduction

This work focuses on the use of Langevin equations applied to nonequilibrium systems and, more specifically, phase transitions. These equations exemplify the usefulness of effective descriptions in Physics. We present an introduction of the type of problems we are concerned with and explanation of the reasons why work remains to do on Langevin equations.

In experiments on a fluid, water for instance, the mechanical properties of fluid are well explained by the macroscopic, continuous, Navier-Stokes equations. However, we know that fluids are composed of discontinuous molecules, if we are working with very large lengthscales, water appears to be continuous, but, as the lengthscale of observation diminishes to the size of the molecules, we start to see effects of the discreteness. The molecules are polarized and interact with each other like dipoles. Many experiments can only be understood taking, the discreteness of the composition of fluids, into account. This is one reason why effective descriptions, adapted and restricted to a particular lengthscale of observation work so well.

The laws governing the interactions between the typically 10^{23} molecules of a macroscopic quantity of water are known. On the other side, Newton's equations of motions allows one to predict the motion of the molecules under some external force. This makes the problem of predicting the behavior of water in theory predictable. In practice, it is virtually impossible to follow the motion of each molecule of water, and to store the position of each molecule. This facts are due to the smallness, of atoms, and molecules, compared to us. This is a reason why effective description like Navier-Stokes equations are an inevitable tool to understand the behavior of fluid matter in general.

At last, another more epistemological and historical reason for the ubiq-

uity of effective descriptions in science is their simplicity. It would be wrong to believe that, fluid dynamics equations were derived because they were more adapted than a molecular description taking into account Quantum Mechanics and the now more established fundamental nature of matter, they were derived because they describe well the phenomena studied in the nineteenth century they constitute an advance in understanding the phenomena we observed. Deriving Navier-Stokes equation from the microscopic scale is a highly non-trivial problem and no one doubts that waiting for deriving Navier-Stokes equations them exactly before using them is not a good idea. The way we access to knowledge, and the habit in Science to apply Occam's razor principle, explain the tendency to favor the solution that assumes less suppositions and that is based on less beliefs. Sometimes, depending on the point of view, this is also the simplest solution to the problems.

From what was explained before, it looks obvious that defining effective theories following the criteria of simplicity sometimes called, parsimony, just because they describe well a macroscopic phenomena is, a common, and a useful habit, of science. It is also obvious that macroscopic phenomena are caused by the subjacent microscopic. The problem of relating, the microscopic world, to the macroscopic one, is the main object of Statistical Mechanics, and of this thesis. The very high number of particles comprising matter make the use of statistical tools very efficient.

An interesting puzzle solved by statistical mechanics is that eventhough, the laws governing the microscopic of Physics are reversible, irreversible processes are ubiquitous in nature. For instance, an ideal gas is constituted of particles whose interactions and dynamics is reversible. If the particles of a gas are confined, by a wall, in the half of a recipient, when removing the wall, the particles will invade the whole recipient. This process is highly irreversible because the new macroscopic configuration is statistically overwhelmingly more probable than the configuration in which all particles are in only half of the recipient. This is naturally solved by the application of statistical ideas. Formally, this is the second principle of Thermodynamics stating that the entropy of isolated systems increases. Therefore, this allows one to chronologically order events in time.

Irreversibility is an exemple of a property that arises from the number of particles and not only from the behavior of individual particles. More generally, it is common that the behavior of particles in big assemblies is different from their behavior when isolated. Systems exhibiting this property are referred to as complex systems. Many definitions of complex system can

be found, one is, a “system of many strongly-coupled degrees of freedom”. This is very general concept and appears in many real systems, in particular, next to a critical point.

Magnetic materials and fluids give good examples of critical points. In a ferromagnetic material, at low enough temperature a spontaneous magnetization appears, when increasing temperature, at a given critical temperature, T_c , or Curie temperature, the spontaneous magnetization disappears.

In the following chapters, we will give many examples of such phenomena. Indeed, order-disorder transitions are very ubiquitous in nature. This is related with universality concepts and reflected by the fact that very many theoretical models have been shown to exhibit phase transitions.

Chapter 2

Phase Transitions with Two Competing Absorbing States

2.1 Motivation

The recent interest of physicists in quantitative problems in social sciences gave rise to important research on “opinion models”. One of the simplest opinion models is called the voter model (VM). This model is an archetypal model of opinion dynamics in which each element/spin is on a lattice and interacts only with its four nearest neighbors. The state of a spin can be modified to the state of another connected spin. Spins behave as individual that can change opinion to the opinion of a friend or someone they talk to. In VM, opinion is limited to 2 values (e.g. 1 or 0) and the interaction takes place on a substrate network that can be a periodic lattice or a disordered network. The dynamics of the model can be described in a few words: a site is selected at random, and its opinion is changed to the opinion of a randomly chosen neighbor. This constitutes an elementary time-step, to be iterated. Following this dynamics, we easily see that if all the individuals adopt value 1 or 0 i.e. they all have the same opinion, the dynamics stops and no individual is anymore able to change opinion. Such states are called absorbing states of the model. One fundamental property of the VM is to have 2 symmetric absorbing states.

The presence and nature of absorbing states are relevant ingredients to determine criticality in phase transition. In the following we will address the question of the relevance of these 2 absorbing states giving first an in-

roduction through examples present in literature and then analyzing the consequences of our results.

2.1.1 Generic Absorbing Phase Transition: Directed Percolation

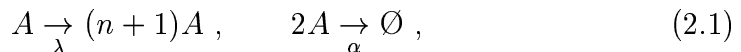
Many natural phenomena like forest fires [3], surface catalysis or propagation of epidemics [4] show similar features. If the presence in one area of the system of, a fire, a started catalytic reaction, or a contagious illness, is called activity, in all these physical situations we have an activity field that propagates in the system. The activity in one area can propagate to all areas in contact (whatever contact means here) and an inactive area that is not in contact with activity will never become active. In order to understand better those general phenomena, models of spreading processes have been studied. Such models involve an activity field $\phi(x)$, site x is active when $\phi(x) \geq 0$ and is absorbing when $\phi(x) = 0$. As was said above, absorbing states are characterized by the absence of fluctuations, when the system finds itself in such a state, it can not escape from it. When the transition probability to access the absorbing state is not zero, this is an extreme case of irreversibility, since the probability to escape from it is zero. Therefore, detail balance condition is violated. Usually, detail balance is prescribed to ensure the existence of a stationary state, a system with a dynamics obeying detail balance can have as a stationary state the state that obeys the detail balance condition. In our cases of interest, there is however a stationary state, which we will study and characterize. We are interested in the situation in which those models are diffusion limited, in low enough dimension, their properties are interesting since the interplay between reaction and diffusion keeps them in a situation with important fluctuations and spatial structures. A paradigmatic model exhibiting this kind of phase transition is the Directed Percolation (DP). In DP each site of the lattice is either active (infected) or inactive (healthy). Infected sites can infect neighboring healthy sites and can heal, according to the balance of infection recovery, the stationary state of the system is either partially infected or completely healthy (active or absorbing phase). When completely healthy it cannot get infected anymore since spontaneous outburst of infection are not possible. One realization of the DP universality class is given by the directed bond percolation which microscopic details are described in [2]. A typical time-evolution of directed

bond percolation is shown in (Fig. 2.1), the first row shows a system initially fully occupied, for three different percolation rates. The time-evolution experiment from a fully occupied lattice to the stationary state of the system is called a 'decay experiment'. The second row shows a time-evolution following an initially completely absorbing configuration with a single seed of activity in the middle of the system. In the first column, the rate of infection is small and the system invariably reaches, in a finite time, a state from which it cannot escape. The quantity defined as the density of active sites, $\rho = \frac{1}{L} \sum_i^L n_i$, where L is the system size and n_i is a variable taking value 1 when site i is occupied and 0 when it is empty, is a convenient order parameter, for this phase transition, measuring it in experiments like the first row of (Fig. 2.1), we see that there is a particular value of $p = p_c$ for which it decays as a power law $\rho(t) \equiv t^{-\theta}$. In (Fig. 2.7), we illustrate that for another system belonging to the universality class of DP, in 2 space dimension and time, noted $2+1$, a log-log plot gives as expected a straight line of slope -0.45. In the beginning of this thesis, we recall that all models belonging to the same universality class, in this case DP, are described the same critical exponents that depend on the dimension of the system. In this chapter, we will present results that illustrate some subtleties on this point. The particular model we consider here, the generalized voter (GV), has the interesting particularity to coincide with a different model, in $D = 1$ (one space dimension and time, sometime noted $1+1$), namely branching-annihilating random walk with parity conservation. However those universality classes coincide in $D = 1$, they are different in higher dimensions. In the case of (Fig. 2.1), dimension is 1, so the decay exponent is around -0.16. As said before, those exponents are important in Nonequilibrium Phase Transition (NEPT) because they are supposed to be reminiscent of a universality class. In this work we apply universality class concepts, very well established for equilibrium systems, to NEPT, all models belonging to the same universality class should have the same exponents. So studying critical behavior and exponents like θ should allow to classify NEPT into universality classes. Under that is the idea that systems presenting different microscopic properties might show the same macroscopic behavior close to their critical point. Another characteristic behavior can be seen, for $p > p_c$. $\rho(t)$ saturates to a finite value $\rho^{stat} = (p - p_c)^\beta$. The system is characterized by two different correlation lengths, the spatial correlation length scale ξ_\perp and temporal correlation length scale ξ_\parallel that behave respectively as $\xi_\perp = |p - p_c|^{-\nu_\perp}$ and $\xi_\parallel = |p - p_c|^{-\nu_\parallel}$ when p is close to p_c . The divergence of length scales can be seen as the reason for the appear-

ance of power laws. Indeed, if there is no more finite length scale in the system, the laws describing the system must be so that they do not have any characteristic length scale and this is one of the properties of power laws.

The nature of phase transitions is governed by very simple ingredients as symmetries, dimensionality of the system and the symmetry breaking of the order parameter. The most generic absorbing phase transition is DP, it is known to be very robust. To obtain a different universality class, it is enough to include some new symmetry not present in DP. So a priori a system with several symmetric absorbing states, should belong to a different universality class. The competition between different absorbing states might alter the critical behavior. There are many models with two symmetric absorbing states, like some cellular automata [12, 13] or nonequilibrium Ising models [14, 15]. They belong to the same universality class called DP2. Reaction-diffusion models of particles with parity-conserving symmetry also belong to DP2 in one spatial dimension but differ in higher dimension.

These are defined by the following reaction-diffusion scheme:



with $n = 2, 4, 6, \dots$. For a review this see [2].

2.1.2 Generalized voter

In previous work [5], number of microscopic models have been shown to belong to the same universality class named “generalized voter” (GV). They are characterized by different common features.

1. No surface tension. Coarsening caused by interfacial noise instead of surface tension.
2. No bulk noise. Existence of two dynamically symmetric absorbing states.
3. Logarithmic ordering instead of common power law induced by surface tension.

This findings lead the authors of [5] to define a universality class encompassing the VM.

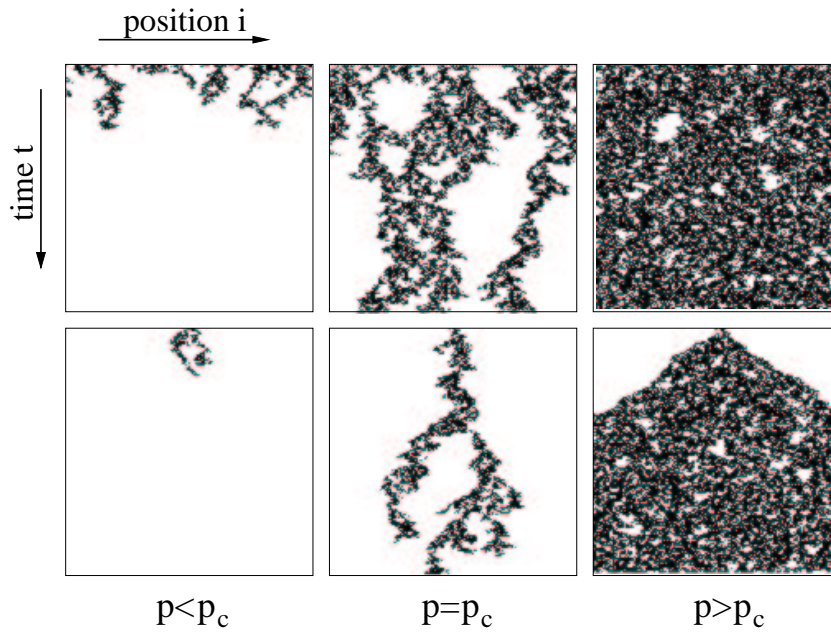


Figure 2.1: Directed bond percolation in 1+1 dimensions starting from random initial conditions (top) and from a single active seed (bottom). Each horizontal row of pixels represents four updates.(taken from [2]).

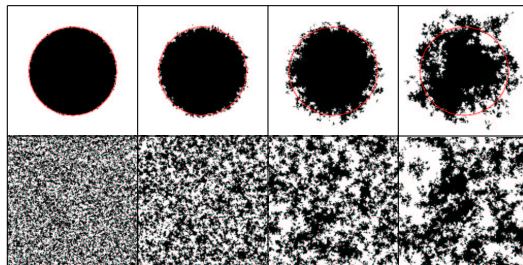


Figure 2.2: Voter coarsening experiments in which we see the absence of surface tension and bulk noise (taken from [5]).

Splitting of voter criticality 2D results

In a work by Droz et al. [6], the authors define a microscopic model with interesting properties. They study two dimensional phase transitions and observed that varying a small ingredient in the dynamics, the neighborhood considered, the model undergoes either a single phase transition apparently

belonging to GV or two transitions. When the neighborhood is small, a spin interacts only with its four nearest neighbor, they observe a GV transition. When the neighborhood is big enough, at least 12 neighbors, including third nearest neighbors, they observe two transitions. Let us precisely describe the dynamics :

Spin at site i , σ_i , can access only two states, $+1$ and -1 . Sequentially update each site, if all spins in the neighborhood of a given site are in the same state as spin i , then spin i cannot be changed (resulting inactive phase or absorbing phase if all site are in this state), if one of the neighboring sites is not in the same state as i , then site i is updated with a Metropolis rate. To use a Metropolis rate, define an energy for the system as :

$$E = - \sum_{(i,j)} \delta_{\sigma_i \sigma_j}, \quad (2.2)$$

where (i, j) refers to, all sites j in the neighborhood $N(i)$ of i . To accept or reject a spin flip, one looks at the energy difference ΔE between the final and initial configuration and accept the move with probability $\min\{1, e^{-\Delta E/T}\}$, where T is temperature. Summarizing, this results in a modified Metropolis rate with two symmetric absorbing states. If all sites are in state ± 1 , the dynamics stops.

According to the neighborhood $N(i)$ considered, the model has a different phase diagram. Here are the two possible scenarios illustrated in (Fig. 2.3) :

- (A) with nearest-neighbor, the system undergoes a single phase transition belonging to the generalized voter universality class.
- (B) with third-nearest-neighbors, 12 neighbors, the system undergoes two phase transitions. First an Ising transition and after a Directed Percolation (DP) phase transition.

So it appears sensible to say that the generalized voter transition is equivalent to the simultaneous breaking of Ising and DP symmetries. The splitting depends on the neighborhood considered it can be clearly finite or apparently equal to zero. This is somehow pathological and can lead to the question : “Is the generalized voter genuinely a new transition or is it only two close well studied transition?”. Another explanation for the above situation is that one of the necessary conditions to observe GV transition is broken. Let us considered the problematic situation: with third nearest-neighbors, in the

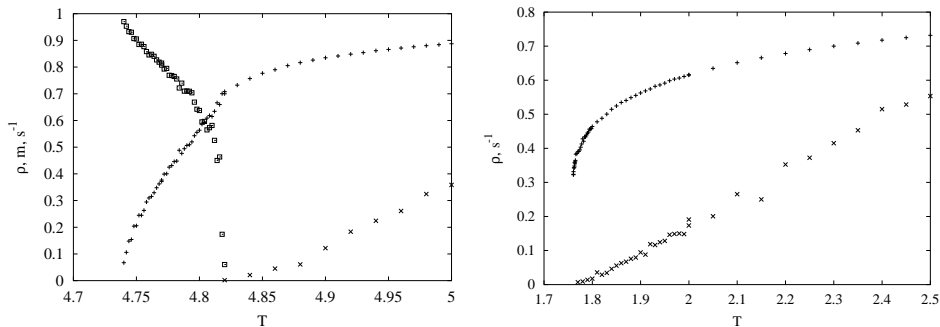


Figure 2.3: The density of active sites ρ (+), the inverse of the variance of magnetization s (x) and magnetization m (□) as a function of temperature. Left, DP and Ising transitions appear to be splitted (scenario B). Right, DP and Ising transition are simultaneous giving rise to a generalized voter transition (scenario (A) taken from [6]).

dynamics, there is two transition. A fundamental condition to observe GV is the absence of bulk noise. In the vicinity of an interface of a model belonging to GV, fluctuations only occur very close to the interface, it is obvious that including third-nearest-neighbors, fluctuations can penetrate in the bulk from the interface, and propagate.

To improve this “hand-waving” answer, we sought for some different description or theoretical framework of the ordering transition. A good step in this direction could be to find a Langevin equation describing this phenomenology. Then this equation can be studied numerically or through the renormalization group tools in order to clarify the above picture. Here, we propose a Langevin equation we numerically proved to encompass these scenarios. This alternative description allows us to understand when the Ising and DP transitions are simultaneous and when they are splitted. It has the advantage of demonstrating that in some case there is no splitting at all and both transition are simultaneous resulting in a different transition namely generalized voter.

2.2 From microscopic to Langevin equation: two symmetric absorbing states

2.2.1 The form of the Langevin equation

In order to find a Langevin equation describing the above picture, we can either heuristically define a Langevin equation. We had different constraints on the noise and the deterministic term. All these constraints lead us to a non uniquely defined Langevin equation which we numerically study in order to check or not it has the good phenomenology.

Noise term

In order to have an absorbing state, the noise term needs to have some particular features. Go to 0 at the absorbing barriers. And in order to be sure to find a DP transition, we use a noise proportional to $\phi^{\frac{1}{2}}$ close to the barriers. We arbitrarily placed the barriers in -1 and 1 so the choice of correlator we made was the following $\langle \eta(r, t)\eta(r', t') \rangle = (1 - \phi^2)\delta(t - t')\delta(r - r')$. This locally makes the job, indeed it behaves like $\phi^{\frac{1}{2}}$ in the vicinity of -1 and 1.

Potential

What form to choose for the deterministic part. We can get intuition from the potential and also from the strength (minus the derivative of the potential). Again, the absorbing barriers create some constraints on the choice. We need a strength that goes to 0 in -1 and 1, so it will be proportional to $(1 - \phi^2)$. In order to get first a symmetry breaking and after an absorbing phase transition we need a strength expression that vanishes at some intermediate value between 0 and one. This can be done taking a strength also proportional to $a\phi - b\phi^3$. It corresponds to the strength of the ϕ^4 potential, so it will easily generate an Ising transition. The resulting expression for our strength is $(1 - \phi^2)(a\phi - b\phi^3)$ The potential giving rise to this strength is the following (Figs. 2.4 and 2.5).

$$V(\phi) = -\frac{a}{2}\phi^2 + \frac{a+b}{4}\phi^4 - \frac{b}{6}\phi^6 \quad (2.3)$$

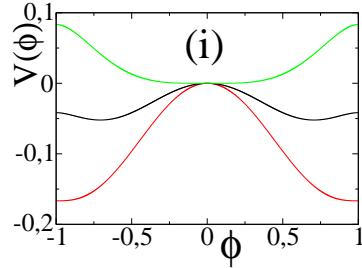


Figure 2.4: (i) In this series, $b=1$, this gives scenario (B). This graph is illustrative of the 2 phase transitions. Green $a=1$ Ising disordered phase. Black $a=1/2$ Ising ordered and DP active phase. Red, $a=0$ DP absorbing phase.

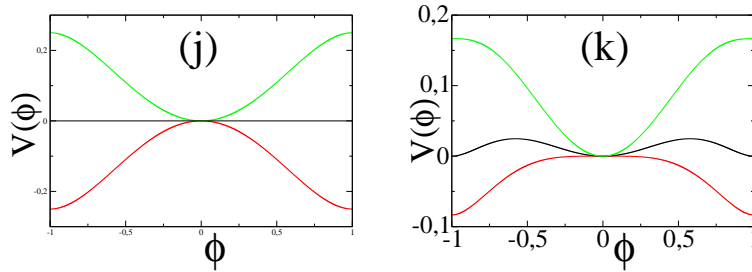


Figure 2.5: (j) $b=0$ gives scenario (A). Green, $a=1$ disordered phase. Black, $a=0$ Voter transition. Red, $a=-1$ ordered phase. (k) $b=-1$ gives scenario (A). Green, $a=1$ disordered phase. Black, $a=1/2$ close to Voter transition. Red, $a=-1$ ordered phase.

Our guess

Just putting together the above information and adding the necessary diffusing term, we end up with the following Langevin equation

$$\frac{\partial \phi(r, t)}{\partial t} = (a\phi - b\phi^3)(1 - \phi^2) + D\nabla^2 \phi(r, t) + \sigma \sqrt{(1 - \phi^2(r, t))} \eta \quad (2.4)$$

2.3 Results for Langevin equation with two symmetric absorbing states

We present results, obtained with different tools, in order to obtain a good understanding of the phenomenology presented by Eq. (2.4). The first tool

we apply to this problem is a mean-field calculation of the phase diagram: in 2.3.1 we explain the meaning of our mean-field approximations, describe our results and their expected limitations. Mean-field results are exact from the upper critical dimension to infinite dimension. Interested in physical dimension, we go down in dimension, and subsequently study numerically Eq. (2.4) in dimension 2, and 1. The numerical scheme we followed is detailed in 2.3.2, results for $D = 2$, are in 2.3.3, results for $D = 1$ in 2.3.4

2.3.1 Mean-field

Self-consistent results

To use a self-consistent approach we first discretize Eq. (2.4) giving Eq. (2.5) and study the case of global coupling (see Eq. (2.6)).

$$\partial_t \phi_i = (a\phi_i - b\phi_i^3)(1 - \phi_i^2) + D\nabla^2 \phi_i + \sigma\sqrt{(1 - \phi_i^2)}\eta \quad (2.5)$$

$$\nabla^2 \phi_i = \frac{1}{N-1} \sum_{j \neq i} (\phi_j - \phi_i) \equiv M_i - \phi_i. \quad (2.6)$$

Assuming $M_i = M$, we are left with only one associated FP equation for Eq. (2.5) in Ito sense:

$$\partial_t P = -\partial_\phi \{[(a\phi - b\phi^3)(1 - \phi^2) + D(M - \phi)]P\} + \frac{\sigma^2}{2} \partial_\phi^2 [(1 - \phi^2)P] \quad (2.7)$$

A stationary solution is:

$$P[\phi; M] \equiv \frac{1}{(1 - \phi^2)^{1-D/\sigma^2}} \exp\left[\frac{2}{\sigma^2} \left(\frac{a\phi^2}{2} - \frac{b\phi^4}{4}\right)\right] \left(\frac{1 + \phi}{1 - \phi}\right)^{DM/\sigma^2} \quad (2.8)$$

The self-consistent solution is obtained when:

$$M = \langle M \rangle = \frac{\int \phi P[\phi; M]}{\int P[\phi; M]} \quad (2.9)$$

This can be solved by numerical approximation of both integrals.

Limitations

Eventhough it is interesting, mean-field analysis is limited by the fact that we do not know how to make a mean-field analysis of the Reggeon field theory itself. The standard method of approximating the laplacian term by a magnetization term in the Langevin equation and solving the associated FP equation does not give satisfactory results. In the particular case of the Reggeon field theory, the constant term M and the noise term $\sigma\sqrt{\phi}$, control the result. If $M = 0$ then we always get an absorbing phase and if M is finite then we always get an active phase. We need an intermediate approximation possibly including more than nearest neighbors. This is an interesting work left to do.

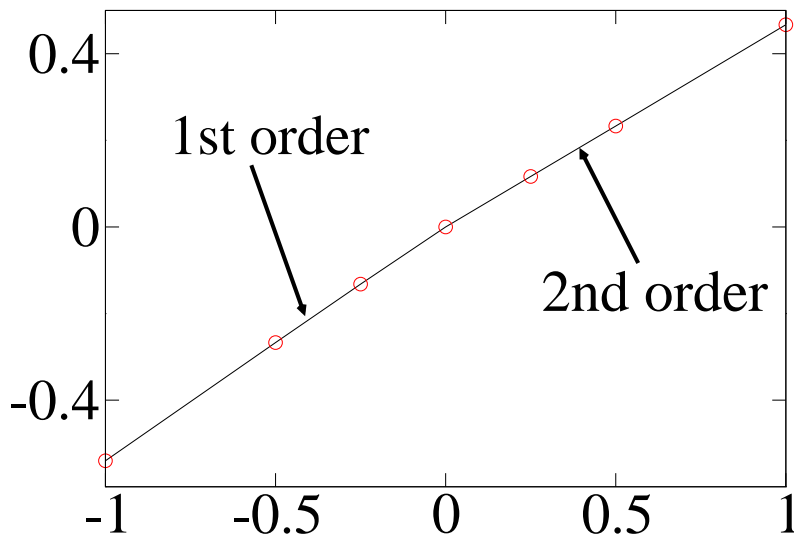


Figure 2.6: Result given by (Eq. 2.9) with $\sigma = 1$, $D = 1$. It captures the general picture given above (Fig. 2.7(a)) even if we cannot obtain the DP transition line by means of this approximation.

2.3.2 Algorithms for Langevin equations

This is quite a tricky problem that has been solved by two manners. It has long been known that some Langevin equation representing systems with absorbing states are difficult to simulate if the noise amplitude power is less than one. This is precisely the case we are interested in. Using a standard Euler method will produce value of the field that cross the barriers and this is physically unacceptable for our problem.

For this kind of problems there are 2 known solutions. The first one has been introduced by Dickman [11]. It consists in discretizing the Langevin equation in a way that the field does not cross the barrier. We first started with this one and had some preliminary results and intuition on the problem but this numerical trick appears somehow unnatural and shows long transients. On the other hand, the method introduced in [8, 9] is much more efficient and has shorter transients so we decided to use it.

The second method, is in itself more elaborated and consists in finding a way of generating a random number following a distribution obtained by analitically iterating the solution of the Fokker-Planck(FP) equation equivalent to our Langevin equation. We then use the new value of the field as the initial solution of the FP equation and iterate again. Since we don't know how to efficiently generate a random number from the solution of the FP, we split the Langevin equation in two parts. We put all the terms we can iterate in one part and iterate the rest with a simple Euler algorithm.

- Noise part for which we know the solution of the FP equation. So we use the following formula. $P(\phi, t + dt) = P\{\phi(t + dt) = \phi | \phi(t) = \phi_0\}$
- Deterministic part we iterate using a simple Euler method.

$$\phi(t + dt) = dt(\nabla^2\phi + F[\phi])$$

It can be shown [10] that the splitting step method has an order of convergence $\mathcal{O}(dt)$ when the second step is integrated exactly. There are different ways of separating the equation in two parts (including more or less deterministic terms in the exact iteration of the noise term), they give the same result but the efficiency of the algorithm depends on how difficult it is to generate a random number with the resulting distribution. This kind of problems are treated in a reference book [7].

It is possible to solve the FP equation associated to $\frac{\partial\phi(r,t)}{\partial t} = \sigma\sqrt{(1 - \phi^2(r,t))}\eta$. But it is more efficient to use two independent noise. Invoking universality

arguments, the universality class in which belong the transitions should not depend on the details of the noise term we study. So we use a gaussian noise of amplitude proportional to $\sqrt{\phi-1}$ if $\phi > 0$ and $\sqrt{\phi+1}$ if $\phi < 0$. This square root noise is generated as explained in [8]. Here is a short explanation of the numerical algorithm used. The FP equation associated to a gaussian square root noise $\partial_t \phi = \sigma \sqrt{\phi}$ is $\partial_t P(\phi, t) = \frac{\sigma^2}{2} \partial_\phi^2 [\phi P(\phi, t)]$.

If the initial condition is $P(\phi, 0) = \delta(\phi_0)$ then at time t we can show [9] that, $P(\phi, dt)$ will be given by Eq. (2.10)

$$P(\phi, dt) = \delta(\phi) e^{-\frac{2\phi_0}{\sigma^2 dt}} + \frac{2e^{-\frac{2(\phi_0+\phi)}{\sigma^2 dt}}}{\sigma^2 dt} \sqrt{\frac{\phi_0}{\phi}} I_1 \left(\frac{4\sqrt{\phi_0\phi}}{\sigma^2 dt} \right). \quad (2.10)$$

The first term is a delta function in the absorbing state showing that there is a finite probability of reaching the absorbing state in time dt . The second term is a smooth probability density distribution. I_1 is a modified Bessel function of the first kind of first order. To generate this distribution we use the same method as in [8],

$$\phi^* = \text{Gamma}[\text{Poisson}[\lambda\phi_0]]/\lambda, \quad (2.11)$$

where $\lambda = \frac{2}{\sigma^2 dt}$, modifying so that $\text{Gamma}[0] = \delta(x)$. Given that, $\text{Prob.}\{\text{Poisson}[\frac{2\phi_0}{\sigma^2 dt}] = 0\} = e^{-\frac{2\phi_0}{\sigma^2 dt}}$. We see that Eq. (2.11) generate exactly Eq. (2.10), the delta function term and the smooth term.

2.3.3 Numerical results in $D = 2$

We obtain a rich phase diagram, presenting a set of 3 universality classes.

Observing the potentials depicted in Fig. 2.4 and 2.4, we expect that fixing "b" and varying "a" as a control parameter, according to the value of "b", we will obtain scenarios A and B. For $b > 0$, we expect to see 2 phase transitions (Fig. 2.3 left, scenario B), first an Ising transition and after a Directed Percolation (DP) transition (Fig. 2.7(d)). On the other hand, when $b \leq 0$, a single transition (Figs. 2.3 right, and 2.7(b), scenario A) corresponding to what Droz et al. described in their article [6] (Fig. 2.7(a)).

This reasoning is mean-field like, it does not take into account fluctuations. In real simulations, one has to expect to see fluctuations effects. In practice, because of fluctuations, we observe that there is a value of $b_c \neq 0$ separating scenarios A and B.

For $b < b_c$, we identify a unique transition as being of generalized voter kind, this universality has been described in detail in Dornic et al. [5] (Fig. 2.7(a,c)). To best observe this, we initialize the whole system in state $\phi(x, t = 0) = 0$ and evolve it with Eq. 2.4 thanks to algorithm adapting Eq. 2.11. The observables we are interested in are the magnetization and the density of kinks, or presence of interfaces. Magnetization is conserved in time as is to expect for GV transition. Kinks can be defined in different ways. The easiest formula to is :

$$\rho = \sum_i \delta_{(\sigma_i, -\sigma_j)}. \quad (2.12)$$

The density of kinks is close to the density of interfaces. Following the time evolution of the system we see an ordering transition with logarithms.

$$\frac{1}{\rho(t)} \sim \log(t). \quad (2.13)$$

The expected behavior for GV being [17, 18] :

$$\rho_m(t) = (1 - m^2) \left[\frac{2\pi D}{\ln t} + \mathcal{O}\left(\frac{1}{\ln^2 t}\right) \right], \quad (2.14)$$

We were also able to realize experiments similar to the one showed in (Fig. 2.2), illustrating the absence of surface tension.

2.3.4 Numerics in $D = 1$: Compact directed percolation, Parity conserving

Numerical results given by Eq. (2.4) in one spatial dimension seem to show that it is a correct Langevin description of parity-conserving, directed ising, DP2 or GV which coincide in one spatial dimension. This is understandable via a mapping Fig. 2.8 of interfaces or kinks separating absorbing (activity of the system) to particles following the reaction scheme 2.1. The transition in GV separates an ordered phase in which all the system is in the same state (+1 or -1) and a disordered state in which kinks separate domains of opposite signs. Domains of opposite signs are separated by an odd number of kinks while domains of identical signs are separated by an even number of kinks. This topological constraint is the conservation law that gives rise to the GV, parity-conserving identity in one spatial dimension. From what is

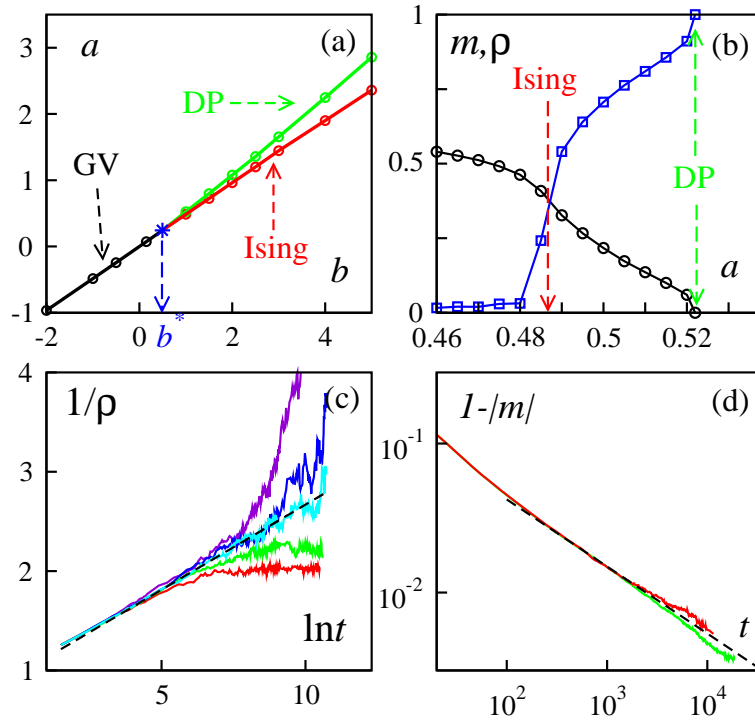


Figure 2.7: Results in two space dimensions. (a) Phase diagram of Eq. (2.4) in the (a, b) plane. For $b \leq b^*$ we observe a GV transition line. (b) Steady-state magnetization (circles) and density of interfaces (squares) for various values of a with $b = 1$. (c) $1/\rho$ vs $\ln t$ at $b = -0.2$ for various values of a around $a_{GV} \simeq -0.115$ (middle curve); the dashed line is a linear fit. (d) Time-decay of $1 - |m|$ for a values around $a_{DP} \simeq 1.6551$ ($b = 3$); at criticality, $1 - |m| \sim t^\theta$ with $\theta \simeq \theta_{DP} \simeq 0.45$ (dashed line).

said above, the ordering dynamic of creation and annihilation of kinks, can only follow: $A \rightarrow 3A$ $2A \rightarrow \emptyset$.

The mapping with annihilating random walker presented in [5] makes clear the fact that in the absorbing phase, the system asymptotically behaves with a power law in $-\frac{1}{2}$ (see Fig. 2.9(b)).

In spreading experiments, we found $\delta = 0.29$ (Fig. 2.10), which is compatible with the known relation for this transition $\delta + \theta = 0.286$ [2].

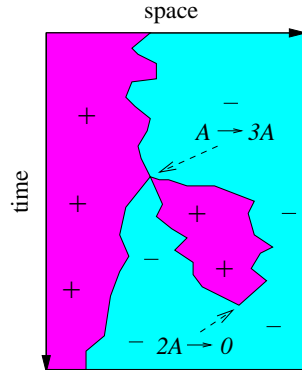


Figure 2.8: The mapping responsible for coincidence of parity-conserving and DP2 in one dimension.

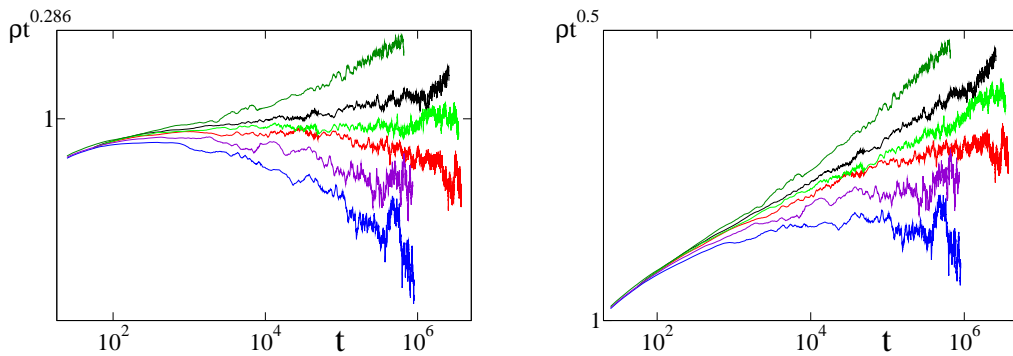


Figure 2.9: Density of kinks multiplied by time to a given power. Left, the power is 0.286 which is the expected value for criticality of system with 2 absorbing states. Right, the power is 0.5, to put in evidence the decay in the absorbing phase.

2.4 Symmetry breaking in Generalized Voter

The results presented so far can be summarized as the following :

- Our effective description for critical phenomena in presence of two symmetric absorbing states improves the understanding of critical phenomena and of the relevance of symmetries in determining universality out of equilibrium.

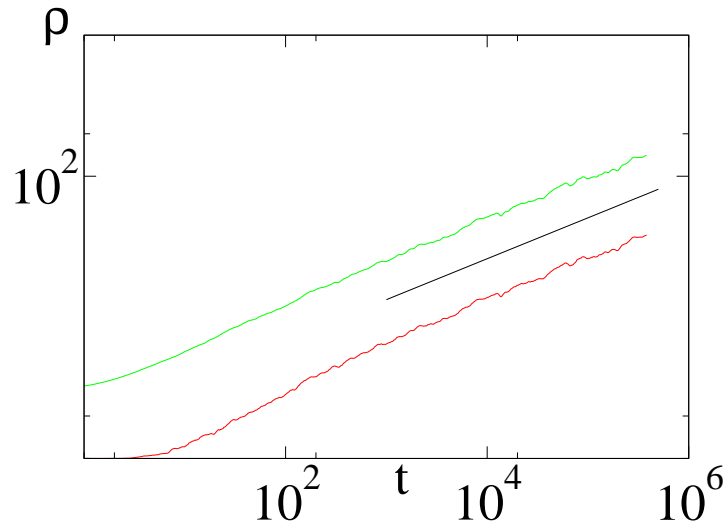


Figure 2.10: Spreading experiment. Two measurements of the density of kinks: green, $N - \langle \phi_x \phi_{x+1} \rangle$; red, $\langle 1 - \Theta[\phi_x \phi_{x+1}] \rangle$. The black straight line has a slope 0.29. We see that both definition of the density of kinks present the same asymptotic scaling ($\delta = 0.29$).

- We also clarified the fact that, in two spatial dimensions, so long as there is no bulk noise, there is only one transition, belonging to the GV universality class.
- In effective descriptions, with two absorbing states, bulk noise can be introduced, dynamically preventing the system to access the absorbing state when symmetry breaks and inducing two splitted transitions, Ising and DP.

Since the study of microscopic models showed that asymmetry and non-integrability are not incompatible with logarithmic coarsening, it might be useful to investigate whether or not coarse-graining procedures conserve asymmetry or non-integrability. One way to approach an answer to this question may be to find a coarse-grained description that breaks the same symmetries as microscopic models do, exhibiting logarithmic coarsening. In the remainder of this chapter, we follow this idea. Firstly, we heuristically define a Langevin equation breaking a given symmetry. Secondly, we study it

numerically and to finish, we give perturbative diagrammatic arguments to consolidate our guess.

2.4.1 Relevant ingredients: coarsening without surface tension

It has been shown that two-dimensional models, where bulk noise is absent and where coarsening is induced only via interfacial noise, all obey voter-like critical coarsening; thus, they form a universality class, referred to as *generalized voter* (GV). Noisy interfaces and hindered bulk noise are naturally present in systems with competing absorbing states. All models belonging to the *generalized voter* universality class present, explicitly or after suitable mapping, two absorbing states. The presence of asymmetry is believed to lead generically to the *Directed percolation* universality class, however some Z^2 asymmetric models, undergo a *generalized voter* transition. This fact underlies that the fundamental property of the *generalized voter* class is the absence of bulk noise. For these reasons, we seek for an asymmetric Langevin equation with two absorbing states undergoing a non-DP transition. Our first task is to find an asymmetric but irrelevant contribution to the theory.

A second interesting result obtained from microscopic models is that some symmetric rules lead to logarithmic coarsening characteristic of GV but, without conservation of the magnetization, more precisely any non-zero magnetization is weakly attracted towards vanishing magnetization.

2.4.2 Microscopic non-integrable model

Here, we investigate another subset of the GV. This consists in a modification of the voter model which is defined by four parameters. A spin flips with probability $r_{s,h}$, $s = \pm 1$ is the value of the spin and h is its local field $h = \{-4, -2, 0, 2, 4\}$. We enforce $r_{s,h} = r_{-s,-h}$ for Z^2 symmetry and are left with 4 parameters. For the voter model those are, $r_{1,h} = \frac{1}{2} - \frac{h}{8}$. $r_{1,4} = 0$ to conserve the absorbing state and $r_{1,0} = \frac{1}{2}$ arbitrarily. We are now left with three free parameters, $r_{1,-4}, r_{1,-2}, r_{1,2}$, the condition $r_{1,2} = r_{1,-4}/4$, leaves only two. In the plane $r_{1,-2}, r_{1,-4}$, this rule exhibits a line of ordering transitions exhibiting logarithmic coarsening and non-conserved magnetization.

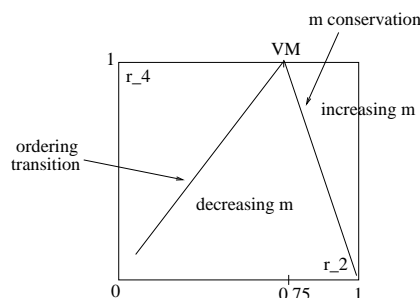


Figure 2.11: Left straight line, ordering transition line for the model described in text. Right, Mean-field results of Eq. (2.15).

Mean-field and simulations

At a mean-field level, assuming that spins are uncorrelated, we can easily derive the simple relation,

$$\frac{\partial m}{\partial t} = \frac{3}{16}m(r_{-2} + r_{-4}/4 - 1). \quad (2.15)$$

From Eq. (2.15), we see that according to the sign of the term multiplying m in the left-hand-side, the zero magnetization is either stable or unstable. This allows us to draw a line in the plane r_{-2}, r_{-4} , separating phase space in which disordered systems have a growing, or a decreasing magnetization (see Fig. 2.11). We see that the transition line obtained in simulation is situated in the phase space where magnetization is expected to be decreasing in absolute value.

In simulations, time evolutions of infinite temperature systems to a finite temperature, with an initial magnetization different from 0, show that the magnetization decreases, logarithmically to 0. This is the reflect of the logarithmically time growing correlation length. We see that this is very similar to voter dynamics, the change is that individual + (respect. -) spins in a sea of - (respect. +) spins have a longer persistence time.

Langevin equation for symmetric non-integrable model: heuristic arguments

In the Langevin equation we conjecture that this is equivalent to replacing $D \rightarrow (D + \phi D_1 \nabla^2 \phi)$. The term $D_1 \nabla^2 \phi$ is of the same sign as ϕ and increases

persistence time. This perturbatively modifies the propagator and therefore the critical point location for Eq. (2.16) has to be re-located, for $b = 0$ it was found around $a = 0.0018$ as shown in Figs. 2.12 and 2.13.

$$\frac{\partial\phi}{\partial t} = (D + \phi D_1 \nabla^2 \phi) \nabla^2 \phi + (a\phi - b\phi^3)(1 - \phi^2) + \eta \sqrt{1 - \phi^2} \quad (2.16)$$

Equation (2.16) appear to be a satisfactory phenomenological proposal for the present subset of rule undergoing GV ordering transition without m conservation.

Numerical results

Without surprises, we can apply the method employed to study Langevin Eq. (2.4), to Eq. (2.16). The results obtained are depicted in Fig. 2.12. In order to observe a GV transition we initialize a two dimensional system in a uniform state $\phi(t = 0, r) = 0$, and evolve the system measuring the average density of kinks and the average magnetization. For $b = 0$, $a = 0$, and D_1 small, we are in a disordered, phase. Showing both that the introduction of D_1 is a relevant perturbation. In order to locate a critical point, we study the $a - b$ phase diagram. For $b = 0$ and $a \geq 0$, two situation are observed. If $a > a_c$, for a given a_c the system orders completely, the density of kinks vanishing and the magnetization taking value ± 1 depending on fluctuations. If $a < a_c$, the system remains asymptotically disordered. Just at $a = a_c$, we observe a GV behavior, namely a logarithmic decay of the density of kinks (see Fig. 2.12) with initial vanishing magnetization conserved in time (Fig. 2.13).

As a complementary result, we observe that a non initial magnetization logarithmically decays to vanishing magnetization.

Perturbative diagrammatic arguments

In order to gain understanding in our problems, we write down the terms we proposed in terms of diagrams. The diagrams representing the terms present in the original theory are depicted in Fig. 2.15.

We see that the new term we introduced, when combined with the noise term generate a mass coefficient. This gives an explanation of why the critical

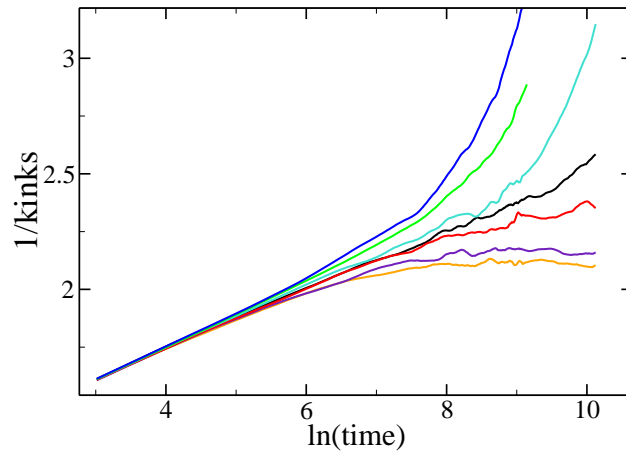


Figure 2.12: Coarsening experiment for system size 1024×1024 in $D = 2$, initial condition completely disordered. We clearly observe a logarithmic time evolution of the density of kinks, for $a = 0.018$. This is characteristic of GV type of ordering.

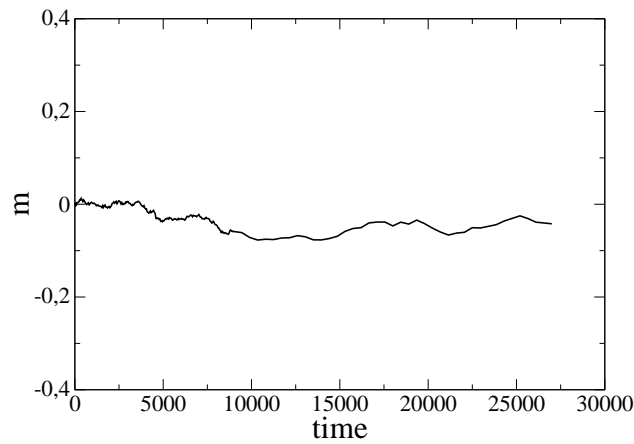


Figure 2.13: Same experiment as Fig. 2.12, we show only result for the critical point, $a = 0.018$, we depict the time evolution of the magnetization. Initial zero magnetization is conserved in time. As expected for GV and from mean-field calculation (Eq. (2.11))

point location is modified by the introduction of hindered diffusion. Moreover, we know that no new divergences are introduced so that the critical

point nature is not modified.

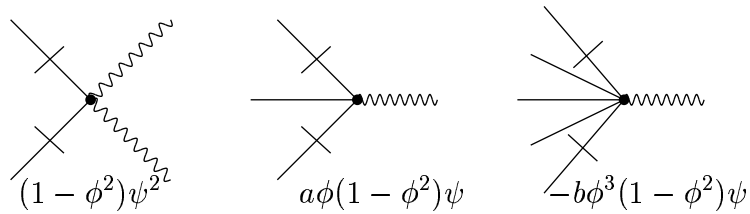


Figure 2.14: The three vertices of the theory. From left to right, we see the noise diagram, the mass, and the saturating term.

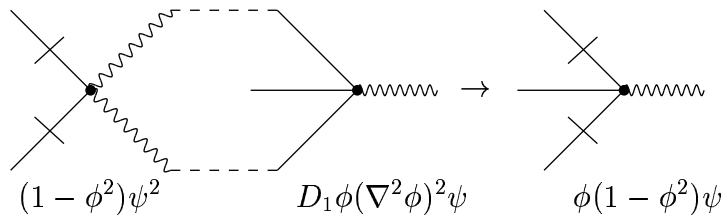


Figure 2.15: The symmetric term together with the noise term generate a mass term. This explains why the critical point location is modified in numerical results.

2.4.3 Asymmetric generalized voter

For microscopic models, the subset of m -conserving Z^2 asymmetric rules was studied using pair-update with an update probability $p_{n^+, n^-} = 1/n^+$ (for inhomogeneous pairs; n^+, n^- are the number of neighboring spins $+$ and $-$). This rule is m -conserving if, with probability $1/2$ the updated pair ends in state $++$ or $--$. The described rule suggests that we should rescale time

for each site by a factor proportional to the local mean-field felt by this site. Applying this without deterministic asymmetry we are directly lead to Eqs. (2.17) and (2.18). Here the dynamic is defined for sites and not for pairs so we have no way of enforcing m conservation(Fig. 2.16(right)).

Langevin equation for asymmetric model: heuristic arguments

A) Field asymmetry

The simplest possibility of asymmetry in the stochastic part is to include a field dependent amplitude to the noise. There are several ways to do it, we have explored the following,

$$\frac{\partial \phi}{\partial t} = D\nabla^2 \phi + \sigma \eta \sqrt{1 - \phi^2} \sqrt{1 + a\phi}. \quad (2.17)$$

B) Laplacian asymmetry

Another possibility of introducing terms linear in the field is a laplacian leading to Eq. (2.18),

$$\frac{\partial \phi}{\partial t} = D\nabla^2 \phi + \sigma \eta \sqrt{1 - \phi^2} \sqrt{1 + a\nabla^2 \phi}. \quad (2.18)$$

Numerical results

Numerical simulation of Eq. (2.17) gives results consistent with GV. As it is to expect, (ordering time) vs. (size) is a growing function. Logarithmic coarsening is recovered in a time-regime depending on system-size (Fig. 2.16(left)), during which $m = 0$ is conserved (Fig. 2.16(right)). This appears to be a good proposal for an asymmetric equation exhibiting GV behavior.

Here again, monitoring (ordering time) vs. (size) is a growing function (Fig. 2.17). Logarithmic coarsening is recovered in a time-regime depending on system-size, during which $m = 0$ is conserved. This is a good proposal for an asymmetric equation exhibiting GV behavior.

Perturbative diagrammatic arguments

Contrarily to the preceding case, here, the critical point $a = b = 0$, is maintained and no mass term is introduced.

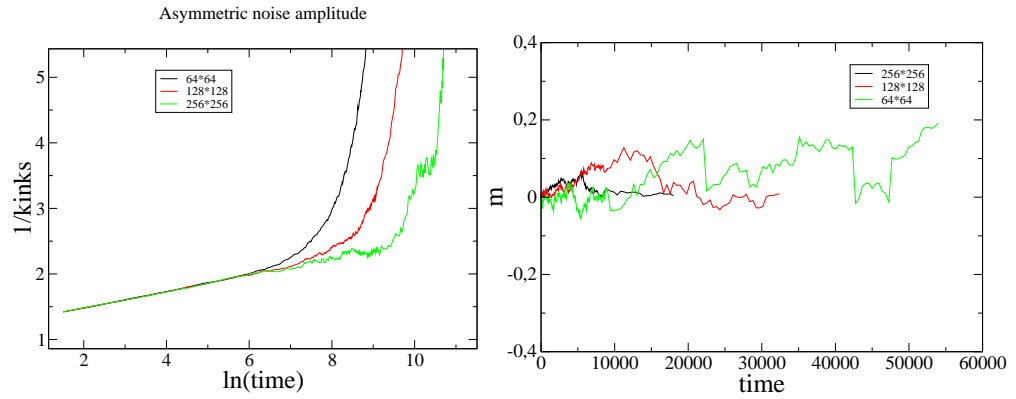


Figure 2.16: Coarsening experiments for different system sizes. Left: inverse number of kinks versus $\log(\text{time})$ this shows that asymptotically Eq. (2.17) exhibits GV behavior. Right: $m = 0$ is conserved (same runs).

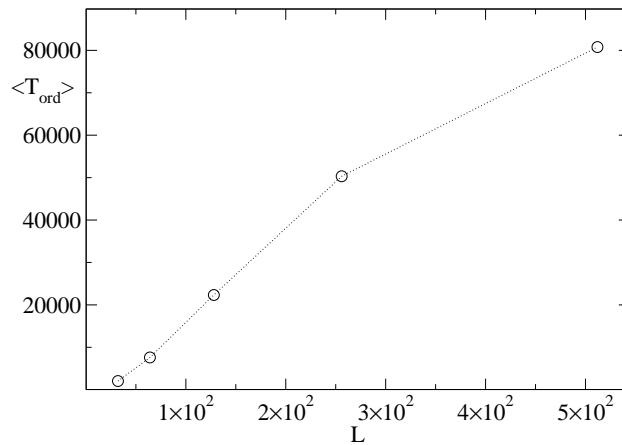


Figure 2.17: Ordering time defined as the average time at which magnetization reaches the value 0.9. For Eq. (2.18), it grows with system size.

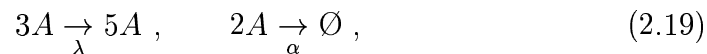
2.4.4 Non-integrable and asymmetric Langevin

From microscopic models we know that putting together contribution of the hindered diffusion term and the asymmetry do not lead to a GV transition. This can be explained by writing together the diagrammatic contribution of the hindered diffusion term, and of the asymmetric noise, term. They result in an asymmetric deterministic contribution leading to DP universality class. In simulations of this case, we see no GV transition needing for an explanation. This means that the symmetry is broken and a DP transition arises.

2.5 Counter-example

Trying to determine which are the relevant ingredients that dictate the nature of a phase transition out-of-equilibrium is a main issue in this thesis. To this aim, we can play at will with our models and study the consequences of our “recipes”. In this section we will explain how parity conservation is not the relevant ingredient in order to have a GV transition, even in one spatial dimension. GV transition occur in one and two spatial dimension. In two dimensions, the GV transition is a transition between two absorbing states, without surface tension, which implies that interfaces between this two absorbed domains govern the coalescence dynamics of the system. There is no activity inside the domains. On the other hand, if we have particles that diffuse in a two-dimensional space and react upon encounter, the dynamics is only present where particles are located, there are no interfaces, and there are no domains without activity. So that the symmetries and the dynamics of the system are completely different and no mapping can possibly connect one to the other (see [2] (p.94) for a nice explanation).

It is also important to notice that parity conservation is not enough to have a GV transition in one dimension. Such an assertion can only be proved by giving a counter-example. For instance, consider the following reaction-diffusion system in one dimension:



These reactions conserve the number of particles modulo 2 so this might be in the universality class of the Parity-conserving equivalent to the GV in 1D. A mapping, to two absorbing state, equivalent to the one performed for

the reaction-diffusion given by 2.1 can be done, but the interface dynamics should be different since, three interfaces should encounter in order to create offsprings. However, numerical simulation show that this is not the case, indeed, the transition observed belongs to the DP universality class (due to the different dynamics). An explanation for this small puzzle can be given. The deterministic part of the Langevin equation one would write at hand to describe reaction-diffusion processes 2.19 writes,

$$\partial_t \phi = a\phi^3 - b\phi^2, \quad (2.20)$$

the first term on the right-hand-side is the contribution of the creation process and the second term is the annihilation. Actually, this is not as easy since, rigorously deriving Langevin equation involving 3 or more particles, encounter upon technical problems, it needs for calculating integrals that are not gaussians. At mean-field level, the transition is expected to occur when $a = 0$ and $\phi = b/a$ is the solution. This implies the transition to be first-order, from $b/a \xrightarrow{a \rightarrow 0} \infty$ to 0. However, there exist reasons to believe that first-order transitions of system with absorbing state do not occur [19], so can be expected to be DP like.

As shown, very briefly here, the technical problems encountered upon deriving systematically a Langevin equation or a field theory from a microscopic model, and the information we can obtain from a heuristic proposal are two good motivations to use physically intuitive continuous effective descriptions.

2.6 Conclusion

The Langevin equation we proposed Eq. (2.4) seems to be a good description of phase transitions with two symmetric absorbing states. It describes the rich phenomenology of order-disorder transitions of microscopic models with two symmetric absorbing states [2, 5, 6, 12, 13, 14, 15].

It shows that, in two space dimensions, systems involving two symmetric absorbing states either undergo a GV transition or a symmetry breaking, Ising, transition followed by an absorbing phase transition into the favored absorbing state belonging to DP universality classe. Which scenario appears depends on, whether or not the potential term allows for bulk noise. If we impose a ϕ^4 shaped potential, we observe an Ising transition, since the absorbing states are unstable against perturbations, they are dynamically unreachable by an infinite system.

In one space dimension, we obtain evidence that what matters in capturing the critical behavior is the presence of two symmetric absorbing states. Here, contrarily to the two dimensional case, general theorems imply that no potential can possibly induce a symmetry breaking transition. The transition we observe is shown to belong to a universality class known from microscopic models of reaction diffusion particles with reactions conserving parity and involving only one particle for creation. In the absorbing phase of such model, the system asymptotically behaves as pure annihilation. Consequently, we also obtained a way of generating the annihilation process $2A \rightarrow \emptyset$, without the need of imaginary noise which is very difficult (see [20] and chapter 6). Since studying and interpreting imaginary noise Langevin equations is difficult, this is promising for future work on reaction-diffusion systems.

The mean-field study we presented comforts our numerical results and our phase-diagram. This work clarified some points that remained obscure from the interpretation of microscopic models into two absorbing states and opened the possibility for further analytical work [21].

In the second part of this chapter, we have shown what are the limitation of the GV universality class. Magnetization conservation is not necessary but only asymptotic magnetization conservation.

Chapter 3

Nonequilibrium wetting phenomena

3.1 Introduction and motivation

Historically, the study of wetting transitions began thanks to previous research on contact angles. For example, a liquid droplet in contact with a solid surface and, at coexistence with a vapor phase (see Fig. 3.1) involves three interfaces, and therefore three surface tensions need to be considered. This problem was solved in the nineteenth century by the innovative Young who found the now well-known relation,

$$\sigma_{wv} = \sigma_{wl} + \sigma_{lv} \cos(\theta), \quad (3.1)$$

called the Young-Dupré law. Here, θ is the contact angle of the wall-liquid interface with the vapor-liquid interface. σ is the surface tension - that is the energy per unit surface of the interface between two different phases - where subindices w, v and l stand for wall, vapor and liquid, respectively. Therefore, σ_{wl} is the surface tension associated to the wall-liquid interface. Knowing the 3 surface tensions, one can predict the contact angle, θ . It was only in 1977 that, in a seminal paper, Cahn realized such systems must undergo a wetting phase transition [22]. In one phase, the contact angle is very small, the solid is wet by the liquid (wet phase) and in the other phase the contact angle is almost 180 the solid is said to be dry (dry phase).

Changing from one situation to the other consists in a wetting phase transition. Cahn's argument is very simple and only uses the Young-Dupré

relationship and the knowledge of some 'bulk' critical exponents of fluids. We know that,

$$\sigma_{wv} - \sigma_{wl} \leq \sigma_{lv}, \quad (3.2)$$

where, in general, both sides approach 0 close to the critical point. The liquid/vapor surface tension behaves as

$$\sigma_{lv} \sim |T_c - T|^{2\mu} = |T_c - T|^{1.3}, \quad (3.3)$$

where μ (or ν ?) is the critical exponent of the bulk correlation length in a three-dimensional space. The left hand side of Eq. (3.2) is governed by a different smaller exponent, which implies the occurrence of a transition. Cahn argued that the surface tension difference behaves as the density difference,

$$\sigma_{wv} - \sigma_{wl} \sim \rho_l - \rho_v \sim |T_c - T|^\beta = |T_c - T|^{0.8}, \quad (3.4)$$

with β the *surface* critical exponent (this is a standard notation for equilibrium wetting and should not be confused with. This assumption has been proved to present exceptions but critical points usually appear for $T \rightarrow T_c$ so we follow this reasoning here. Since $\beta < 2\mu$, as the critical point is approached, inequality (3.4) becomes an equality and the wall is completely covered by the liquid : this is called complete wetting. Subsequently in the 80's, experimental and theoretical work on wetting, lead to a good understanding of this field. It was only in the middle of the 90's, when their nonequilibrium counterpart was studied. In this chapter, we will try to clarify what is a nonequilibrium interface. As often, it is more easy to define the rules that an equilibrium system has to follow and, to break one of these rules, to obtain a nonequilibrium system.

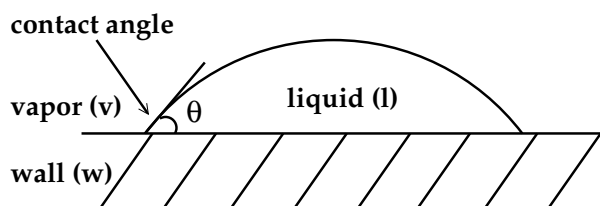


Figure 3.1: Droplet in contact with a wall. The angle between the interfaces, wall-vapor, wall-liquid and liquid-vapor depends on the respective surface-tensions.

Wetting phenomena are important in nature, they can occur in different real situations involving a lubricant, a paint or an ink. A porous media

absorbs a liquid because its surface tends to be wet by the liquid. In an experimental setup, the situation of interest occurs when a fluid presents two phases separated by an interface, one phase being favoured by the presence of a wall. The interface can be described by defining, the bulk dynamics and, the interaction with the substrate of the two phases. Another way to study the interface is to define a suitable effective interface dynamics. This interface dynamics is sometime derivable from the bulk dynamics but we will not linger much on this point. Thanks to universality concepts, we need not worry too much about the difficult task of deriving exactly (eventhough it would be very interesting) our effective interfacial description.

Studies of wetting problems at equilibrium, started more than 20 years ago, experiments (see [23], for a recent review) and theory (for a pedagogical review, see [24], [51]) show two complementary facets. The knowledge of theoretical results at equilibrium is a fundamental basis in order to tackle nonequilibrium problems. The study of nonequilibrium wetting (sometime called depinning, since it is the transition from a pinned state of the interface to a depinned phase) is richer than the equilibrium case and was undertaken for the first time only some 10 years ago [25]. Nonequilibrium situations encompass richer phenomenology, since there are fewer constraints on the system, in particular on the rules of the microscopic dynamics. However, a large gap persists in this research field, consisting of the absence of experimental evidence. Nonequilibrium interfaces have been observed and quantitative measurements have been performed, allowing to compare harmoniously experiments with theory. On the reverse, the theoretical situation of a nonequilibrium interface depinning from a substrate *has not yet been experimentally quantified*. This remains as a very important task to be undertaken. This is not the only case of important theoretical studies about nonequilibrium phase transitions lacking of experimental evidences, another prominent one is the well established (at least theoretically) *Directed Percolation* [2, 26]. One of the reasons why the experimental study of depinning processes could be very important is that they could be related to the experimentally elusive DP (see chapter 4).

This facts lead people to study more realistic models in the field of depinning transitions, as the work of [27] which includes details of the diffusion process and show that the nature of the transition is not altered by such details. As expected, and necessary for experimental successes, adding some details to the models do not alter universality class. Part of this work (chapter 4) is focused on this same point, in the sense that it shows the generatlity,

and robustness of the studied transition with respect to the interaction potential. As a side point, this *suggests a way to measure DP exponents*. In this case, we show that the system also present some insensibility to a certain type and strength of spatial quenched noise. Other models exhibiting DP transition, in particular, the most paradigmatic model one, the *Contact process* are known to exhibit a strong dependence on the presence of quenched noise [28, 29]XXX +Janssen XXX. As Hooyberghs et al. [28] showed with analytical tools and Vojta et al. [29] confirmed by Monte-Carlo simulations, the presence of quenched noise leads to a strong disorder fixed point. The presence of noise is likely to be one of the reasons why it has been so difficult to observe the DP transition in experimental systems. We stress that there are possibilities to believe that depinning under nonequilibrium conditions could lead to observe DP for the first time. Even if this does not work, it would be an interesting experiment. Another interesting point is that in this work we show two different universality classes, named 'MN1' and 'MN2', that are irrelevant to quenched noise is irrelevant (under some restriction to precise later) and as said before, fluctuations in the potential intensity do not destroy the absorbing state. We hope that experimental work will soon confirm these experimental predictions.

In this chapter, we start with microscopic models describing free interfaces, both equilibrium and nonequilibrium like. Afterwards, we turn to the equivalent interfacial continuous descriptions, Edwards-Wilkinson(EW) [30] and Kardar-Parisi-Zhang(KPZ) [63] of free interfaces. Eventhough this seminal piece is by now twenty years old, the complete elucidation of the behavior of the KPZ equation is still a debated subject : (i) the existence of strong coupling fixed point invalid perturbative approaches, (ii) the upper critical dimension, above which mean-field results are valid, is not determined.

Once concepts necessary are settled, we give an introduction to equilibrium wetting and to nonequilibrium depinning, showing the features they have in common and their differences. Our focus is on models undergoing these transitions, on how equilibrium models are designed and on how to define their extension to the nonequilibrium case. For microscopic models a simple way is to break detailed balance [34], while in a continuous description, we need to introduce the KPZ non-linearity. Such a continuous description is difficult to study due to the instabilities present in the KPZ equation and has not been thoroughly investigated. We present known results for nonequilibrium wetting transitions and explain how they are partially incomplete. Our work is aimed at filling this gap. The particular case on which we have

focused deals with an interface with positive nonlinearity and a “lower wall” suppressing negative values of the interface. We are able to perform *mean-field* calculations predicting the phase diagram and show numerical results in agreement with previous results known for microscopic models. The detailed study we performed of continuous descriptions of nonequilibrium depinning transition improves understanding of the problem and open new gates to tackle theoretically this problem.

3.2 Free interface: microscopic description

Since the celebrated Ising model has been solved, it is a widespread belief that lattice models are useful in understanding critical phenomena [?]. This is the reason why we start by presenting microscopic models which indeed were very useful in understanding interface growth at and out of equilibrium [34].

3.2.1 Equilibrium

We refer here to the simplest case of interface, separating two bulk phases co-existing at equilibrium. At equilibrium means that one phase is not growing at the expense of the other. This situation can be encountered in magnetic systems: an experimental situation would consist in a magnetic system with two different magnetizations imposed at the opposite boundaries of the system. Below the Curie temperature, there is a well-defined interface separating the opposite boundaries. An equivalent theoretical example could be an Ising model, with a non-conserved dynamics, and opposite magnetization at two opposite open boundary conditions. Below the critical temperature, a well defined interface between + and – spins takes form. This interface is well described by the Edwards-Wilkinson theory. Turning on a small external magnetic field sets the interface in motion and conduct to a nonequilibrium situation. This is described in the next section and the useful theory here is KPZ. In this case, care needs to be taken in order to avoid effects of nucleation in the unstable phase. In the time scale where no nucleation is present, the behavior of the interface is well described by a KPZ equation (an alternative is to turn on the field only in the vicinity of the interface). Alternatively, two immiscible fluids would also have an equilibrium interface separating them.

Random deposition with surface relaxation

The first model we describe in a few words is the random model. Particles fall vertically, and sequentially at a random position. A particle sticks on top of the substrate or of the first particle on the column under it. So that the heights of the different columns are not correlated. A column near a very high or a very low column has the same probability of being high or low. This means that the height in one column do not influence the height in a neighboring one. To modify this particular trait and, introduce correlations, surface relaxation is a sufficient mechanism. Including relaxation in the model modify very much the shape of the interface. In random deposition with surface relaxation, a particle deposited on top of a column do not stick directly but look first if a neighboring column is lower, in which case, it relax to this column. Compared to the previous case, a column next to a very high column has a higher growth rate since particle falling on the very high column relax onto the lower neighbors. In other words, the rate of growth somehow depends on the height of the neighboring columns. This mechanism obviously creates spatial correlations that develop as the system evolves in time. If the system is small as in numerical simulation runned long enough, it will reach a point when correlation extend over the entire system and, measured quantities saturate. This phenomena is what allows to measure χ , the exponent governing the saturation of the roughness due to system size. The height and the roughness of an interface can be defined as,

$$\bar{h}(t) \equiv \frac{1}{L} \sum_{i=1}^L h(i, t), \quad (3.5)$$

$$w(L, t) \equiv \sqrt{\frac{1}{L} \sum_{i=1}^L [h(i, t) - \bar{h}(t)]^2}. \quad (3.6)$$

The random deposition with surface relaxation illustrated in Fig. 3.2 can be studied numerically. The interface asymptotic properties can be characterized by a few parameters, the dynamic roughness exponent β_W defined by $w(L, t) = t^{\beta_W}$ and the stationary roughness exponent given by the relation, $w(L, t) = L^\chi$. Simulations in one dimension of the model sketched in Fig. 3.2 showed that the exponents have values compatible with $\beta_W = 1/4$ and, $\chi = 1/2$ [35]. These are the values predicted by the theory associated to this growth process. In order to find a good theory, the guide to follow

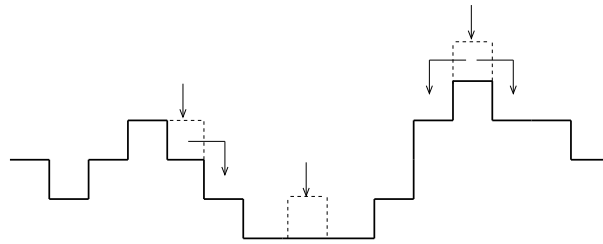


Figure 3.2: Random deposition with surface relaxation. Before sticking definitively, deposited particles can relax to a nearest neighbor if this has a lower height.

is, to consider symmetry principles and to write the simplest possible theory compatible with the symmetries of the problem. It is one of the central point of this thesis to illustrate that this is a method is very often succesful. At equilibrium, fluctuation-dissipation relation makes it is often easy.

Nonequilibrium

Out-of-equilibrium, fluctuation-dissipation relations are generically absent (KPZ equation is a rather exceptional case) and correlations are more difficult to guess, they sometime can be computed, but it is usually very hard. In avoiding this very hard step, eventhough the problem under study do not accept fluctuation-dissipation relations, phenomenologically inspired guesses can be of good help. This is a reason why, it becomes a more difficult task. In order to test prediction, numerical methods, especially when they are fast, are very useful to descriminate between possible candidates. As presented in [36], it is easy to modify this model to obtain different universality classe. For instance if we suppress surface relaxation we obtain a different model without correlations so the roughness does not saturate and $\beta_W = 1/2$, each site performs a random walk about the average height and, $\chi = \infty$, due to the absence of saturation. If instead, we suppress surface relaxation, and make falling particle to stick to the first nearest neighbor they find in their fall, we obtain $\beta_W = 1/3$, $\chi = 1/2$. This last case is characteristic of the well-known Kardar-Parisi-Zhang nonequilibrium interface. In the rest of this chapter and, in the following one, we review different models designed as growth processes of this type of interfaces. And try to clarify what governs their growth dynamic.

3.3 Bounded interface microscopic description

Microscopic interface description were the first attempts at treating the problem of nonequilibrium wetting. Numerical studies as well as analytic approaches based on those models have improved the understanding of depinning transitions. Effective continuous descriptions were also able to describe these transitions properly. In general, continuous descriptions are more amenable to analytic approaches. In reference [34], a restricted solid-on-solid (RSOS) model is studied. The term solid-on-solid means that overhangs are not allowed, i.e., the surface is perfectly single valued. The model is defined on a one-dimensional with N sites and periodic boundary conditions. To each site of the lattice is associated an integer value h_i being the height of the interface at site i . h_i is restricted to positive values. The term restricted implies the condition $|h_{i\pm 1} - h_i| \leq 1$, this introduces an effective surface tension. Four processes are the basic ingredients of this model:

1. Deposition on the substrate $h_i = 0 \rightarrow h_i = 1$, with rate q_0 .
2. Deposition on the interface (on top of already deposited atoms) $h_i \rightarrow h_i + 1$ if $h_i \geq 1$, with rate q .
3. Evaporation of an atom at the edge of a terrace. This is often implemented by applying the rule $h_i \rightarrow \min(h_{i-1}, h_i, h_{i+1})$ with rate 1.
4. Evaporation of an atom in a plateau, $h_i \rightarrow h_i - 1$ if $h_{i-1} = h_i = h_{i+1} \geq 1$ with rate p .

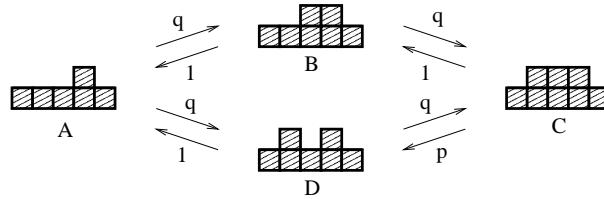


Figure 3.3: This shows how the rate are implemented on a closed cycle and provide a simple representation of the detailed balance requirement. As explained in [34], detailed balance is fulfilled if and only if, $p = 1$. Clockwise and anti-clockwise cycles both have the same probability (in a given time dt , it is $q^2 dt^4$ and $pq^2 dt^4$) to occur. Reversibility is only achieved if $p = 1$ (taken from [34]).

3.3.1 Equilibrium $p = 1$

We briefly describe the phenomenology of equilibrium wetting phase transitions. The discrete model we just described with $p = 1$ (between others), and the continuous Edwards Wilkinson equation [30] with short-ranged interactions (to be presented in the next section) both show an equilibrium wetting phase transition. These are two very different models, one is continuous and the other is discrete, both belonging to the same universality class (presenting the same phase transition, characterized by the same exponents). Langevin descriptions have other very interesting particularities. They are in principle derivable from all equivalent discrete models. It is a very difficult task in general and only a few derivations exist. In this sense, all those models can be thought as equivalent and the most representative one is the Langevin representation, equivalent to a field theory. After the field theory has been established, the possibility to use the machinery of field theory to obtain analytic predictions on the behavior of the system is very useful. Another particularity making Langevin representations an interesting object in studying universality issues is, the fact that the symmetries of the problem in Langevin descriptions are usually more transparent than in discrete models. This allows one to classify transitions into classes with the general criterion of symmetries that apply so well at equilibrium.

Hard-core repulsion : $q = q_0$

The substrate has no interactions with the wetting layer, it is neither repulsive, neither attractive. This problem is exactly soluble in the case $p = 1$ (see Fig. 3.3). Detailed balance is verified, we are in an equilibrium situation in which we can apply a hamiltonian distribution and work out the Gibbs distribution describing the system. This corresponds to a critical wetting transition, path (3) in Fig. 3.4.

Repulsive wall : $q \leq q_0$

In experiments of wetting, usually, the contact energy of the two fluid phases with the wall are unequal, resulting in an attraction or a repulsion of the interface and the wall. This can be seen as an interaction term between the interface and the substrate. The interaction is usually short-ranged though not always. In the RSOS model presented here, to model short-ranged interactions between the substrate and the interface we can simply modify the

value of q_0 . If $q_0 > q$, the substrate is repulsive and if $q_0 < q$, the substrate is attractive. As long as $p = 1$, we obtain an equilibrium wetting transition as q is changed, as a control parameter. For $q > q_c = 1$ (not always critical), we obtain a moving phase and for $q < q_c = 1$, a bounded phase. When $q \leq q_0$, the interface is repulsive, this corresponds, in Fig. 3.4, to a complete wetting transition, path (1). Along path (1), when getting closer to the moving phase, the average distance between the interface and the substrate diverges with the correlation lengths.

Attractive wall : $q > q_0$

If $q \geq q_0$, the interface is attractive, this corresponds, in Fig. 3.4, to a discontinuous transition, path (2). For this last case, in the bound phase, the interface is at a typical distance from the substrate, the small corresponding correlation length and jump discontinuously to ∞ when the moving phase is reached.

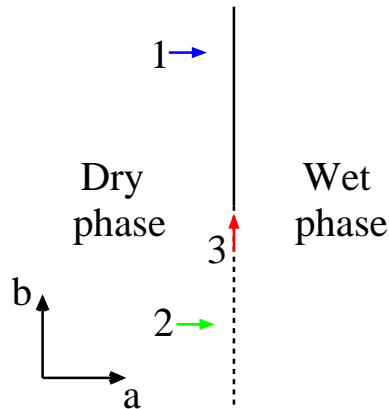


Figure 3.4: Phase diagram for the equilibrium wetting transition. Horizontal axis is the chemical potential difference, vertical axis describes the character attractive or repulsive of the substrate. The bigger b the more repulsive, and the smaller, the more attractive. For $b > 0$ the interface is purely repulsive and for $b < 0$ it is attractive. In $a = 0$ is the transition point between a dry and a wet phase. In $a = b = 0$ is the critical wetting point. Path (1) is the complete wetting transition, (2) is a first order transition and (3) is the critical wetting.(to compare to the nonequilibrium diagram)

3.3.2 Nonequilibrium $p \neq 1$

In this case, it was pointed out in [34], that this model does not obey detailed balance and therefore, can not be at equilibrium, the correct Langevin description is forcefully nonequilibrium like. Here, as before, when $q > q_c \neq 1$, for a given q_c , the interface starts to move to infinity and, as $q < q_c$ it remains bounded.

As it is the case for the equilibrium models, many different microscopic models show the same transition. The equivalent effective Langevin description is given by the Kardar-Parisi-Zhang (KPZ) equation presented below. Someone used to this kind of models can guess that when $p < 1$, ($q_c < 1$) the interface forms cusps pointing down so the KPZ nonlinearity of the interface is positive (equivalently a tilted interface grows faster). On the other hand, when $p > 1$, ($q_c > 1$) the interface forms cusps pointing up so that the KPZ nonlinearity is negative (tilted interfaces grow slower).

- **a. $p > 1$ and $q_o > q$**

In this case, the phase diagram is very interesting. For the repulsive case, the transition is continuous (as for the equilibrium case). It is to remark that $q_c > 1$ to equilibrate for $p > 1$.

- **b. $p > 1$ and $q_o < q$**

For a strong enough attraction, it becomes a finite discontinuous jump (pre-wetting line) followed by another continuous transition showed to belong to the DP universality class. These value of parameter also allow for phase coexistence to be observed, for a wide range of parameters, a typically nonequilibrium feature [54].

- **c. $p < 1$ and $q_o > q$**

In the same way as in (a), the transition is continuous, with different critical exponents.

- **d.** $p < 1$ and $q_o > q$

This last case is different, for the transition is simply discontinuous. There is no mechanism to make it continuous.

3.4 Free interface Langevin description

In the two following short sections, we make a short review of known results for the Langevin descriptions of equilibrium and non-equilibrium interfaces. For the equilibrium case, we focus on the Edwards-Wilkinson theory given by Eq. (3.9), for the nonequilibrium case, there are several possible theories describing interfaces, either with conservation law, or without any. We also describe the simplest extension of the Edwards-Wilkinson to nonequilibrium which is the Kardar-Parisi-Zhang.

3.4.1 Equilibrium: Edwards-Wilkinson

There are several approaches to study the interface between two different phases. One is to write a full description of a two-phase system, including bulk and interfaces of the system. Another possibility is to consider the interface dynamics alone, this dynamics depends on the nature of the forces between particles in the two phases. Typically, in an equilibrium system, there is a hamiltonian describing these interactions and, a different hamiltonian describing the interface dynamics. Such a hamiltonian describing the interface dynamics is described below. Deriving the interface hamiltonian from the bulk hamiltonian is often a very hard task [32]. The other possibility is to make a phenomenological description of the interface. In order to do that, it is necessary to consider the symmetries at play in the problem, and find the simplest possible theory compatible with these symmetries. This allows for a number of simplifications at the expense of having parameters whose values are not related to measurable bulk properties of the homogeneous system. However, as is generally the case, the effective model usually allows one to experimentally access measurable quantities and to adjust the parameters of this effective description according to the measurable quantities. In any case, the universal quantities that interest us in this work are not sensitive to the particular values we take for the parameters.

Equilibrium interface description can be derived from a potential. The

important ingredients to take into account are, the differences of chemical potential, the surface tension and an additive noise taking into account fluctuations. The resulting potential including these effects is then given by,

$$V(h) = \int a h(r, t) + \nabla^2 h(r, t). \quad (3.7)$$

The prototypic equilibrium reasoning is that if a configuration of $h(r, t)$ is close to a minimum of the potential, its rate of variation is small. The bigger is the functional derivative, the faster is the evolution of the system in the direction of the closest minimum. Therefore, the functional derivative of $V(h)$ has to be proportional to $-\frac{\partial h}{\partial t}$. However, even for a local minimum, the system undergoes fluctuations able to make it evolve towards a more stable minimum. This fluctuation effect is taken into account introducing an additive (additive means that the noise amplitude is independent of the state of the system) noise term. This gives the Edwards-Wilkinson (EW) equation [30],

$$\frac{\partial h(r, t)}{\partial t} = -\frac{\partial V(h)}{\partial h} + \sigma \eta(r, t) \quad (3.8)$$

$$\frac{\partial h(r, t)}{\partial t} = a + \nabla^2 h(r, t) + \sigma \eta(r, t). \quad (3.9)$$

This equation is linear, passing to Fourier space, one can easily obtain the exponents governing this kind of growth processes [59]. It gives, a dynamic roughness exponent β_W governing the time evolution of the spatial interface variance $\sqrt{\langle (h(r, t) - \langle h(r, t) \rangle_r)^2 \rangle_r} = t^{\beta_W=0.25}$ (where $\langle \rangle_r$ stands for spatial average). As will be seen later, in order to describe the wetting transition of an equilibrium interface we only need to add a potential term $V(h) = \frac{b}{p} e^{-ph} + \frac{c}{q} e^{-qh}$, short-ranged or $V(h) = \frac{b}{ph^p} + \frac{c}{qh^q}$, long-ranged. In the following, $b < 0$ is called attractive because it contributes in an attractive component and $b > 0$ is called repulsive or purely repulsive, ($p < q$, always, to account for strong hard-core repulsion).

3.4.2 Nonequilibrium: Kardar-Parisi-Zhang

Surface growth processes observed in solids are genuinely irreversible processes so it would be interesting to modify the previous description adding some irreversible ingredient. An easy way to have a nonequilibrium model is to include a new term which breaks the up-down symmetry in the previously presented (EW) [63]. Often, as was explained for DP in chapter 2 ,

the equivalence of the different spatial directions is a necessary condition in order to be in equilibrium. Isotropic percolation is an equilibrium problem, but if the percolation process is directed, one direction is favoured compared to the others and the system is then out-of-equilibrium. A series of terms modifying the behavior of the (EW) equation are possible, the lowest order one, not deriving from a potential is $(\nabla h(r, t))^2$. This term can also be seen as the first order contribution of a local velocity perpendicular to the surface (FIG) (as if one phase was set on fire and the other one was being consumed). In this sense also, we are again supposing a given phase is favored compared to the other and this is indeed a nonequilibrium situation. The celebrated KPZ equation writes,

$$\frac{\partial h}{\partial t} = \nu \nabla^2 h + \frac{\lambda}{2} (\nabla h)^2 + \sigma \eta. \quad (3.10)$$

The first term on the right-hand side is a relaxation term coming from a surface tension ν . In an experiment, this takes into account evaporation/absorption phenomena of the vapor phase surrounding the solid. The second term is the lowest-order nonlinear term that can be included in the growth of an interface. In the case of a growth in a direction locally normal to the interface, this is the first-order of the projection along the h axis of this growth. Higher order terms could be included but no new effects are expected. The last term is a gaussian white noise reflecting the stochastic behavior of effective descriptions.

In this case, the equation is no longer linear and cannot be solved through the same methods as for the EW equation. The nonlinearity couples different modes and renders the problem intractable analytically. However, in one spatial dimension, the lucky existence of a fluctuation dissipation theorem (unexpected for nonequilibrium systems) allows one to find exactly the exponents. For KPZ in one dimension, $\beta_W = \frac{1}{3}$. The new term increases the roughness of the interface compared to EW, and goes against the smoothing effect of the diffusion term. This interface is not symmetric under up-down reversal so that the introduction of an impenetrable wall above the interface or below it lead to two different physical pictures (ref MA-Grinstein).

As said in the introduction of this chapter, the interesting KPZ description is not fully understood. This constitutes a motivation to study related problems and hopefully to gain intuition on it. The problem of a KPZ interface with a wall is presented in the following sections.

3.5 Langevin description of nonequilibrium interface depinning 47

KPZ: a mapping to *Multiplicative noise*

The problem of a KPZ interface, Eq. (3.10), can be mapped onto a *Multiplicative noise* (MN) equation, Eq. (3.11), changing of variable $h(x, t) = (2\nu/\lambda) \ln(n(x, t))$ in Eq. (3.10) we are left with,

$$\partial_t n = \nabla^2 n + n\sigma\eta. \quad (3.11)$$

ν is always taken positive but λ can be either positive or negative. Even though it appears innocuous here, it is important to note that in this condensed way of writing the mapping, is hidden that the change of variable is quite different according to the sign of λ . To follow the rest of the work presented here, it is important to notice that as soon as a wall is present, the change of variable we choose makes a big difference. Equation 3.11 describes the problem of *Directed polymer in random media*.

Another interesting change of variable is $\phi(x, t) = \nabla h(x, t)$, this gives,

$$\frac{d\phi}{dt} = \partial_t \phi + \phi \nabla \phi, \quad (3.12)$$

this is the *Noisy Burgers equation of turbulence*.

For additive noises, the smaller the noise amplitude the more ordered systems are. This appears very natural but actually it is not always the case. For multiplicative (the correlator involves the square of the field) and RFT (the correlator involves the field only) noises, when noise amplitudes increases the system becomes more ordered. This is somehow surprising and can lead to new interesting phenomena.

3.5 Langevin description of nonequilibrium interface depinning

After having introduced the problem we focus on and related important results, we turn to the description of the work we have realized and of the obtained results. In Sec. 3.3, we describe a microscopic model giving a useful description of nonequilibrium depinning. As said in [34] and above in 3.3.2, the results obtained for the microscopic model, for $p > 1$ and $p < 1$, is equivalent to a KPZ interface interacting with a wall and different signs of nonlinearity. Here we present what??

3.5.1 Multiplicative Noise 1

In this section, we review the case of a KPZ interface with a lower wall and a negative non-linearity (λ in the following). This has already been profusely studied [38, 42, 43, 44, 45]. A convenient introduction of the known results allows to understand better the results obtained in the case of a lower wall and a positive λ . The KPZ equation has been shortly introduced in Sec. 3.4.2. We now modify it in order to include terms accounting for the wall-interface interaction. The interaction we choose derives from the potential,

$$V(h) = -ah + \frac{b}{p} \exp(-ph) + \frac{c}{q} \exp(-qh), \quad (3.13)$$

shown in Fig. 3.5. Parameters are, $q > p$, c is always kept positive for stability purposes. It is a strongly repulsive lower wall at very short distances. If b is negative, the potential is attractive at intermediate distances, and purely repulsive if b is positive.

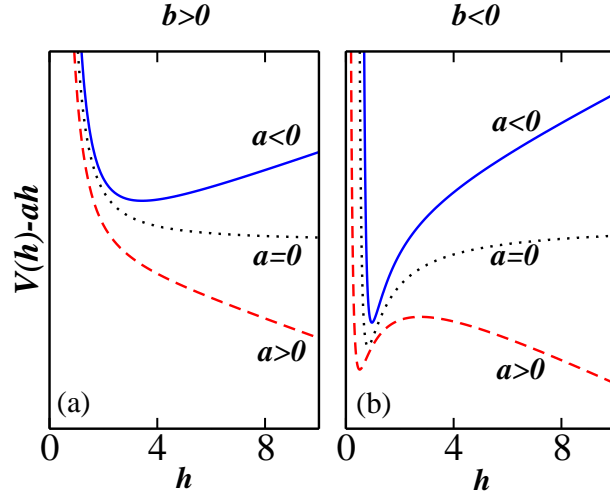


Figure 3.5: Effective potentials derived from Eq. (3.13) in the pinned ($a < 0$) and the depinned ($a > 0$) phases, and at coexistence ($a = 0$). (a) repulsive walls ($b, c > 0$); (b) attractive walls ($b < 0, c > 0$).

The modified KPZ equation with short-ranged interaction is written below,

$$\partial_t h = \nabla^2 h + \lambda(\nabla h)^2 + a + b \exp(-ph) + c \exp(-qh) + \sigma \eta. \quad (3.14)$$

3.5 Langevin description of nonequilibrium interface depinning 49

According to the value of a , the interface average distance from the wall, $\langle h \rangle$, remains finite or grows indefinitely. Separating this two regimes, the equation has a critical point, for which power-law are observed. We can argue that when h goes to infinity, the wall is not felt by the interface, taking spatial averages on both sides of $\langle h \rangle$. Performing in Eq. 4.8 a Cole-Hopf transformation, $n(x, t) = \exp(-h)$, one obtains, if $\lambda = -1$ (without loss of generality),

$$\frac{\partial n(r, t)}{\partial t} = \nabla^2 n(r, t) + an(r, t) - bn(r, t)^{1+q} + \sigma n(r, t)\eta(r, t), \quad (3.15)$$

it bears the name of *Multiplicative Noise 1*.

3.5.2 Multiplicative Noise 2

As said before, in the KPZ equation, the up/down symmetry is broken, therefore inverting the sign of λ and keeping a lower wall, lead to probe a different side of the interface on the wall, naturally leading to a different critical phenomena.

If contrarily to the case presented above $\lambda = +1$, after the mapping $\bar{m}(x, t) = \exp(-h)$, the MN equation resulting is:

$$\frac{\partial m(r, t)}{\partial t} = \nabla^2 m - 2 \frac{(\nabla m)^2}{m} - am - bm^{1-q} + \sigma m\eta(r, t). \quad (3.16)$$

So in the presence of a “lower wall” and a positive nonlinearity, a more convenient change of variable is, $n = \exp(h)$, leading to,

$$\frac{\partial n(r, t)}{\partial t} = D\nabla^2 n + an + bn^{1-q} + \sigma n\eta(r, t), \quad (3.17)$$

now the order parameter we are interested in is not anymore the average of the stochastic variable but $\langle \frac{1}{n} \rangle$. This is the new variable that tells us the number of contact points between the interface and the wall. The main result of this chapter is to show that this equation constitutes a sound description of the depinning transition, and that all the relevant information is included in it [39]. From now on, Eq. (4.10) is referred to as MN2 equation.

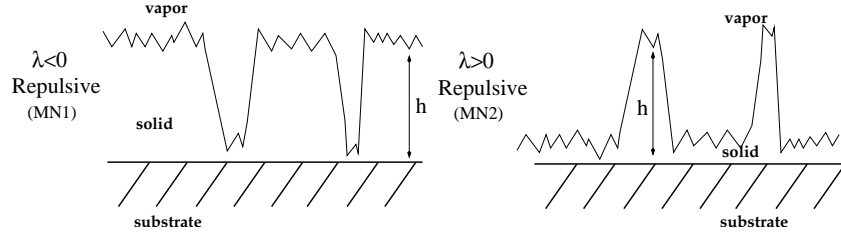


Figure 3.6: Representative sketches of the “solid-vapor” interface for repulsive interaction and a lower wall. Left: in the case of MN1 ($\lambda < 0$) and MN2 ($\lambda > 0$) universality classes. Flat pieces of the interface are subjected to an effective repulsion (attraction) from the substrate in the case of MN1 (MN2). Here we see the definition of h and n variables. h is the interface-substrate wall distance and n is a variable which is 1 when the interface is in contact with the substrate and 0 otherwise

Tails or tales

A different way to see that positive and negative nonlinearity give rise to different transitions is the following. We present an argument similar to the one presented in [46] even if we do not have a way of computing the probability distribution of h . We only suppose that the interface follows the Family-Vicsek scaling [47], and particularize it to a stretched exponential as standard KPZ tails.

$$P(h, t) \sim t^{-\gamma} f\left(\frac{h - \langle h \rangle}{t^\gamma}\right) \quad (3.18)$$

The order parameter we have defined is the number of pinned sites. Supposing we know $P(h, t)$, this can be evaluated integrating from the barrier to an arbitrary small h_0 .

$$\rho_t = \int_0^{h_0} dh P(h, t) \quad (3.19)$$

We perform the change of variables $z = \frac{h - \langle h \rangle}{t^\gamma}$, $dz = \frac{dh}{t^\gamma}$ we are left with,

$$\rho_t = \int_{-\frac{\langle h \rangle}{t^\gamma}}^{-\frac{\langle h \rangle}{t^\gamma} + \frac{h_0}{t^\gamma}} dz f(z). \quad (3.20)$$

Now suppose we have $\frac{\langle h \rangle}{t^\gamma} \rightarrow C$ and $f(-C) \neq 0$, then in the asymptotic limit we obtain,

$$\rho_t = f(-C) h_0 t^{-\gamma}. \quad (3.21)$$

3.5 Langevin description of nonequilibrium interface depinning 51

It is well known that MN1 and MN2 have different tails [46] and that the scaling functions must approach 0 in different ways since $\theta_{hMN1} \neq \theta_{hMN2} \neq \gamma$. So, if scaling holds asymptotically, we would expect the approach to be with a power respectively bigger and smaller than one.

Instead, if $\frac{\langle h \rangle}{t^\gamma} \rightarrow \infty$, then

$$\rho_t = f\left(-\frac{\langle h \rangle}{t^\gamma}\right) h_0 t^{-\gamma}, \quad (3.22)$$

which is expected to be very different from a power-law behavior. Indeed in the case of a KPZ, the tails are stretched exponential.

$$P(h, t) \sim t^{-\gamma} \exp[-\mu(|h - \langle h \rangle|/t^\gamma)^\eta] \quad (3.23)$$

Supposing this still holds we expect a stretched exponential corrected by a power-law.

$$\rho_t = \exp\left[-\mu\left(\frac{\langle h \rangle}{t^\gamma}\right)^\eta\right] h_0 t^{-\gamma}, \quad (3.24)$$

at criticality, $\frac{\langle h \rangle}{t^\gamma}$ is expected to be a power of t .

In numerical experiments, we qualitatively observe this two different behaviors. For $p \geq 1$, ρ_t exhibits a power-law behavior and we expect $\langle h \rangle = t^{1/3}$ to hold asymptotically. For $p \leq 1$ we see a clear stretched exponential. We have checked that for $p \leq 1$, $\langle h \rangle = t^{1/p+2} \gg t^{\gamma=\frac{1}{3}}$, which is all consistent.

Short discussion on quasi-absorbing states

The difference between the “quasi-absorbing” state of MN and the “true” (RFT) absorbing state is sometimes presented as coming from the integrability of the stationary distribution. For the RFT case it presents a singularity at $\phi = 0$, (independent of the phase and of the potential chosen, as long as no constant term is present). On the other hand, for MN the distribution remains integrable in the active phase with no singularity at $\phi = 0$. Here, we present a simple explanation of this fact, constituting in itself an explanation of the fundamental differences between noises ϕ^α for $\alpha = 0.5$ or $\alpha = 1$.

Starting from a typical condition ($\phi \neq 0$), in the case of $\alpha = 0.5$, it is known that after a finite time dt , the probability of reaching the absorbing state is non vanishing, let say p_1 ($(1 - p_1)$ is the probability of ϕ to be different from 0). The normalized probability density distribution is constituted by a delta pic multiplied by p_1 and a continuous function of integral

$1 - p_1$. The probability of going out from the absorbing state is always 0 by definition. So after n steps, writing p_i the probability of reaching the absorbing state in the i^{th} step, the probability to have $\phi \neq 0$ is given by, $(1 - p_0)\dots(1 - p_i)\dots(1 - p_n)$. One is easily convinced that this tends to 0. Since the stationary state is defined by averaging the system evolution from a typical initial condition over a time window going to infinity. This is a simple way to explain how the non-integrability arises. On the other hand for MN type of noise, $\alpha = 1$, in the active phase, the probability of reaching the absorbing state in any finite time is 0 and the above presented scenario do not appear. However, as was shown in [41], a multiplicative noise equation with an appropriate potential, can undergo a transition in the *directed percolation* universality class. The main reason for this is that for multiplicative noise, typically, the absorbing state is never reached so that the noise can create new activity. The authors of [41] used a potential such that, even if some small activity still exists, a small well ensures that the system does not return to full activity.

3.5.3 Mean-field results

In order to get intuition on the behavior of the solutions of Eq. (4.10) we apply mean-field tools to it. The crudest *mean-field* approach would be to remove the noise term and the laplacian. This turns out to be a very simple approximation and does not allow to get much insight into the problem. In this section, we apply a more elaborate *mean-field* approximation already applied in chapter 2 to a different Langevin equation. The features of the approximation presented here are very much the same as in chapter 2. It consists in transforming the very complicated system of N -coupled variables into a more simple system of only one variable. To do this, we suppose all sites to be equivalent, this cancels out spatial fluctuations. The trick consists in replacing in the Langevin Eq. (4.10) the laplacian term $\nabla^2 n = 1/2d \sum_j (n_j - n_i)$ coupling sites to its neighbors by $\nabla^2 n = 1/2d \sum_j (\bar{n} - n_i)$. In this way, we take into account the effects of the noise and only neglect some of the spatial information. Since this is very important, we expect to lose some information. However, we can hope to obtain a good phase diagram and the order of the transition to be predicted successfully. The starting point of our mean-field calculation is to write the self-consistency of the probability density in the stationary state:

3.5 Langevin description of nonequilibrium interface depinning 53

$$\bar{n} = \frac{\int_0^\infty dn n P(n, \bar{n})}{\int_0^\infty dn P(n, \bar{n})}. \quad (3.25)$$

The stationary probability density can be obtained from the Fokker-Planck equation equivalent to our Langevin Eq. (4.10) with the true laplacian replaced by the above mentioned approximation,

$$\frac{\partial n(r, t)}{\partial t} = D(\bar{n} - n) + an + bn^{1-q} + \sigma n \eta(r, t). \quad (3.26)$$

The Fokker-Planck equivalent is then,

$$\partial_t P(n, t) = -\partial_n((a - D)n + bn^{-q+1} + D\bar{n}) - \frac{\sigma^2}{2} n \partial_n(nP). \quad (3.27)$$

Imposing stationarity, we have,

$$\partial_t P(n, t) = 0 = -\partial_n((a - D)n + bn^{-q+1} + D\bar{n}) - \frac{\sigma^2}{2} n \partial_n(nP), \quad (3.28)$$

which admits for solution,

$$P_{sta}(n) = \frac{1}{n} \exp\left[\left(\frac{2}{\sigma^2} \int_0^n \frac{(a - D)x + bx^{-q+1} + D\bar{n}}{x^2} dx\right)\right], \quad (3.29)$$

$$P(n, \bar{n}) \propto n^{\frac{2(a-D)}{\sigma^2}-1} \exp\left\{-\frac{2b}{\sigma^2 q n^q} - \frac{2D\bar{n}}{\sigma^2 n}\right\}, \quad (3.30)$$

$$I_p(m) = \int_0^\infty dn n^p P_{sta}(n), \quad (3.31)$$

where , $n = \frac{2D}{\sigma^2 x}$.
With $\gamma = \frac{2(a-D)}{\sigma^2}$,

$$I_p(m) = \left(\frac{2D}{\sigma^2 x}\right)^{p+\gamma} \int_0^\infty dx x^{-1-p-\gamma} \exp(-mx - cx^q), \quad (3.32)$$

with $c = \frac{2b}{q\sigma^2} \left(\frac{\sigma^2}{2D}\right)^q$.

With I_p we can compute the moments we are interested in.

3.5.4 Numerics for MN2

In order to integrate equation (4.10) as efficiently as possible we have employed a recently introduced split-step scheme for the integration of Langevin equations with non-additive noise. In this, the Langevin equation under consideration is studied on a lattice and separated in two parts: the first one includes only deterministic terms and is integrated at each time-step using any standard integration scheme: Euler, Runge-Kutta, etc [75] (we choose here a simple Euler algorithm). The output of this step is used as the input to integrate (in the same discrete time interval) the second part which contains the remaining linear deterministic terms and the noise. This is done by sampling in an exact way the probability distribution function associated to this part of the equation. In the case under study (noise proportional to the field) the second step corresponds to sampling a log-normal distribution solution of $\partial_t n = an + \sigma n \eta$ ([8]).

This is in details, the way it was done:

$$dn_t = an_t dt + \sigma n_t dW_t, \quad (3.33)$$

where dW is a Wiener process. Since this is interpreted in the Stratonovich sense, we can safely perform the change of variables $Y_t = \ln n_t$ and obtain

$$dY_t = a dt + \sigma dW_t. \quad (3.34)$$

This is a drifted Brownian motion equation whose solution is:

$$Prob(Y_{t+dt} = y | Y_t = y_0) = N(y_0 + a dt, \sigma^2 dt). \quad (3.35)$$

Inverting the previous change of variable, we are left with

$$n[t + dt | n(t) = n_0] = n_0 \exp(a dt + \sigma \sqrt{dt} N(0, 1)). \quad (3.36)$$

Therefore the two-step algorithm is finally given by:

$$n_1 = n(i, t) + (b n(i, t)^{1-q} + D \nabla^2 n(i, t)) dt \quad (3.37)$$

where $\nabla^2 n(i, t) = n(i + 1, t) + n(i - 1, t) - 2n(i, t)$ and,

$$n(i, t + dt) = n_1 \exp\left(a dt + \sigma \sqrt{dt} N(0, 1)\right) \quad (3.38)$$

3.5 Langevin description of nonequilibrium interface depinning 55

where $N(0,1)$ is a Normal distribution with zero-mean and unit variance. Note that the linear part can be included in either the first or the second step, or partially incorporated in both of them.

We have considered one-dimensional lattices, and fixed $\sigma = 1$, $b = 1$, $D = 0.1$, space-mesh is $dx = 1$ and time-mesh is $dt = 0.1$. As an initial condition we take $n(r, t = 0) = 3$. We took $q = 4$ for all simulations except for results presented in Fig. 3.8(a) where we show that asymptotic results do not depend on the value of q (as long as it is positive). We then iterate by employing the previous two-step integration algorithm, consisting in first (3.37) and then (3.38), at each site i , in parallel.

First, to accurately determine the critical point, we perform decay experiments and average over many independent runs in a system of size $L = 2^{17}$. At criticality, $a_c = -0.143668(3)$, the average density, $\bar{m} = \overline{(1/n)}$ decays as a power-law, with an associated exponent $\theta \approx 0.229(5)$ (see Fig. 3.7). This is to be compared with the previous estimates $\theta \approx -0.215(15)$ [69] and $\theta \approx 0.228(5)$ [48]. On the other hand, for smaller sizes, we observe saturation at this value of a_c , and the scaling of the saturation values for different system sizes (inset Fig. 3.7(a)) gives $\beta/\nu \approx 0.335(5)$ (to be compared with 0.34(2) in [69]).

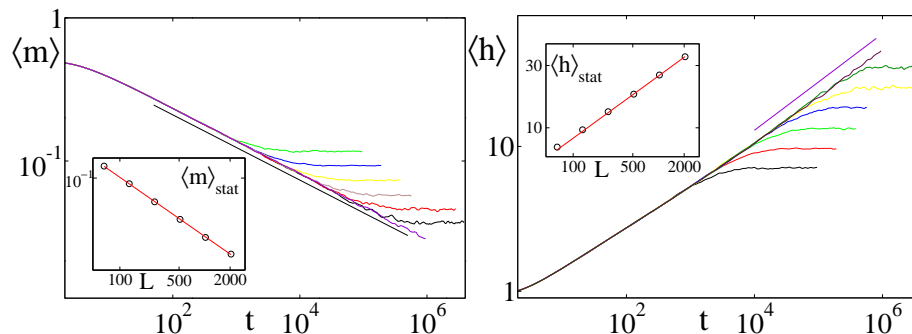


Figure 3.7: Left: Log-log plot of the time decay of the average order-parameter at the critical point, $a_c = -0.143668$, for system sizes 2^6 , 2^7 , 2^8 , 2^9 , 2^{10} , 2^{11} , and 2^{17} respectively. In the inset, the average saturation values of the previous curves are plotted as a function of the system size, L , in a log-log plot. Right: Log-log plot of the time growth of the value of $h = -\log(n)$ for the same value of a and same system sizes as before. In the inset, the average saturation values of the previous curves are plotted as a function of the system size, L , in a log-log plot.

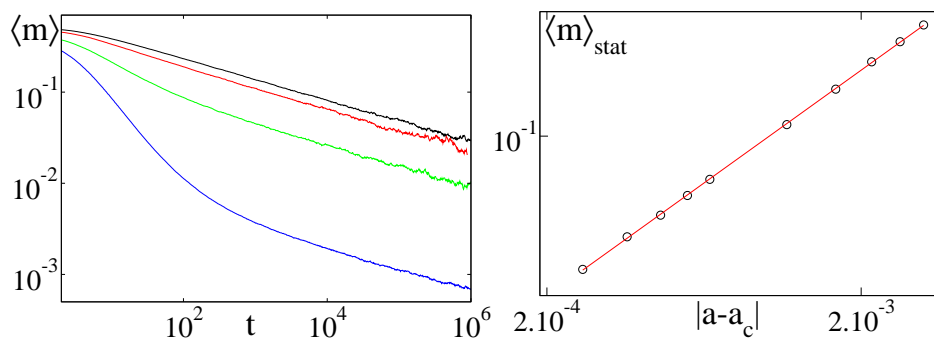


Figure 3.8: Results for $L = 2^{17}$. Left: Averaged decay experiment for equation (4.10) with $q = 0.5, 1, 2, 4$ (from top to bottom) and. For any $q > 0$ we observe the same decay exponent and the critical point location remains unchanged. Right: Log-log plot of the saturation values of \bar{m} for different values of a nearby the critical point. From the slope we estimate $\beta = 0.332(5)$.

3.5.5 Quenched noise for MN1 and MN2

The effect of quenched noise and of inevitable fluctuations is what is believed to avoid any experimental realization of the theoretically predicted nonequilibrium transitions. In this section, we investigate on the effect of quenched noise on the two absorbing phase transitions presented above, MN1 and MN2.

3.6 Experimental realizations

After the Cole-Hopf mapping of the h variable, $n = \exp(-h)$, we are left with a variable noted n . The stochastic differential equation for n was shown to be relevant in synchronisation phenomena. All our results, either *mean-field* calculation or numerical work were obtained in terms of the n variable. This naturally lead to think that an experimental realization of our results could be obtained in synchronisation phenomena. Working on such an experiment, the measurement of n would directly allows one to distinguish from MN1 and MN2 behavior. It will then be probably feasible to observe DP critical exponents. It is often quoted that Grassberger, a few years ago, placed the experimental realization of DP as one of his first priorities. However, the ubiquitous presence of fluctuations in natural systems allow to escape from the 'absorbing state'.

The phenomena we investigate in this chapter is close to the phenomena

of equilibrium wetting phase transition. For the equilibrium case, theoretical results have been obtained which later were experimentally confirmed. This gives a playground to develop both theoretical and experimental knowledge and tools. This valuable achievement might bring even more new information if it were carried out in the equivalent nonequilibrium situation.

Theoretical work showed that in any non isotropic media, the nonlinear term of the KPZ theory is perturbatively generated[50]. So in principle any non isotropic crystal growth could do. However, the nonequilibrium KPZ-like growth has been observed in experimental situations, it appears difficult to observe due long-ranged mediated interaction generating transients(cite Cuerno, others and other mechanism). Even if it is not easy to observe, so one can argue about the relevance of this growth mechanism, it was succesfully observed.

3.7 Conclusion

In this chapter, we have presented an introduction supposed to help readers to understand the problem addressed and the presented results. We have studied the dynamics of KPZ-like interfaces bounded by a lower wall. The results and phenomenology differ from that of “upper wall”. By performing a Cole-Hopf or logarithmic transformation, we have observed that the resulting order-parameter Langevin equation, equation (3.16) is singular and no sound result can be derived from it. Instead, the main result of this paper, a sound Langevin equation can be written in terms of a non-order-parameter, diverging-at-the-transition field, equation (4.10). For such an equation we have performed (i) a mean-field analysis, using a self-consistent approach, leading to the result $\beta = 1/q$, and quite strangely, there is no trace of any strong-coupling regime (noise-dependent β exponent value), contrarily to what happens for the case of “upper wall”. This is also expected because the KPZ equation presents a strong-coupling fixed-point. (ii) Extensive numerical integrations of the stochastic equation, performed employing the recently introduced very-efficient *split-step* scheme. The obtained exponent values are in good agreement with previously known ones obtained from simulations of discrete models, and improve the level of accuracy and precision. This gives a consistent representation for bounded KPZ in terms of *multiplicative noise* equations and allow for further studies using this effective description.

We have shown that an apparently ill-behaved non-order-parameter Langevin

equation constitutes a sound continuous representation of the pinning-depinning transition experienced by interfaces in the Kardar-Parisi-Zhang class under the presence of a lower bounding wall. Performing further analytical analyses, renormalization group, possibly non-perturbatively in order to investigate the strong-coupling fixed point (cite Leonie KPZ), of the presented description remains as a challenging task.

Going much further ahead the aim of this work, it is to point out that (to the best of my knowledge), no experiments attempted to reproduce the depinning of KPZ interfaces. The phase diagram, obtained from complementary past works, has a very rich phenomenology, first-order transition, DP transition [41] (never cleanly confirmed experimentally), *generic phase coexistence* only possible out-of-equilibrium, *tricritical* transition point. Taking all that into account, it would be extremely interesting to have a working experiment on nonequilibrium depinning. This lead theoretical work to explore more realistic variants of the presented model, to have convincing evidences that an experiment would not be very to dependent of the precise model we use. Since the precise shape of the interaction potential is not necessarily exponential. It can be rather power-law and slowly decaying, like van der Waals. Changing from exponential to power-law in equilibrium wetting problem is known to produce different results so it is to expect that the same might happen for the nonequilibrium problem. This is the question we will answer in the next chapter.

Chapter 4

Long ranged nonequilibrium wetting

4.1 Motivation

This chapter does not need an introduction since it is a development of the precedent chapter and the necessary introducing information have been presented in the previous chapter. However, a few important points are to notice here :

1. the generic form of interaction between particles is the van der Waals potential which decays as a power law and not as an exponential. This is interesting since experimental realizations of nonequilibrium depinning might involve effective interactions modified by many factors as screening effects and therefore, the precise form of the potential cannot be known beforehand.
2. precisising the understanding of this point would open the gate to possible ways of measuring *Directed Percolation* exponents as well as *Multiplicative Noise* absorbing transitions. Here the problem of defects, or small fluctuations, inducing activity in the middle of inactive regions is probably naturally inexistent since a point of the interface far away from the substrate needs a big fluctuation to become pinned to the substrate (however in DP, when close from the critical point, only a very small fluctuation is able to create activity in inactive regions and destroy the absorbing state).

4.2 Introduction

Spatial constraints in systems where two (or more) bulk phases coexist may lead to wetting transitions. This is the case, for example, of confined fluids where one of two coexisting equilibrium phases (the liquid, say) is in contact with a substrate with an interface separating it from the second phase (the gas) at infinity. The liquid *does not wet* the substrate if the thickness of the liquid film is finite (there is a microscopic quantity of liquid). On the other hand, the substrate is *wet* if there is a macroscopically thick liquid film on it. A wetting transition is said to occur when the substrate changes from not being wet by the liquid to being wet. Typically, two types of wetting transitions can be considered: by increasing the temperature at bulk coexistence one may find either *critical wetting* or a discontinuous transition; by varying the chemical potential while the temperature is fixed above the wetting transition temperature one finds a *complete wetting* transition, at bulk coexistence. Under equilibrium conditions, a completely analogous transition (often called drying) may occur when the substrate preferentially adsorbs the gas phase [51].

Effective interfacial potentials are useful coarse-grained models that have played a key role in understanding a large variety of equilibrium wetting problems [52, 51]. These potentials, $V(h)$, are functionals of the interfacial height (measured from the substrate), $h(\mathbf{x})$. In this framework, wetting transitions are described as the unbinding of the (say liquid-vapor) interface from the substrate, with the effective binding potential determined by the microscopic forces between the constituents of the substrate and those of the bulk phases. Typically, exponentials and power-law decaying potentials $V(h)$ have been considered for systems dominated by short-ranged and long-ranged forces, respectively.

There exist a large amount of phenomena describable in terms of equilibrium wetting, either under short-range or under long-ranged interactions, while it has only recently been recognized that non-equilibrium effects, such as anisotropies in the interface growing rules, may play a crucial role in describing some experimental situations. Within this perspective, short-ranged *non-equilibrium wetting* has been studied [53, 54], and some interesting novel phenomenology has been elucidated (see [55] for recent reviews). In particular, liquid-crystals [56], molecular-beam epitaxial systems, as *GaAs* [57], or materials exhibiting Stranski-Krastanov instabilities [58], appear to be good candidates to require a non-equilibrium wetting description. However, some

of these systems, as well as many others not enumerated, might include effective long-range substrate-interface effects as also occurs in the equilibrium case.

In this chapter, we fill this gap by providing a general and systematic theory of non-equilibrium wetting under the presence of effective long-ranged interactions. First, we briefly review the equilibrium situation to set up the theoretical framework and, afterwards, generalize it to embrace non-equilibrium situations.

In equilibrium, two types of analytical approaches are available: static studies based on the ensemble theory [51] and dynamical, stochastic approaches that allow investigating relaxational aspects. The second approach is amenable to non-equilibrium extensions and is the one we employ. Thus, consider the simple Edwards-Wilkinson dynamics [59] subject to a bounding force (i.e. the derivative of the bounding potential) [60]:

$$\partial_t h(\mathbf{x}, t) = \nabla^2 h + a - \frac{\partial V(h)}{\partial h} + \sigma \eta(\mathbf{x}, t). \quad (4.1)$$

This includes **(i)** the usual diffusion term, computed as minus the derivative of a standard surface-tension term, **(ii)** the driving force, a , related to the chemical potential difference between the two phases, **(iii)** the Gaussian white noise, $\eta(\mathbf{x}, t)$, and **(iv)** the bounding force, which may derive from a short-ranged potential

$$V(h) = \frac{b}{p} e^{-ph} + \frac{c}{q} e^{-qh}, \quad (4.2)$$

or from a long-ranged one

$$V(h) = \frac{b}{ph^p} + \frac{c}{qh^q}, \quad (4.3)$$

where, $b, c > 0$, and $p < q$ are parameters. This last form, Eq.(4.3), is known to be the correct functional form for systems where the molecules interact through van der Waals forces [61].

By varying the chemical-potential, a , one controls the average interfacial distance from the wall: small for $a < a_c$ (non-wet phase), large for $a \approx a_c$, and increasing steadily with time for $a > a_c$ (wet phase), i.e. the system exhibits an unbinding transition at $a = a_c$. The interface potentials $V(h)$ are, in all cases, harshly repulsive at small h to model the impenetrability of the substrate. The parameter b vanishes linearly with the temperature,

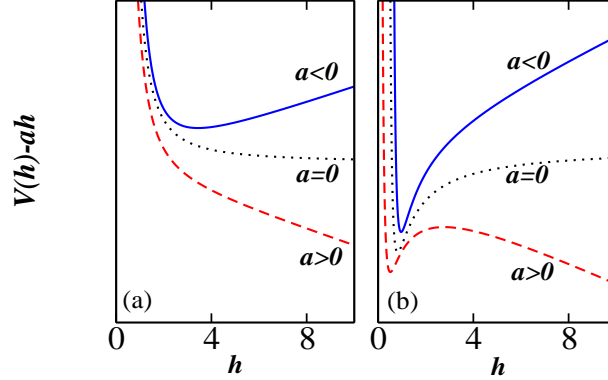


Figure 4.1: Effective potentials as derived from Eq. (4.3) in the pinned ($a < 0$) and the depinned ($a > 0$) phases, and at coexistence ($a = 0$). (a) repulsive walls ($b, c > 0$); (b) attractive walls ($b < 0, c > 0$).

at the (mean-field) critical wetting temperature, and represents the affinity or preference of the substrate for one of the bulk phases (usually the liquid). We consider three distinct situations (see Fig. 6.4):

1. *Repulsive potential: complete wetting.* If $b > 0$ the potential describes the presence of a bounding substrate alone. In this case, the broken symmetry induced by the substrate leads to the divergence of the average position of the interface, at coexistence, $a_c = 0$: i.e. the system undergoes a *complete wetting* transition.

The latter is described by Eq. (4.1) with the potential taken from Eq. (4.2). Two different regimes depending on the value of p have been reported: for $p < 2$ mean-field scaling holds and $\langle h \rangle \sim t^{1/(p+2)}$, while if $p > 2$ fluctuations take over and the velocity is controlled by the intrinsic roughness of a free Edwards-Wilkinson, leading to a fluctuation-dominated regime characterized by $\langle h \rangle \sim t^{1/4}$ (0, or logarithmic growth for two-dimensional interfaces). These results are derived in a formal way and extended in the appendix.

2. *Attractive potential: first order unbinding.* For $b < 0$, by contrast to the complete wetting case, the surface does not promote the growth of the liquid phase and consequently there is no wetting phase even at bulk coexistence, $a = 0$. $V(h)$ exhibits a local minimum near the substrate, that binds the interface in the presence of thermal fluctuations, and the width of the wetting layer is finite (microscopic) at $a = 0$. We may, however, observe a first-order

unbinding transition that occurs as a changes from positive (stable bulk liquid) to negative (stable bulk gas) values.

3. Critical wetting. At a particular value of $b = b_c$ ($b_c = 0$ in mean-field but more generally b_c is small and negative) critical wetting may be observed, with a characteristic non-trivial phenomenology. This situation requires the fine tuning of two independent parameters ($b = b_w$, $a = a_c$). This critical transition is more difficult to treat theoretically and less likely to be found in real systems and will not be discussed here.

The best way to extend equilibrium approaches to more general, non-equilibrium, situations is to consider the simplest and widely studied non-equilibrium extension of the Edwards-Wilkinson equation, i.e. the Kardar-Parisi-Zhang (KPZ) [63, 59] interfacial dynamics [64], in the presence of effective bounding potentials, as the ones we have described before. This strategy has been followed in a series of recent papers for systems with short-ranged (attractive and purely repulsive) potentials [55] and will be extended in the present work to the case of long-ranged potentials. We will discuss the phase diagrams for both purely repulsive and attractive potentials, paying special attention to criticality and to the comparison with equilibrium wetting and non-equilibrium short-ranged unbinding. We will focus on one-dimensional interfaces (separating two-dimensional bulk phases), and mention briefly two-dimensional interfaces in the conclusions.

The chapter is organized as follows. In section 2 we introduce the non-equilibrium unbinding model. In section 3, we review known results for non-equilibrium short-ranged unbinding. Section 4 contains the main results of the chapter, including both analytical and numerical results for purely repulsive and attractive potentials. Finally, the main conclusions are presented together with a discussion of our results.

4.3 Non-equilibrium long-ranged unbinding: the model

Our model consists in a KPZ non-equilibrium interface [63, 59] in the presence of a long-ranged, bounding potential Eq. (4.3),

$$\partial_t h = \nabla^2 h + \lambda(\nabla h)^2 + a + \frac{b}{h^{p+1}} + \frac{c}{h^{q+1}} + \sigma\eta(\mathbf{x}, t), \quad (4.4)$$

where $\lambda \neq 0$ is the coefficient of the non-linear KPZ term, the only new ingredient added to the equilibrium wetting Langevin Eq. (4.1).

Note that in equilibrium the time-dependent probability distribution $P(h, t)$ is symmetric for the free interface and therefore it does not make any difference which side faces the substrate. By contrast, under non-equilibrium conditions, owing to the $h \rightarrow -h$ asymmetry of the KPZ-equation, it depends on the sign of λ that the substrate probes either one tail or the other of a KPZ probability distribution that is no longer symmetric. Thus, for a given bounding potential two different situations must be considered. Therefore, we will investigate systems with positive and negative values of λ (without loss of generality we take $\lambda = \pm 1$), and with both attractive ($b < 0$) and repulsive ($b > 0$) potentials, i.e. we consider *four distinct cases*. The focus is mainly on one-dimensional interfaces.

For *analytical studies* we employ simple power-counting arguments to establish the relevance or irrelevance of the new terms at the equilibrium renormalization group fixed points. These will be combined with heuristic and scaling arguments, to relate the emerging critical behavior to equilibrium wetting and short-ranged non-equilibrium unbinding.

For *numerical studies*, we consider one-dimensional discretizations of Eq. (4.4). As direct integrations of KPZ-like equations are known to be plagued with numerical instabilities [65], we resort to the exponential or Cole-Hopf transformation, $n = \exp(\pm h)$, that leads to well-behaved, numerically tractable, Langevin equations with multiplicative noise [55, 66]. In order to integrate these equations we employ a recently proposed efficient numerical scheme [8], specifically designed to deal with stochastic equations with non-additive noise. More than just a useful technical trick, this transformation has an interesting physical motivation, as we discuss next. For negative values of $a - a_c$, the average interfacial height $\langle h \rangle$ (thickness of the liquid film) may be large but finite, and the interface fluctuates around its average position, occasionally touching the substrate. As the interface moves to infinity when $a \rightarrow a_c$, its average height grows (i.e. the liquid film completely wets the substrate) thereby suppressing contact (dry) sites. An appropriate order-parameter (OP) for the unbinding transition is the number of contact (dry) sites [53, 67], or equivalently the surface order parameter [68]. This OP is finite and positive when the interface is bound, and vanishes at the unbinding transition. The variable, $\langle n \rangle = \langle \exp(-h) \rangle$, that vanishes exponentially far from the wall, is an adequate mathematical representation of such an OP (though not the only one).

The main goal of our study is the description of the scaling behavior of the OP. $\langle n \rangle$, is expected to obey simple scaling near the critical point, for sufficiently large times, t , and large system-sizes L . Denoting $\delta a = |a - a_c|$,

$$\langle n(\delta a, t, L) \rangle = L^{-\beta_{OP}/\nu} \langle n(L^{1/\nu} \delta a, L^{-z} t) \rangle, \quad (4.5)$$

while right at the transition $\langle n(\delta a = 0, t) \rangle \sim t^{-\beta_{OP}/\nu z} \sim t^{-\theta_{OP}}$ and therefore $\langle n(\delta a, t = \infty) \rangle \sim \delta a^{\beta_{OP}}$, where the critical exponents were introduced following standard nomenclature. Analogously, for the interfacial height we can define $\langle h \rangle \sim \delta a^{-\beta_h}$ and $\langle h(\delta a = 0, t) \rangle \sim t^{\beta_h/\nu z} \sim t^{\theta_h}$, although in terms of h a single universality class, with exponents related to the free KPZ [66], is observed for both signs of λ . Determining all of these critical exponents by the aforementioned techniques will allow us to assign the emerging critical behavior to specific universality classes, providing a comprehensive classification of non-equilibrium unbinding transitions in the presence of long-ranged forces.

Before proceeding to the presentation of our results, we notice that it is expected that the behavior for short-ranged interactions is recovered in the large- p limit of the long-ranged ones. Next, a brief review of the former is provided.

4.4 Brief review of equilibrium wetting

The action associated with Eq. (4.1) [107, 82] (setting $c = 0$) is

$$\mathcal{S}(h, \tilde{h}) = \int d^d x dt \left\{ \tilde{h}^2 - \tilde{h} [\partial_t h - \nabla^2 h - a - b h^{-p-1}] \right\}, \quad (4.6)$$

where \tilde{h} denotes, as usual, the response field [107, 82]. If one assumes first that the interaction term is the dominant one, from naïve dimensional analysis, imposing b to be dimensionless at the upper critical dimension, and equating the dimensions of the time-derivative and the potential terms, one obtains $[h]_{MF} = L^{2/(p+2)}$ and consequently, within mean-field, $\theta_h = 1/(p+2)$ since time scales naïvely as L^2 . The exponent values $\beta_h = 1/(p+1)$ and $\nu = (p+2)/(2p+2)$ are then obtained by matching $[a] = [h]_{MF}^{-p-1}$ and by identifying L with the characteristic correlation length, respectively.

On the other hand, when fluctuations (i.e. the noise term) dominate, we require the noise amplitude to be dimensionless at the upper critical

dimension, which leads to $[\tilde{h}]_{FL} = L^{(2+d)/2}$, and therefore $[h\tilde{h}] = L^{-d}$, $[h]_{FL} = L^{(2-d)/2}$. From this, proceeding as before, $\theta_h = (2-d)/4$, $\nu = 2/(d+2)$, and $\beta_h = (2-d)/(d+2)$. These results (which may be obtained using a number of different procedures [52, 83, 85, 84, 60, 51]) are exact as long as h and \tilde{h} do not have anomalous dimensions, which has been shown to be the case [83].

The upper critical dimension is defined by $[h]_{MF} = [h]_{FL}$, which yields $d_c(p) = 2p/(2+p)$. Note that for $d > d_c(p)$ the critical exponents depend on the details of the interaction (i.e. on p) whilst for $d < d_c(p)$, they depend only on d . In particular, in one dimensional systems, $p = 2$ marks the transition between a *mean-field regime* and a *fluctuation regime*:

i) If $p < 2$ mean field theory is valid, and consequently $\theta_h = 1/(p+2)$, $\beta_h = 1/(p+1)$, $z = 2$, and $\nu = 1/2$.

ii) For $p \geq 2$, the substrate interaction decays fast enough for the fluctuations to take over and the exponents become p -independent: $\theta_h = 1/4$, $\beta_h = 1/3$, $z = 2$, and $\nu = 2/3$.

Note that at the limiting value $p = 2$ the exponents change continuously from the mean field to the fluctuation regime. It is also remarkable that the fluctuation regime exponents coincide with those of short-ranged equilibrium wetting (characterized by exponential bounding potentials [51]).

Until now we have considered the scaling properties of $\langle h \rangle$, but as was mentioned earlier the number of dry sites or contact points between the interface and the substrate, measured by $\langle \exp(-h) \rangle$, is known to exhibit interesting scaling behavior in wetting problems [68].

i) For $p < 2$ simple mean field scaling holds, and the h -distribution is a Gaussian detaching from the wall at a speed controlled by its mean value. As the interface is well described by its average position, it is expected that

$$\langle e^{-h} \rangle \sim e^{-\langle h \rangle} \sim e^{-At^{1/(p+2)}}, \quad (4.7)$$

yielding a *stretched exponential* decay.

ii) For $p > 2$, $\langle a + b \exp(-h) \rangle = 0$ holds in the stationary state, and therefore $\langle n \rangle \propto a$; using simple scaling, $[\exp(-h)] = [a] = [\partial_t h] \sim t^{1/4-1}$, giving $\langle \exp(-h) \rangle \sim t^{-3/4}$. This result can be derived in a number of ways, including explicit calculations for discrete models in this class [86], and remains valid for long-ranged potentials in the fluctuation regime. Note the difference between this fluctuation-induced power-law behavior and the previously reported stretched exponential behavior in the mean-field regime.

For attractive walls, $b < 0$, a positive value of c is required to ensure the impenetrability of the substrate (see Fig. 6.4). In this case it is easy

to argue that the interface jumps discontinuously from a bound state (for $a < 0$), localized at the minimum of $V(h)$, to an unbound state (for $a > 0$) through a first-order phase transition. Clearly, in terms of the contact points, $\langle \exp(-h) \rangle$, the transition is also discontinuous.

4.5 Brief review of non-equilibrium short-ranged unbinding

The KPZ equation with exponential bounding potentials is

$$\partial_t h = \nabla^2 h + \lambda (\nabla h)^2 + a + b e^{-ph} + c e^{-qh} + \sigma \eta, \quad (4.8)$$

with $q > p > 0$. The results for the four possible physical situations are:

Repulsive wall and $\lambda < 0$

If $\lambda < 0$ (we set $\lambda = -1$) the change of variables $n = \exp(-h)$ transforms (4.8) (with $c = 0$) into

$$\partial_t n = \nabla^2 n - a n - b n^{1+p} + n \sigma \eta. \quad (4.9)$$

This describes complete wetting transitions (along path 1 in Fig. 6.3(a)) characterized by (see [55]) a dynamic exponent $z = 3/2$, identical to KPZ, $\nu = 1/(2z - 2) = 1$, and non-trivial exponents β_{OP} and θ_{OP} that were determined by simulations. The exponents for h have been measured also and the transition was shown to be in the *multiplicative noise 1* (MN1) universality class: $\beta_{OP} \approx 1.78$, $\theta_{OP} \approx 1.18$, $\theta_h \approx 0.33$ and $\beta_h \approx 1/2$ in $d = 1$ [55].

Repulsive wall and $\lambda > 0$

As for the $\lambda < 0$ case, it is more convenient [39] to use the transformation, $n = \exp(+h)$ leading to

$$\partial_t n = \nabla^2 n + a n + b n^{1-p} + n \sigma \eta. \quad (4.10)$$

This equation describes the transition along the path 1 in Fig. 6.3(b). Numerical estimates for the associated universality class have been recently obtained from this (non-order-parameter) Langevin equation [39]. By measuring the order parameter $m = \langle 1/n \rangle$ (that vanishes at the transition), the

following set of exponents was obtained: $\theta_{OP} \approx 0.22$, $\beta_{OP} \approx 0.32$, different from MN1 and $\theta_h \approx 0.33$, $\beta_h \approx 0.5$, $z = 3/2$ and $\nu = 1$ in line with the corresponding exponents of the MN1 class [39, 69, 53]. This universality class is known as *multiplicative noise 2* (MN2). A detailed discussion of the differences between the MN2 and MN1 universality classes, may be found in [55].

Note that, apart from the signs, the difference between Eq. (4.9) and Eq. (4.10) is in the leading power of n . It is possible, however, to summarize these two Langevin equations in

$$\partial_t n = \nabla^2 n + \alpha a n + \alpha b n^\gamma + n\sigma\eta, \quad (4.11)$$

with $\alpha = \lambda/|\lambda|$ and $\gamma = 1 - \alpha p$. Then $\alpha > 1$ and $\alpha < 1$ correspond, respectively, to the MN1 and MN2 universality classes. In the first case the leading power for large values of n is the non-linear term while this role is taken by the linear term in the second case. The transition at the boundary $\gamma = 1$ ($p = 0$) is obviously discontinuous, as both terms are linear and there is no saturating term.

In MN1 the order parameter is n , while in the MN2 case, it is $m = 1/n$. In both cases a is the control parameter.

Attractive wall and $\lambda < 0$

For attractive walls, $b < 0$, a positive value of c is required for stability, for any value of λ . In systems with $\lambda < 0$ (see Fig. 1(a)), a new phenomenology including a broad coexistence region, and a directed-percolation unbinding transition emerges [70, 55, 71, 53]. In the broad-coexistence region the stationary solution is either bound or unbound depending on the initial conditions [55, 54]. Such a region is delimited on the right (where the bound phase loses stability) by a directed percolation transition, where the scaling properties are controlled by the effective dynamics of the particle-like interface-surface contact points (i.e. points trapped in the potential well). Its leftmost border corresponds to the abrupt (discontinuous) binding of initially unbound interfaces. Again we refer the reader to [55] for a detailed discussion and to [71] for a review on generic phase-coexistence in non-equilibrium systems.

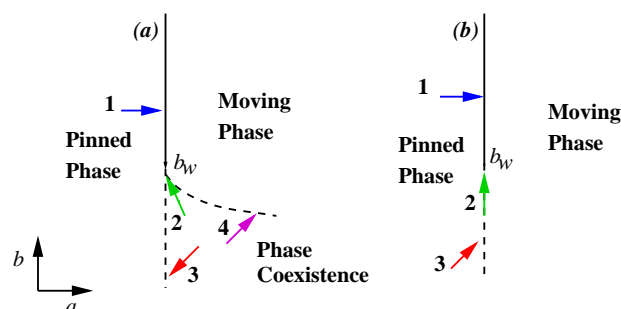


Figure 4.2: Phase diagrams for $\lambda < 0$ (a), $\lambda > 0$ (b). Paths labeled 1 correspond to non-equilibrium complete wetting transitions; 2, critical or first-order unbinding transitions (not studied); 3, first-order unbinding transitions; 4, unbinding transition in the directed percolation universality class. For $\lambda < 0$ and $b < b_w$ (attractive substrates), two-phase coexistence is observed in the area delimited by the two lines.

Attractive wall and $\lambda > 0$

For $\lambda > 0$ (see Fig. 1(b)) a first-order transition separates bound from unbound phases (akin to the equilibrium discontinuous transition for attractive walls). No broad coexistence region, nor directed percolation transition, exist in this case.

4.6 Non-equilibrium long-ranged unbinding: results

We are now set to discuss the long-ranged non-equilibrium problem described by Eq. (4.4). There is a singularity at $h = 0$ and thus only positive values of h are allowed (mimicking the impenetrability of the substrate). As before, if $b > 0$ we take $c = 0$ for simplicity. Proceeding as in the short-ranged non-equilibrium case, we perform the change of variables $n = \exp(\alpha h)$, with $\alpha = \lambda/|\lambda|$, in equation (4.4), obtaining

$$\partial_t n = \nabla^2 n + \alpha a n + \alpha b \frac{n}{|\alpha \log(n)|^{1+p}} + n \sigma \eta, \quad (4.12)$$

where a term $+\alpha c n / |\alpha \log(n)|^{1+q}$ has to be added when $b < 0$. As before, for positive λ ($\alpha = 1$), the order-parameter is $m = 1/n$, while for $\lambda < 0$ the

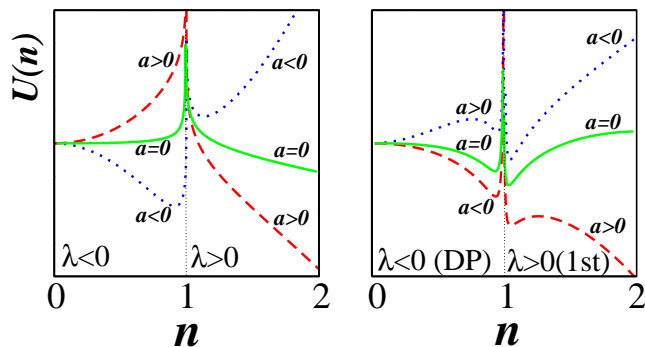


Figure 4.3: Effective potentials in terms of n obtained from the numerical integration of the interaction part of eq. (4.12). Left and right panels correspond to, respectively, repulsive ($b = 1$) and attractive ($b = -1$) interactions. For both b we show results for negative and positive λ , and different values of a corresponding to the bound and unbound phases, as well as at coexistence. Note that for $\lambda < 0$ (> 0) the unbound phase corresponds to a minimum of n at 0 (∞). Transitions for attractive walls can be either first-order or continuous (directed-percolation).

order-parameter is n itself. Note also that as there is a singularity at $n = 1$ (inherited from the singularity at $h = 0$ in Eq. (4.4)), for $\lambda > 0$, where n diverges at the transition, the initial condition is fixed at $n(x) > 1 \quad \forall x$, while for $\lambda < 0$, where n vanishes at the transition, $0 < n(x) < 1 \quad \forall x$, is taken. The deterministic one-site terms of Eq. (4.12) may be written as minus the derivative of a potential, $U(n)$, that is depicted in Fig. 4.3.

It is instructive to compare this model with the two universality classes reported for non-equilibrium short-ranged wetting, i.e. MN1 and MN2. In fact, it is expected that, in the limit of sufficiently large p , the power-law force yields the same dynamics as short-ranged (exponential) forces. Thus, for $\lambda < 0$ and large p we anticipate MN1 behavior while MN2 scaling should obtain when $\lambda > 0$, in the same limit.

4.6.1 Analytic results

In an early work the KPZ non-linearity was argued to be irrelevant above the (mean-field) wetting temperature $b = b_w = 0$, and an equilibrium (complete) wetting transition was predicted to occur as $a \rightarrow a_c$, at constant $b > b_w$, for any λ [72] (transitions along path 1 in Fig. 6.3). In the following we show that such a prediction is untenable and that the non-equilibrium term leads

to new physics.

Let us start by employing naïve power counting arguments, based on equilibrium scaling, to decide whether λ is a relevant or an irrelevant perturbation, at the mean-field fixed point and at the fluctuation one. In order to do that, we first fix $\lambda = 0$ in equation (4.4). If $b > 0$, then the upper critical dimension depends only on the repulsive part of the potential and is $d_c(p) = 2p/(2+p)$ [73, 107], as shown in the appendix. Now, from dimensional analysis $[\lambda] = L^{-1+d/2}$. Upon evaluating it at $d_c(p)$ one finds $[\lambda] = L^{-2/(2+p)}$ which, in terms of momenta, has a positive dimension for any value of p . Therefore, the KPZ non-linearity is relevant at the mean-field equilibrium wetting transition.

Relevancy at the fluctuating regime fixed-point is proved using the known one-dimensional scaling dimension of the field $[h] \sim t^{1/4} \sim L^{1/2}$ at the fluctuation-dominated fixed point (see appendix). Then, it follows, $[\lambda] = L^{-(d+1)}$, implying that λ is strongly relevant in any space-dimension. To be rigorous we would need to include perturbative corrections generated by the new non-linear term proportional to λ , but even without computing these, one can say that it is very unlikely that such corrections reverse the strong lowest-order relevancy of λ . The relevancy of λ , is strongly supported by the results of numerical simulations of the corresponding Langevin equation as we will show next.

As in one-dimensional equilibrium interfaces, where $p = 2$ separates the mean-field and the fluctuation-dominated regimes, it is easy to argue that in non-equilibrium the two regimes are separated by $p = 1$. From Eq. (4.4) in the absence of noise, the mean-field velocity exponent at the critical point, given by $\lambda \langle (\nabla h)^2 \rangle + a_c = 0$, is obtained by integrating $\partial_t h \sim h^{-p-1}$, and found to be $\theta_h = 1/(p+2)$. On the other hand, when noise (fluctuations) is included, the (one-dimensional) free KPZ equation has a roughening exponent of $1/3$ and, therefore, a velocity proportional to $t^{1/3}$ [59]. Which of these contributions dominates? Clearly, if $p < 1$ the wall-induced velocity is larger and fluctuations give only a higher order correction (i.e. they are irrelevant). By contrast, if $p \geq 1$ the effective repulsion generated by the wall (through suppression of the intrinsic interfacial roughness) controls the scaling. Thus, in non-equilibrium long-ranged wetting, $p = 1$ separates the mean-field from the fluctuation-dominated regimes.

Transient effects, that are significant before the non-equilibrium interface develops its full (asymptotic) time-dependent roughness, may prevent the KPZ exponent $\theta = 1/3$ from being observed, leading to an effective ex-

ponent, $\theta_{eff} < 1/3$. Furthermore, at short times, the interface is expected to grow with an Edwards-Wilkinson exponent, $\theta = 1/4$, and therefore θ_{eff} , increases progressively from $1/4$ to its asymptotic KPZ value, $1/3$, in the long time regime. Comparing these values with the wall induced velocity exponent $1/(p+2)$, we anticipate that for potentials with $1 < p < 2$ severe transient effects will occur before the fluctuation-dominated scaling sets in. By contrast, for $p > 2$ fluctuations dominate from the early stages of interfacial growth.

4.6.2 Numerical Results

In order to avoid numerical instabilities, typical of KPZ direct numerical integration schemes [65], we chose to study the associated multiplicative noise Eq. (4.12) obtained after performing a Cole-Hopf transformation. To solve Eq. (4.12) efficiently we have used a recently proposed *split-step* scheme for the integration of Langevin equations with non-additive noise [8]. In this scheme, the equation under consideration is discretized in space and time and separated into two contributions: (i) the first includes deterministic terms only and is integrated at each time-step using a standard integration scheme: Euler, Runge Kutta, etc [75] (here we have chosen a simple Euler algorithm) (ii) the output of the first step is used as input to integrate (along the same discrete time-step) the second part which includes the noise and, optionally, linear deterministic terms. This is done by sampling the probability-distribution, i.e. the solution of the Fokker-Planck equation associated with this part of the dynamics. In the case under study (noise proportional to the field), the second step can be carried out exactly. At each site, one has to sample a log-normal distribution, i.e., the solution of the Fokker-Planck equation associated with $\partial_t n = \alpha n + \sigma n \eta$ (for more details see [76] and [8]). The two-step algorithm for Eq. (4.12) is then implemented as follows. At each site $n = n(x, t)$, we compute

$$n_1(x, t) = n + dt \left[\frac{\alpha b n}{(\alpha \log(n))^{1+p}} + \nabla_{discr}^2 n(x, t) \right] \quad (4.13)$$

where the discretized Laplacian is defined by

$$\nabla_{discr}^2 n(x, t) = \frac{n(x + \Delta x, t) + n(x - \Delta x, t) - 2n(x, t)}{\Delta x^2} \quad (4.14)$$

with Δx the space-mesh, and

$$n(x, t + \Delta t) = n_1(x, t) \exp\left(\alpha a \Delta t + \sigma \eta \sqrt{\Delta t}\right) \quad (4.15)$$

where η is a random variable extracted from a Normal distribution with zero-mean and unit variance. Note that the linear deterministic term can be included in either the first or the second step, or partially incorporated in both of them. For systems with $b < 0$, the stabilizing term, proportional to c has to be included.

We set $\sigma = 1$, $\Delta x = 1/\sqrt{0.1}$, and the time-mesh $\Delta t = 0.1$ (note that in this scheme Δt can be taken larger than in the usual integration algorithms [8]). In some simulations we used different values of b , which by default was set to $b = \pm 1$. We take as initial condition $n(x, t = 0) = 3$ if $\lambda > 0$ (recall that $n \in]1, \infty[$) and $n = 0.5$ if $\lambda < 0$ ($n \in [0, 1[$). Then, the dynamics is iterated by employing the two-step integration algorithm at each site and using parallel updating.

The numerical procedure is as follows. In order to determine the critical point for any set of parameters we take the system-size as large as possible and look for the separatrix between upward-bending and downward-bending curves in the order-parameter (either n or $m = 1/n$ depending on the case) versus t in a double-logarithmic plot. The asymptotic value of this slope gives an estimation of θ_{OP} . Also, for the same parameters, $\langle h \rangle$ grows as a power-law with an exponent θ_h (bending downward and upward in the bound and the unbound phases, respectively). Generally the order parameter is more sensitive to control-parameter variations, providing the most reliable way of determining the critical point. For completeness, and in order to check the validity of analytical approximations, we measure the global interface width, W , at the transition, which is expected to grow with the KPZ exponent $\beta_W = 1/3$, in the regime where it is asymptotically free.

Once the critical point is determined accurately we compute β_{OP} and β_h by measuring the stationary values of the order parameter and of $\langle h \rangle$ at different distances from it. A complementary approach is based on finite-size scaling analysis: the values of the order parameter and of $\langle h \rangle$, at saturation, are measured for a fixed value of a as a function of system-size. At the critical point these values scale with exponents β_{OP}/ν and β_h/ν , respectively. In addition, the scaling of the saturation times for different system-sizes allows to determine the dynamical exponent z . This standard finite-size scaling analysis is not always possible (see below), and in such cases z is measured

through spreading-like experiments. Finally, an alternative to spreading consists in measuring the distribution of gaps between contact points at a given time. For small gaps this function decays with an exponent $z\theta_{OP}$ giving yet another estimate of z [77].

The correlation length critical exponent ν is obtained by measuring the location of the effective critical point, i.e. the value of a for which the order-parameter falls below a fixed threshold, say 10^{-3} , as a function of system-size: $a_{c,eff}(L) \sim L^{-1/\nu}$. This exponent may also be determined indirectly by employing scaling relations and using the value of β_{OP}/ν from finite-size scaling analysis and the value of β_{OP} obtained from direct measurements. The results of these measurements, in conjunction with the scaling laws, provide an over-complete estimation of the set of critical exponents, that was also used to verify scaling relations.

Before discussing the differences between the various universality classes and regimes (i.e. different values of λ , p and b) we first give an overview of the common features of all simulations.

1. Once the KPZ equation parameters (D, λ, σ) are fixed, the location of the critical point is universal, meaning that it does not depend on the details of the substrate, i.e. on the values of b, c , and p . The critical point is determined by the value of a where the free-KPZ interface changes the sign of its velocity, from positive, i.e. diverging to an unbound state, to negative, becoming bound at the wall: $a_c + \lambda\langle(\nabla h)^2\rangle = 0$. As we consider two different values of λ , $+1$ and -1 , there are two critical points: $a_c(\lambda = \pm 1) \approx \mp 0.143668(3)$.
2. At the critical point, the asymptotically unbound interface is a free KPZ one, and thus $z = 3/2$ and $\beta_W = 1/3$. These values were consistently checked in all simulations (see Fig. 4.4(a),(b)).
3. A simple argument, originally given in [66], predicts $\nu = 1$ for all bounded KPZ interfaces. This prediction was confirmed in all of our cases (see inset of Fig. 4.4(a)).

Repulsive walls and $\lambda > 0$.

We have to distinguish two regimes, depending on the range of the attractive substrate, i.e. the value of p .

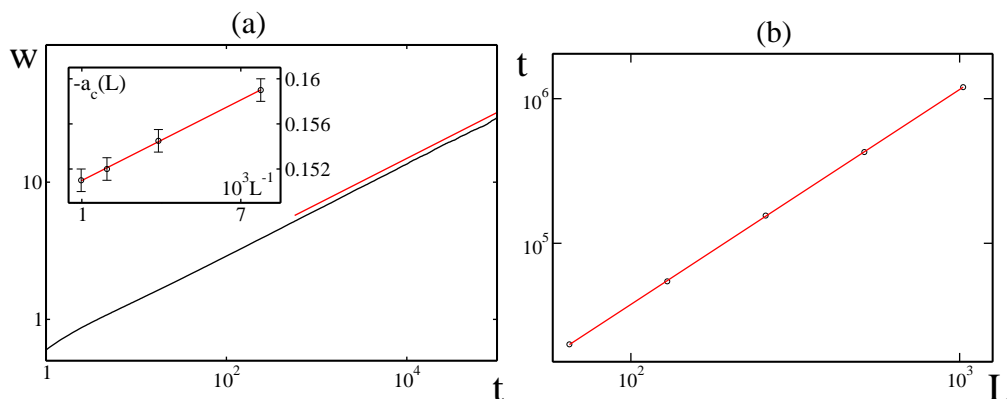


Figure 4.4: Features common to all simulations. (a) Roughness vs t gives $\beta_W = 0.33(1)$; (inset) $-a_c(L)$ vs $10^3 L^{-1}$ falls on a straight-line that yields $\nu \sim 1$ (data for $\lambda = -1$ and $p = 2$). (b) Saturation time vs system-size leads to $z = 1.48(4)$ (data for $\lambda = 1$ and $p = 2$).

Mean-field regime. The theoretical discussion indicates that for $p < 1$, and any sign of λ , a mean-field regime controlled by the exponents $\theta_h = 1/(p+2)$ and $\beta_h = 3/(2p+4)$ is obtained. By changing variables in a naïve way a stretched exponential behavior for the order-parameter is predicted. Figures 4.5 and 4.10 illustrate the confirmation of these predictions (both for positive and negative λ).

Fluctuation regime: Multiplicative Noise 2. A strong-fluctuation regime is predicted for systems with $p > 1$ but, as argued above, severe transient effects are expected for $2 > p > 1$. We start with the analysis of the, a priori, simpler $p > 2$ sub-regime and offer simulation results for $p = 2, 2.5, 3, 4, 7$. In all cases the order-parameter was found to decay at criticality with an exponent $\theta_{OP} \approx 0.229$ while the average height diverges with $\theta_h \approx 1/3$ (see Fig. 4.6, data shown for $p = 2$). A standard finite-size scaling analysis can be performed (see Fig. 4.6), yielding $\beta_{OP}/\nu = 0.34(2)$ and $\beta_h/\nu = 0.46(2)$.

These results, together with the previously reported general ones, unambiguously place the fluctuation regime for repulsive walls with positive λ into the MN2 universality class.

For systems with $1 < p < 2$, where strong transients are expected, after fixing $b = 1$ and running simulations up to $t = 10^6$, continuously varying power-law exponents are found (see Fig. 4.7). We note, however, that these

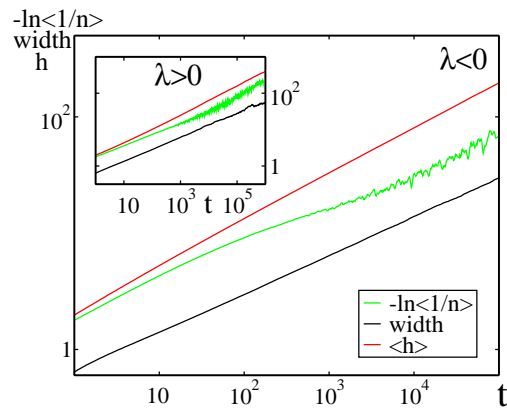


Figure 4.5: Log-log plot of the time evolution at a_c of $\langle h \rangle$ (upper, red curves), $-\ln\langle n_{OP} \rangle$ (middle, green curves), and the width w (lower, black curves), in the mean-field regime $p = 0.5$, for $\lambda < 0$ (main) and $\lambda > 0$ (inset). Irrespective of the sign of λ , $\langle h \rangle$ and the roughness may be fitted to a power-law with the predicted exponents $\theta_h = 1/(p+2)$ and $\beta_W = 1/3$, respectively. $-\ln\langle n_{OP} \rangle$ falls on a straight-line in a double logarithmic plot, confirming the stretched-exponential behavior of the order parameter.

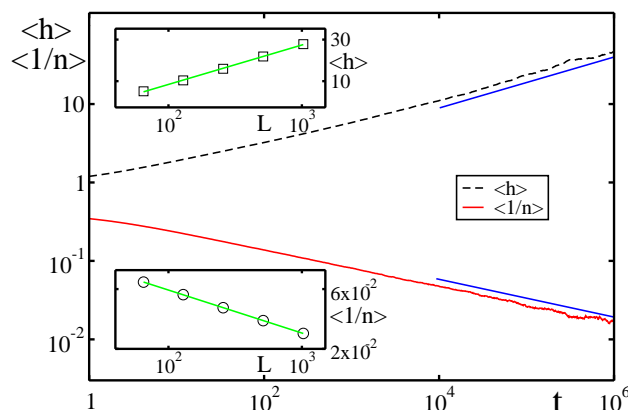


Figure 4.6: Log-log plot of the time evolution at a_c of $\langle h \rangle$ (dashed, black curve), and $-\log \langle n_{OP} \rangle$ (solid, red curve), in the fluctuation regime ($p = 2$) and for $\lambda > 0$. From the slopes of the straight-line fits one finds $\theta_h = 0.32(2)$ (upper-curve) and $\theta_{OP} = 0.228(6)$ (lower-curve). Upper-inset: finite-size scaling of $\langle h \rangle$ yielding $\beta_h/\nu = 0.46(2)$. From the lower-inset one obtains $\beta_{OP}/\nu = 0.34(2)$. These exponents agree with those of the MN2 universality class.

fits give effective rather than asymptotic exponents. In fact, the change in the effective exponents from mean-field (wall-controlled) to the fluctuation (intrinsic-interface) regime is expected to occur at shorter times when the effect of the substrate is less pronounced, implying that reducing the value of b decreases the crossover time. This was confirmed by simulating systems with $b = 0.1$ and $b = 0.05$ and observing a monotonic decrease of the effective exponents that converge to the expected asymptotic value $\theta_{OP} \approx 0.228$, $\theta_h \approx 1/3$ (see inset (a) of Fig. 4.7) in line with the hypothesis that the transition belongs to the MN2 universality class.

In order to check that $p = 2$ is the boundary between the strong and weak transient sub-regimes, we have plotted in Fig. 4.7, inset (b), the average order-parameter for systems with the same initial condition, at time $t = 10^6$, and different values of p . This is a non-stationary value of the OP that is strongly affected by transients. It is clear from the figure that the behavior of the order parameter changes qualitatively at $p = 2$ corroborating the result that this value of p marks the boundary between the sub-regimes with and without severe transients.

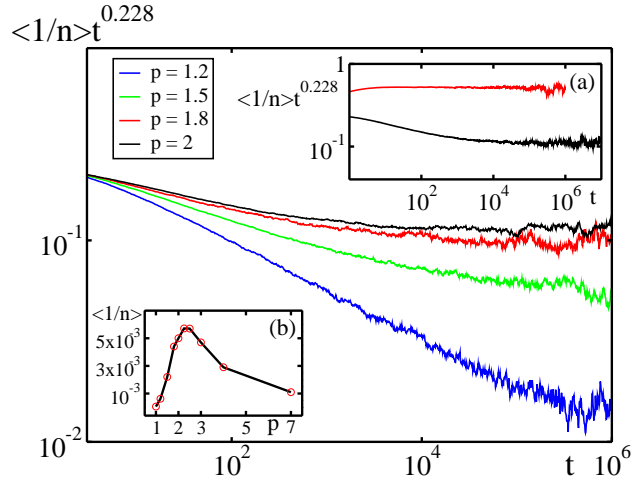


Figure 4.7: Main: Order-parameter multiplied by the expected power-law $t^{0.228}$. For systems with $b = 1$, long transients that depend on p are observed for systems with $1 < p < 2$. Inset (a): The crossover times are reduced as b decreases; compare the upper, red curve for $b = 0.05$ with the lower, black one for $b = 1$ ($p = 2$). Inset (b): Order-parameter at $t = 10^6$ vs p ($b = 1$). $p = 2$ marks the boundary of the strong transient region as illustrated by the different behaviors observed above and below $p = 2$.

Repulsive walls and $\lambda < 0$.

Mean-field regime. In parallel with the positive λ case, the results of Figs. 4.5 and 4.10 show that the theoretically predicted mean-field regime is clearly observed for systems with $p < 1$.

Fluctuation regime: Multiplicative Noise 1. Again we have to distinguish two sub-regimes, with and without severe transients, depending on whether p is larger than or smaller than 2. Simulations in the weak transient regime were performed for $p = 2$ and 3. In both of these systems the order-parameter decays at criticality with an exponent $\theta_{OP} = 1.19(1)$ while the average height diverges with $\theta_h = 0.33(1)$ (see Fig. 4.8(a),(b) data shown for $p = 2$). As was first pointed out in [77], finite-size scaling measurements are non trivial in this case due to the presence of two different characteristic times. Namely, the correlation length reaches the size of the system at times $\sim L^z$, whilst the interface typically detaches from the wall at times $\sim L^{1/\theta_n}$. As the latter grows with a larger exponent for MN1, the interface detaches from

the wall before it reaches the saturation regime for finite samples, rendering the evaluation of β_{OP}/ν and z through standard finite-size scaling methods problematic. An estimation of β_{OP} is possible by taking a large system-size, $L = 2^{17}$, and measuring the order-parameter stationary-state value upon approaching a_c . We find $\beta_{OP} = 1.76(3)$ and $\beta_h = 0.51(3)$ (see Fig. 4.8(c)). z is accessible through spreading experiments from an initial condition with only one active (pinned) site. The measurement of the mean-square deviation from the origin $R^2(t) \approx t^{2/z}$, gives $z = 1.52(5)$ (not shown). Alternatively, one can investigate the gap distribution function of the distances between neighboring contact points at a given time or, equivalently, the average size of inactive islands in the n -language [77]. For small gaps this function decays with an exponent $z\theta_{OP}$, and we find $z\theta_{OP} = 1.75(10)$ which leads to a value of z compatible with $3/2$ (see Fig. 4.8(d)).

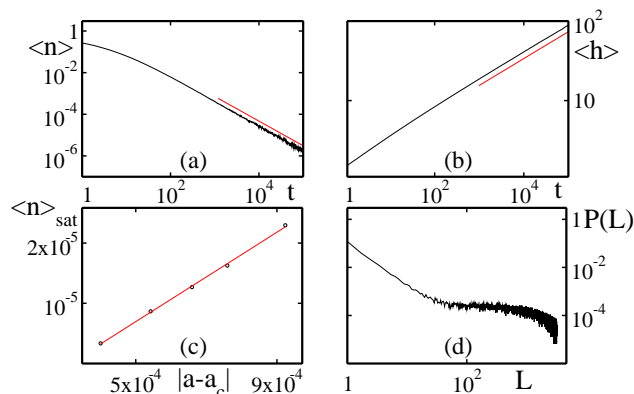


Figure 4.8: Results for $\lambda < 0$ and $p = 2$. (a) Log-log plot of the time decay of the order-parameter. The straight-line is a guide to the eye, and has a slope $\theta_{OP} = 1.19(1)$. (b) Log-log plot of the average distance from the wall vs time, leading to $\theta_h = 0.33(1)$. (c) The scaling of the saturation value of the order-parameter yields $\beta_{OP} = 1.76(3)$. (d) Log-log plot of the gap (between contact points) distribution function at $t = 2^{10}$. The initial slope gives $z\theta_{OP} \approx 1.75(10)$.

These results, together with the general ones, place unambiguously this fluctuation regime for repulsive walls with negative λ into the MN1 universality class.

Again, for systems with $1 < p < 2$, different effective exponents are obtained at a fixed maximum time for different values of b (unity and smaller), confirming the existence of strong transients. Upon decreasing b , the influ-

ence of the wall is reduced and a behavior compatible with the MN1 class is observed: $\theta_{OP} \approx 1.19$, $\theta_h \approx 1/3$, $\beta_{OP} \approx 1.76$ and $\beta_h \approx 0.5$ (figure not shown).

Attractive wall and $\lambda < 0$.

The phase-diagram, depicted on the left panel of Fig. 6.3, is similar to that found for short-ranged interactions [55]. For a fixed b , by varying a one of two transitions may occur depending upon the initial interfacial state. Initially unbound interfaces experience an unbinding-binding transition at a_c where the free-interface velocity inverts its sign (in full analogy with the previous case; see path 3 in Fig. 6.3). On the other hand, initially bound interfaces unbind at a different non-trivial value of a , noted $a^* > a_c$, inside the free-interface unbound phase (path 4 in Fig. 6.3(a)). This transition is analogous to the one observed for short-ranged forces, and is expected to be controlled by the unbinding of interface-sites trapped in the potential minimum. Bound sites (located around the potential minimum) are identified with particles; unbound sites are described by holes. The effective particle dynamics is very similar to that of the contact-process [2] (a well-studied model known to be in the directed percolation class): an occupied site can become empty when a point is detached, and can induce also the binding of a neighboring site. Furthermore, empty sites cannot become spontaneously occupied in the absence of occupied (bound) neighboring sites. Indeed, as soon as the interface is locally out of the potential well, it is pulled away from it. This corresponds to the absorbing state characteristic of the directed percolation class. Note that the statistics of the average number of such pseudo-particles is completely analogous to that of $\langle \exp(-h) \rangle$.

Before the depinning transition, typical *triangular structures* are observed, consisting of pinned sites (lying in the potential well), and depinned sites being pulled from the substrate. This triangular shapes (pyramidal in two-dimensions) are similar to those in the analogous short-range case, and are reminiscent of pyramidal mounds obtained in the non-equilibrium growing of some interfaces, as for instance, in the so called Stranski-Krastanov effect [58].

Our numerical results show that this transition is controlled, as in the short-ranged case, by directed percolation critical exponents (see Fig. 4.9). In particular, we have determined $\beta_{OP}/\nu = 0.26(2)$ and $\theta_{OP} = 0.161(2)$, in excellent agreement with the one-dimensional directed percolation values.

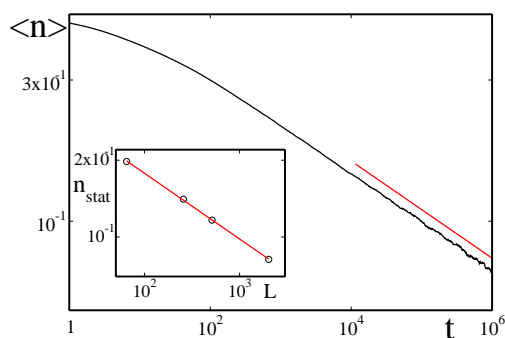


Figure 4.9: Time decay of the order-parameter at the critical point $a = 0.38448$. From the slope in the log-log plot we find $\theta = 0.161(2)$. Inset: finite size scaling of the order parameter. From the slope in the log-log plot we estimate $\beta/\nu = 0.26(2)$, in agreement with directed percolation values.

Let us remark that, as the bound sites remain inside the potential well, and the dynamics controlling their final “escape” is likely to be insensitive to the exponential or power-law tails of the potential at large values of h , the parallel between this behavior and the directed-percolation transition for short-ranged forces is to be expected. Interestingly, Ginelli et al. investigated a lattice model of a generalized contact process with long-ranged interactions between the edges of low-density segments and found a transition in the directed percolation universality class for forces that decay sufficiently slowly, and a first-order transition otherwise [78]. Clearly, in terms of h this translates into a long-ranged interaction between the vertices forming the triangle bases, and it is reasonable to assume that, in turn, an effective long-ranged attraction between the substrate and the interface must be obtained. In the light of these results it is reasonable to assume, that both short- and long-ranged interactions in similar models will be characterized by the same behavior below b_w .

In the region between a_c and a^* one observes generic (broad) phase coexistence: the stationary solution is either bound or unbound depending on the initial condition. Within this region, the bound phase is characterized by some bound sites trapped in the potential minimum, and pseudo-unbound regions separating them [55]. In full analogy with short-ranged forces, close to the unbinding transition $a \lesssim a^*$ initially bound interfaces are stable owing

to a mechanism that eliminates local fluctuations into the unbound phase: once formed, islands of the unbound phase rapidly transform into triangular mounds of fixed slope, which subsequently shrink from the edges.

Attractive wall and $\lambda > 0$.

When $\lambda > 0$, the situation is rather similar to the one for equilibrium and for non-equilibrium ($\lambda > 0$) short-ranged systems. At the critical value a_c where the free interface inverts its velocity sign, there is a discontinuous unbinding-binding transition (path 3 in Fig. 6.3). This value does not depend on the value of p nor on b or c [79].

The multicritical point. Finally, for either sign of λ , path 2 in Fig. 6.3 corresponds to a multi-critical point analog to an equilibrium critical wetting transition when the critical point is approached at coexistence. Most likely, its location will not coincide with its mean-field value $b = 0$, but exhibits some renormalization shift. The analysis of this multi-critical point will be considered elsewhere.

4.6.3 Discrete Model

As a final check of universality issues, we simulated a discrete interfacial model, known to belong to the KPZ class, in the presence of a long-ranged substrate. The model is the same as that studied in the context of short-ranged wetting in [69]. Even if plagued with long transient effects (much larger than in the short-ranged case) all of the previously reported phase diagrams and universality classes seem to be confirmed for the different types of walls (i.e. values of b and p) and signs of the non-linearity. Generally, the discrete model provides slightly better results for the height variable as compared with the continuum model, and worse for the order-parameter.

Figure 4.10 displays the time growth of the mean separation $\langle h \rangle$ in the mean-field like regime ($p < 1$), for both positive and negative λ . Additionally, the ratio $\beta_{OP}/\nu = 0.251(2)$ and $\theta_{OP} = 0.156(2)$ were obtained for the directed percolation transition, which compares favorably with the accepted estimates 0.25208(5) and 0.1595 [80].

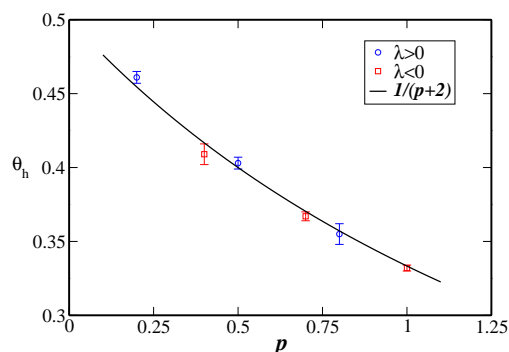


Figure 4.10: Time growth exponents θ_h in the mean-field like regime for $\langle h \rangle$ at the critical point, as results from the discrete interfacial model. Blue circles (red squares) stand for $\lambda > 0$ (< 0) data points, and the solid line is the predicted curve $1/(p+2)$.

4.7 Discussion and Conclusions

We have studied the unbinding of KPZ interfaces in the presence of limiting substrates, interacting via long-ranged potentials. This is the simplest model for interfacial effective descriptions of wetting and in general, unbinding transitions, of systems interacting through van der Waals forces under non-equilibrium conditions.

We have presented the results of systematic analytical and numerical studies of one-dimensional KPZ-like interfaces in the presence of long-ranged forces Eq. (4.4), supporting the following conclusions:

i) Repulsive interactions drive a non-equilibrium complete wetting transition for either sign of λ . This transition belongs to different universality classes depending on the strength of the repulsion, i.e. on the value of p in Eq. (4.4) and on the sign of λ . For $p < 1$ a mean-field like regime is observed in both cases, while for $p > 1$ the fluctuation regime obtains and the transition is in the multiplicative noise 1 (MN1) class for $\lambda < 0$ and in the multiplicative noise 2 (MN2) for $\lambda > 0$. Systems in the fluctuation regime, exhibit severe crossover effects for bounding potentials with $1 < p < 2$. This should be contrasted with the behavior of equilibrium systems where the value of p that separates the mean field from the fluctuation regimes was found to be $p = 2$. More importantly, in non-equilibrium systems the symmetry of

Exponent	$\lambda < 0$			$\lambda > 0$		
	$p < 1$	$p > 1$	$p = \infty$ [5]	$p < 1$	$p > 1$	$p = \infty$ [20]
$\theta_{OP}, \langle n \rangle \sim t^{-\theta_{OP}}$	stretched exp.	1.19(1)	1.18	stretched exp.	0.228(6)	0.229(5)
$\beta_{OP}, \langle n \rangle \sim \delta a^{\beta_{OP}}$	n.a.	1.76(3)	1.78	n.a.	0.34(2)*	0.335(5)
$\theta_h, \langle t \rangle \sim t^{\theta_h}$	$1/(p+2)$	0.34(1)	0.33	$1/(p+2)$	0.32(2)	0.323(10)
$\beta_h, \langle h \rangle \sim \delta a^{-\beta_h}$	$3/2(p+2)^*$	0.51(3)	0.5	$3/2(p+2)^*$	0.46(2)*	0.48(3)
$z, \xi \sim t^{1/z}$	$3/2^\dagger$	1.52(5)	3/2	$3/2^\dagger$	1.48(4)	1.46(5)
$\beta_W, W \sim t^{\beta_W}$	$1/3^\dagger$	0.33(1)	–	$1/3^\dagger$	$1/3^\dagger$	–
$\nu_x, \xi \sim \delta a^{-\nu_x}$	1^\dagger	1	1	1^\dagger	1^\dagger	0.99(3)

Table 4.1: Summary of the critical exponents in the mean-field ($p < 1$) and the fluctuation ($p > 1$) regimes for non-equilibrium, complete wetting transitions with long-ranged forces. To facilitate the comparison, the exponents for the MN1 and MN2 universality classes are also included ($p = \infty$). *, exponent from finite-size analysis or scaling relations; †, estimated value from short simulations; n.a., not applicable.

the equilibrium wetting and drying transitions is broken and the fluctuation regime of the corresponding equilibrium wetting transitions is split into two different non-equilibrium universality classes, MN1 and MN2 respectively. Our results are collected in table 4.1.

ii) For attractive walls, i.e. below the critical wetting temperature, phase-diagrams analogous to those of systems with short-ranged forces have been found: generic phase-coexistence over a finite area limited by directed percolation and first-order boundary lines for $\lambda < 0$, and a first-order phase transition from an unbound to a bound interface for $\lambda > 0$. This transition should not be called “wetting” as the interface detaches below the wetting transition temperature.

The unbinding transition at the critical wetting point (which in the language of this chapter corresponds to a multicritical point) requires a higher degree of fine-tuning and is therefore expected to be more difficult to observe in experimental situations. Its study is also more laborious and is deferred to future work.

For more realistic two-dimensional interfaces, corresponding to three-dimensional bulk systems, the situation is expected to be very similar: all universality classes (mean-field, multiplicative noise 1, multiplicative noise 2, and directed percolation) are expected to be substituted by their two-

dimensional counterparts, with analogous phase diagrams and overall phenomenology.

We hope that the results described here will help to motivate an experimental study of wetting and unbinding transitions under non-equilibrium situations. In these systems one expects to find the rich phenomenology described here, and they can be used to test some of our quantitative predictions, concerning the values of the exponents and the existence of various universality classes. Liquid-crystals [56], molecular-beam epitaxial systems, as *GaAs* [57] claimed to grow following KPZ scaling, or materials exhibiting Stranski-Krastanov instabilities [58], appear to be good candidates that are at least worth investigating in this context. Indeed, it is rather exciting to think that non-equilibrium complete wetting exponents are measurable. This would be a way of measuring the multiplicative noise critical exponents, and brings new hope of measuring directed percolation exponents in real systems [81].

Chapter 5

Disordered substrates: Stochastic DNA models

In this chapter we will present results of work under progress.

5.1 Introduction

In life reproduction and normal living functions, DNA has a great importance. It is the vector of information in most known living forms. It is difficult to know the part of the information contained in the sequence and the part which is due to physical processes taking place in growing processes. In the same way, recently it was argued that the nonlinear dynamics of DNA itself could play an important role in the process of transcription, therefore in the expression of the information contained in the sequence. The transcription process takes place when *RNA polymerase* breaks its way into the double helix. It is believable that *RNA polymerase* will most easily enter inside the double helix in regions where they are more distant. Following this argumentation line, we find it useful to have a model that could describe the dynamics of the double helix. This model could be use to find and explain *transcription start site* location and mutation effects outside genes location. Some mutations are known to inhibit gene expressions and can cause severe illness(ref).

5.2 Continuous Langevin equation with disordered substrate

As a first case of interest, even if this stands a bit away from DNA models, we present here a numerical study of the Reggeon-Field-Theory with quenched disorder. The main result is that its behavior is equivalent to the well studied *Contact process*(CP) with disorder [29, 28]. We first explain how to implement the model and, shortly after present our results.

5.2.1 Quenched disorder for Reggeon-Field-Theory

The CP is a very well known model and simple modifications of it allowed [29] to investigate the properties of the strong noise fixed point. The only needed ingredient to add is a spatially dependent rate of creation $\lambda(x)$. To implement the RFT with quenched disorder, we apply a very similar pattern. Since the creation rate of the microscopic model is equivalent to a mass in the RFT we use a spatially dependent mass term or control parameter which is an almost straightforward modification of the RFT. After seeing the effects

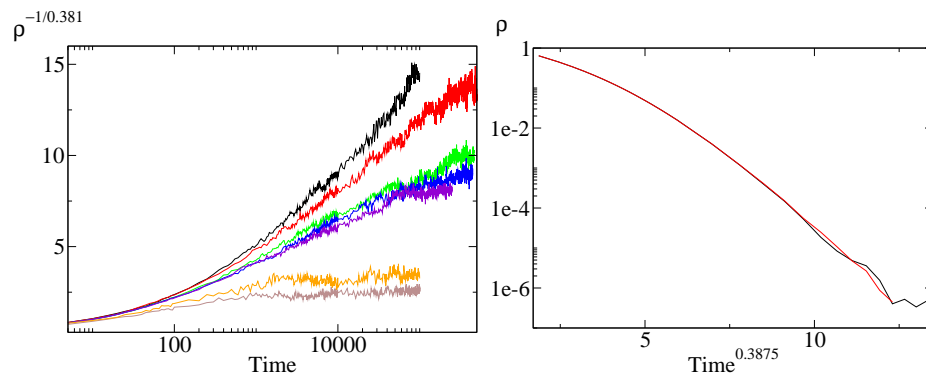


Figure 5.1: Left: Evidence of active dynamics also observed in disordered CP. Right: Stretched exponential behavior instead of exponential in the absorbing phase, at the “clean”(refers to the critical point without defects) critical point.

of disordered on the paradigmatic class of absorbing phase transition, one naturally wonders what would be the effect of this disorder on other known universality classes. Harris criterion is useful to predict relevance of quenched disorder. This is why we investigated this for MN1 and MN2.

5.2.2 Quenched disorder for Multiplicative noise Langevin equation

In the same way as presented above, we can easily generalize the study of RFT with quenched disorder to the study of *multiplicative noise* equation with disorder. The implementation is otherwise identical to the method explained in chapters 3 and 4. The main result of this section is that quenched disorder is irrelevant for this phase transition. One of the reasons for the impossibility of observing DP exponents in natural systems is the presence of instability to noise of the RFT. If contrarily, MN1 and MN2 transitions are stable under the introduction of quenched noise, this leads one to think that they could more easily be observed in natural experiments. It was suggested in recent papers studying these transitions (chapter 4 shows that the nature of the potential, either Van der Waals or short-ranged, is also irrelevant) but has unfortunately never been tackled by experimentalists.

5.3 Peyrard-Bishop-Dauxois: a Langevin equation

The first version of this model was introduced by Peyrard and Bishop in [87]. Compared to older DNA models, it uses a continuum description allowing for inclusion of nonlinear effects, which microscopic models would exclude. The choice of the dimensionality of the model, 1+1D, allows to study dynamic effects. The model describes the distance between pairs of bases and interactions are taken through a Hamiltonian including a Morse potential, equation 5.3. The shape of the potential is very important but as long as it includes a wall and a finite well before a flat part extending to infinity, this particular choice is not expected to be critical for the behavior of the system (it is a clever choice that allows one to obtain analytic results via standard Transfer Integral methods). The rigidity of the chain makes clear that an interaction term between subsequent pairs is important $W(h_n, h_{n-1})$. Different choices of W have been used, the first one is a simple harmonic term. This led the authors of [87] to see a very smooth transition, however denaturation curves from experiments have a rather steep shape. This was successfully accounted for in a modified version including stacking terms of subsequent bases in [88]. Bases are constituted of cycles so that subsequent bases of a given chain interact together, not only through the backbone (justifying a

harmonic term) but also via hydrophobic interactions and overlapping of π electrons. Those interactions are taken into account by the 'stacking term', 5.4.

Denaturation processes observed by cryomicroscopy is undergone in the same way as in our model(see figures).

5.3.1 An equilibrium model

Since the model under study is characterized by an Hamiltonian, it is an equilibrium model, i.e., the whole information about stationary states is stored in the Gibbs distribution. Therefore in evaluating the partition function, the kinetics terms coming from the mass and the potential terms decouple. The kinetic part only contribute in a prefactor $(\sqrt{2\pi mk_b T})^N$. In studying the stationary state, the inertial terms can be neglected, so that a dynamical model including only first-order time derivative(no acceleration or mass effects) would be sufficient. In this sense, we will define a Langevin equation we can study and compare to problems treated in previous sections. Following the above-mentioned analogy, we write:

$$\frac{\partial h_n(r, t)}{\partial t} = -\frac{\partial V(h_n)}{\partial h_n} + \sigma\eta(r, t), \quad (5.1)$$

with

$$V(h_n) = W_{morse}(h_n) + W_{interaction}(h_n) \quad (5.2)$$

$$W_{morse}(h_n) = D_n(e^{-a_n h_n} - 1)^2 \quad (5.3)$$

$$W_{interaction}(h_n) = \frac{k}{2}(1 + \rho e^{-\beta(h_{n+1}+h_n)})(h_{n+1} - h_n)^2 + symmetric. \quad (5.4)$$

In the following sections we use 5.1 as a starting point to study properties of DNA. We focus on establishing the nature of the 'melting transition'. Afterwards, in 5.5 we will discuss the locality of the effects of mutations.

5.4 Melting: critical wetting

DNA double stranded structure is be stable at low temperature. However, when temperature increases, it is expected that entropy effects will be more important than engerical consideration and the strand are expected to separate. Since the absorbance of U.V. light is much greater for individual bases

than for matched G-C or A-T pairs, it is possible to find experimentally the proportion of matched and individual bases. This was done on homopolymers artificially synthesized and a sharp transition was observed. Instead, for natural sequences, the unbinding followed a multistep fashion depending on the sequence. This can also be observed in numerical simulation of small disordered systems. As the system size tends to be bigger, much bigger than individual structures of the disorder, the transition is expected to become smooth.

5.4.1 Numerical study of the transition

In what follows we will show that the model 5.1 also gives a very sharp phase transition. The protocol we followed is very simple we initiated a series of system at different temperatures in a completely ordered state, all bases at the same distance 2 and let the system evolve. We study the simplest, homogeneous case of only G-C bases. The correct parameters for this simulations are taken from reference [90] in which the authors compared the model to real experiments in order to find out the correct parameter values to use. We then monitor several quantities of interest,

- the average distance between bases, $\langle h \rangle$
- the number of bases at distance less than 2, $\langle n \rangle$
- the average value of $\langle \exp(-h) \rangle$.

From intuition and ideas developed in the two previous chapters those quantities are expected to carry relevant information to determine the nature of the transition. At least if this transition coincides with a transition presented in the previous two chapters, it should be evident by this measurements. Looking for a possible analogy, can be done supposing the interbases distance $\langle h \rangle$ might behave in the same way as the average distance between an interface and the substrate on which it grows. In the previous chapters the studied transitions were of complete wetting, i.e. we would vary the shape of the potential to induce a pinned or depinned phase, here instead, the potential is fixed and we change the temperature.

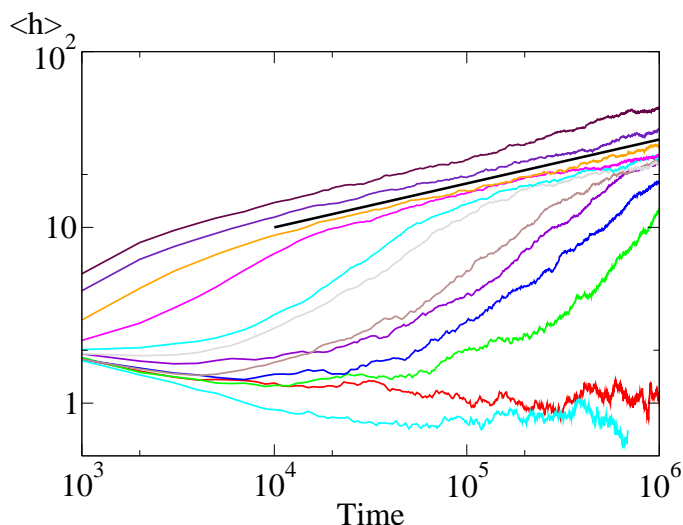


Figure 5.2: Results for Eqs. (5.1) and (5.4), with $\rho = 1$. For the PBD model, with stacking term, there is an apparently discontinuous phase transition or melting transition when temperature is increased above a given T_c . This is traduced by a divergence of the average distance between bases. The black line is a power law with exponent $\frac{1}{4}$, in agreement with equilibrium critical wetting.

5.5 Localized effect of mutation : bubbles statistics

The DNA chain stores all the information in the sequence of the bases. Some parts of the sequence are known to code for proteins. Others are not expressed in amino-acids and proteins. Understanding what their function is remains as an open question. Some are identifiable as archaic genes but other are just repetitions of a pattern not including much information. Recently, the hypothesis has been made that these unexpressed parts might play a relevant role in the dynamics of DNA. Since the expression of genes is a mechanical/biochemical process, it is natural to think that transcription of DNA into RNA is influenced by the dynamics of DNA. In this sense, it is natural to expect that the sequence and particularly the part that are not expressed might also play a relevant role in the dynamics and expression of DNA.

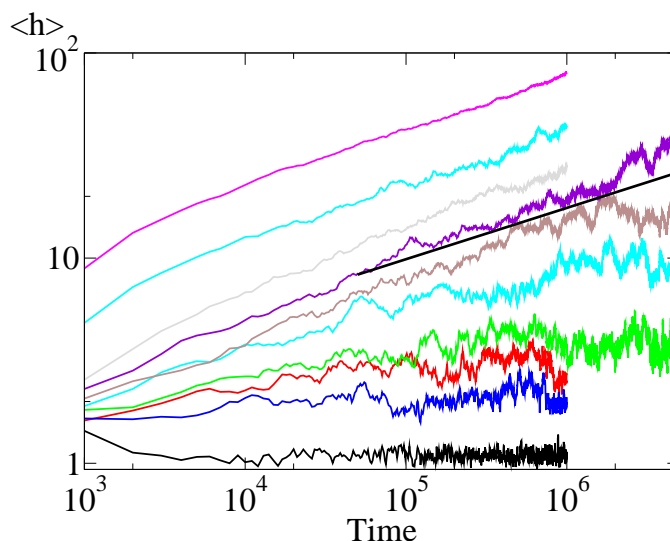


Figure 5.3: Results for Eqs. (5.1) and (5.4), with $\rho = 0$. For the PB model, there is an apparently continuous phase transition or melting transition when temperature is increased above a given T_c . This is traduced by a divergence of the average distance between bases. The black line is a power law with exponent $\frac{1}{4}$, in agreement with equilibrium critical wetting.

5.5.1 DNA tanscription start site

Mutations can occur anywhere in DNA chains, if they occur in the coding part of a gene, this gene might be modified, possibly resulting in a genetic illness. It has been observed by biologists that mutations occuring in non-coding parts could result in the non-expression of a closeby gene. A possible explanation for this events can be that the transcription of DNA into RNA helped by *RNA polymerase* could be hindered by the mutation. There is a so-called transcription start site where *RNA polymerase* fixes on DNA and starts the transcription process.

5.6 Conclusion

In this chapter, we have shown that our methodology allows to study Langevin equation with quenched disorder using as a benchmark the known absorbing phase transitions of DP including quenched disorder. The following tasks we have performed is to reproduce part of the known results obtained for

the PB and the PBD models with the same methodology. This allows one to easily study bubbles statistics and dynamics. This could be biologically relevant quantities in understanding effects of mutations. Our conclusion is that mutations can modify the statistics of bubbles in a non-local way. Due to the spatial inhomogeneities, and to the possible displacement of bubbles, non-local interaction effects are to expect. Considering a given A-T region, surrounded by G-C pairs. It opens less often than a A-T region surrounded by more A-T bases. In this way, if a mutation modifies the surrounding of the A-T region we are considering, it will alter the behavior of this A-T region. Some mutations might hinder the opening of transcription start sites and alter normal patterns of gene expression. The models we have studied are harsh simplifications of the complex reality and already allow for qualitative understanding of many phenomena. A subsequent complication of the model would allow to study more complicated phenomena.

Chapter 6

Non-accessible absorbing state in reaction-diffusion systems

6.1 Introduction

We analyze from the renormalization group perspective a universality class of reaction-diffusion systems with absorbing states. It describes models where the vacuum state is not accessible, as the set of reactions $2A \rightarrow A$ together with creation processes of the form $A \rightarrow nA$ with $n \geq 2$. This class includes the (exactly solvable in one-dimension) *reversible* model $2A \leftrightarrow A$ as a particular example, as well as many other *non-reversible* sets of reactions, proving that reversibility is not the main feature of this class as previously thought. By using field theoretical techniques we show that the critical point appears at zero creation-rate (in accordance with known results for the reversible case) and it is controlled by the well known pair-coagulation renormalization group fixed point, with non-trivial exactly computable critical exponents in any dimension. Finally, we report on Monte-Carlo simulations, confirming the field theoretical predictions in one and two dimensions for various reversible and non-reversible sets of reactions.

In a recent paper Elgart and Kamenev [91] have proposed a classification of absorbing state phase transitions, a subject that has been one of the central pillars of non-equilibrium statistical mechanics over the last decade [1, 2, 92]. The strategy they follow is elegant and powerful. The main idea is to (i) write down using standard techniques the generating functional (or, equivalently, the effective Hamiltonian) for a given reaction-diffusion system; (ii) inspect

the phase space in saddle-point approximation paying special attention to the “zero-energy” manifolds which determine the topological properties; (iii) detect possible structural changes in the phase portrait: the birthmark of phase transitions, and (iv) classify them according to basic topological properties. This procedure is a natural extension to non-equilibrium problems of the rearrangement of thermodynamic-potential minima occurring at equilibrium phase transitions. Hence, it allows for a categorization of universality classes attending to symmetry principles, conservation laws, and few other relevant ingredients, which determine the phase-space topology and its possible structural changes. Establishing the limits of validity of the saddle-point approximation within this context and developing systematic improvements to it remain as fundamental open problems.

Using this strategy, Elgart and Kamenev report on 5 non-trivial universality classes with absorbing states, occurring in one-dimensional systems with just one type of particle [93, 94]. The first 4 ones are: (i) *directed percolation* (DP) characterizing generic systems with an absorbing phase transition and without extra symmetries, conservation laws, quenched disorder, nor long-range interactions [92, 95], (ii) the usually called *parity conserved* (PC) [96] also known as DP2 or generalized voter class [16] which includes two symmetric absorbing states, (iii) the very elusive *pair-contact-process-with diffusion* (PCPD) class in which all reactions involve pairs of particles [98, 99], and (iv) the *triplet-contact-process-with diffusion* (TCPD) in which reactions involve triplets of particles [100].

In this paper we focus on the fifth class in [91]. It describes the reversible reactions $A \rightarrow 2A$ and $2A \rightarrow A$ occurring at rates μ and σ respectively. This model was solved exactly in one dimension more than twenty years ago in a seminal paper by Burschka, Doering, and ben-Avraham [101] by employing the *empty interval method* [102]. Finite-size properties, scaling functions, and critical exponents have also been exactly computed for this reversible model and for variations of it [101] in one dimension. Note that except for the absence of one-particle spontaneous annihilation, $A \rightarrow 0$, this set of reactions coincides with the contact process [1] a well-known model in the robust DP class [92]. It is, therefore, interesting to elucidate which is the main relevant difference in the renormalization group sense, giving rise to a non-trivial non-DP type of scaling. From considerations in [91] it seems that the fact that the reactions are reversible plays such a relevant role, but as we will illustrate, *reversibility is a sufficient, but not a necessary, condition.*

From the field theoretical point of view, Cardy and Täuber had obtained

in their seminal article [103] a one-loop calculation of critical exponents for the closely related set of reactions $2A \leftrightarrow 0$, while in a recent paper Jack, Mayer, and Sollich have shown that such one-loop results are also valid for $2A \leftrightarrow A$ and have to be exact owing to the existence of *detailed balance* for reversible reactions [104]. Therefore, two or more loop corrections should cancel out, even if this is not explicitly shown in [104]. In any case, the main results are that the critical point is located at $\mu_c = 0$ (any non-vanishing branching rate leads to sustained activity) and the order-parameter critical exponent is $\beta = 1$. The long-time long-distance properties turn out to be controlled by the well-known “pure” pair-coagulation ($2A \rightarrow A$) RG fixed point [105, 103, 106, 104] and all exponents can be computed in any dimension.

In this paper, we perform a full diagrammatic expansion of various reaction-diffusion models extending previous analyses to all orders in perturbation theory. First, we recover the previously known results for the reversible model $2A \leftrightarrow A$. Afterward, using the intuition developed from the previous full diagrammatic analysis we construct different sets of *non-reversible* reactions, and argue that they belong to this same universality class. Its key ingredient turns out to be the absence of an accessible vacuum state, i.e. there is no reaction $mA \rightarrow 0$ but just pair-coagulation, combined with creation reactions of the form $A \rightarrow nA$. The *reversible reaction*, $n = 2$ discussed in [91] and [104] is just a representative of this broader class: reversibility (which tantamount to the detailed-balance condition in [104]) is a sufficient but not a necessary requirement.

Let us remark that reactions as $2A \leftrightarrow 0$ and its non-reversible extensions $2A \rightarrow 0$, $0 \rightarrow 3A$, $4A$, ... can also be argued to belong to this same class. In these cases, the vacuum state is accessible, but it is not stable, so they are not genuine absorbing state models.

To verify the field-theoretical predictions we perform Monte-Carlo simulations for various non-reversible sets of reactions, implemented with and without hard-core exclusion (“fermionic” or “bosonic”, respectively) in one and two dimensions. All critical exponents, are in perfect agreement with the RG predictions, confirming the existence of a robust universality class, broader than thought before.

Before proceeding, we should underline that while many of the results contained in this paper are already known (some from exact solutions of the reversible model in one dimension [101] and some from similar perturbative calculations combined with symmetry arguments [91, 105, 103, 106, 104]), a systematic presentation of them, focusing the attention on universality

aspects is, to the best of our knowledge, lacking in the literature. This paper aims at filling this empty space and at providing a comprehensive picture of this universality class, extending it to non-reversible reactions without an accessible vacuum state.

6.2 Field theory analysis of $A \leftrightarrow 2A$

The techniques employed in this section are standard and we refer the reader to [107, 82] and more specifically to [105, 103, 106] for more detailed calculations and/or pedagogical presentations.

Let us apply the Doi-Peliti formalism [107, 103, 106] (see also [108, 109]) to the reversible set of reactions $A \rightarrow 2A$ and $2A \rightarrow A$ occurring at rates μ and σ respectively. They can be cast into a generating functional whose associated (bosonic) action is

$$\begin{aligned} \mathcal{S}[\phi, \pi] &= \int dt \int d^d x [\pi(\partial_t \phi - D\nabla^2 \phi) - H[\phi, \pi]], \quad \text{with} \\ H[\phi, \pi] &= (\pi^2 - \pi)(\mu\phi - \sigma\phi^2), \end{aligned} \quad (6.1)$$

where $\phi(\mathbf{x}, t)$ and $\pi(\mathbf{x}, t)$ are the density and the response fields respectively (some spatial and time dependences have been omitted for simplicity). For a general process $kA \rightarrow jA$ with k and j integer numbers, the associated effective Hamiltonian in this formalism includes a factor $[\pi^j - \pi^k]\phi^k$, which is proportional to $[\pi^2 - \pi]$ if and only if the absorbing state is not accessible, i.e. $j > 0$ and $k > 0$.

For readers with more intuition in terms of stochastic equations, an associated Langevin equation can be easily derived:

$$\partial_t \phi(\mathbf{x}, t) = D\nabla^2 \phi + \mu\phi - \sigma\phi^2 + \sqrt{\mu\phi - \sigma\phi^2} \eta(\mathbf{x}, t) \quad (6.2)$$

where $\eta(\mathbf{x}, t)$ is a Gaussian white noise. Let us emphasize the similarity between Eq.(6.2) and the Langevin equation for the DP class [95, 92]. Despite of this likeness, Eq.(6.2) is not free from interpretation difficulties as the density field is not a real-valued one, but develops an imaginary part [109]. For this reason we avoid using it and center the forthcoming discussion on Eq.(6.1).

Owing to the fact that the effective Hamiltonian in Eq.(6.1), $H[\phi, \pi]$, is proportional to $(\pi^2 - \pi)$, $\pi = 0$ and $\pi = 1$ are zero-energy manifolds. The

existence of these two constant- π solutions is, according to [91], at the basis of the non-DP behavior of this model. Indeed, the four zero-energy solutions: $\pi = 0$, $\pi = 1$, $\phi = 0$, and $\phi = \mu/\sigma$, define a rectangular geometry in the phase portrait (see Fig. 1b and [91]), which should be compared with the standard, triangular, DP topology, for which only one constant- π solution exists (see Fig. 1a and [91]) as we illustrate now.

It is worth noticing that the common factor $(\pi^2 - \pi)$ in Eq.(6.1), arising from the fact that the absorbing state is not accessible, can be interpreted as a *subtle symmetry* between all the coefficients of (noise) terms proportional to π^2 and their corresponding (deterministic) ones proportional to $-\pi$. Indeed, it is closely related to the detailed-balance symmetry discussed in [104]. If an additional reaction $A \rightarrow 0$ occurring at rate λ is switched on, a term $\lambda\phi(1 - \pi)$ has to be added to the Hamiltonian. In such a case, $(\pi^2 - \pi)$ is not a common factor, the subtle symmetry is broken and $\pi = 0$ is not a zero-energy solution anymore. This leads to the triangular topology for zero-energy manifolds in the phase space (Fig 1a) and, hence, to DP-scaling. Something similar occurs by switching on any other reaction as $mA \rightarrow 0$, with $m \geq 2$, converting the vacuum into an accessible state.

Let us present a different argument leading to the same conclusion. From standard naïve power counting and relevance arguments one could be tempted to conclude that this problem is in the DP class, and that the critical dimension is $d_c = 4$. Indeed, as said before, the leading (lowest order) terms in both the deterministic part and the noise are identical to their analogous ones in the DP field theory [95, 92], for which $d_c = 4$. The only way out of this naïve (and wrong) conclusion is that, at the critical point where the linear-deterministic term coefficient vanishes, the coefficient of the leading DP-like noise term $\pi^2\phi$ also vanishes owing to the abovementioned subtle symmetry. This opens the door for higher order noise terms to control the (non-DP) scaling. Indeed, a proper power counting analysis reveals that, as the interaction Hamiltonian is proportional to $(\pi^2 - \pi)$, π has to be dimensionless, which leads to $[\phi] = \Lambda^d$ (where Λ has dimensions of momentum) to ensure a dimensionless action, and consequently to $[\mu] = \Lambda^2$ and $[\sigma] = \Lambda^{2-d}$. Therefore, the theory upper critical dimension is $d_c = 2$ [103, 104, 91].

The existence of the common factor $(\pi^2 - \pi)$ in Eq.(6.1) implies that the μ -dependent non-trivial manifold and the trivial one, $\phi = 0$, merge at the critical point rather than intersecting in just a point as in DP. This is the key reason for the models without an accessible vacuum to exhibit a different type of scaling. To substantiate this assertion we need to prove that the previous

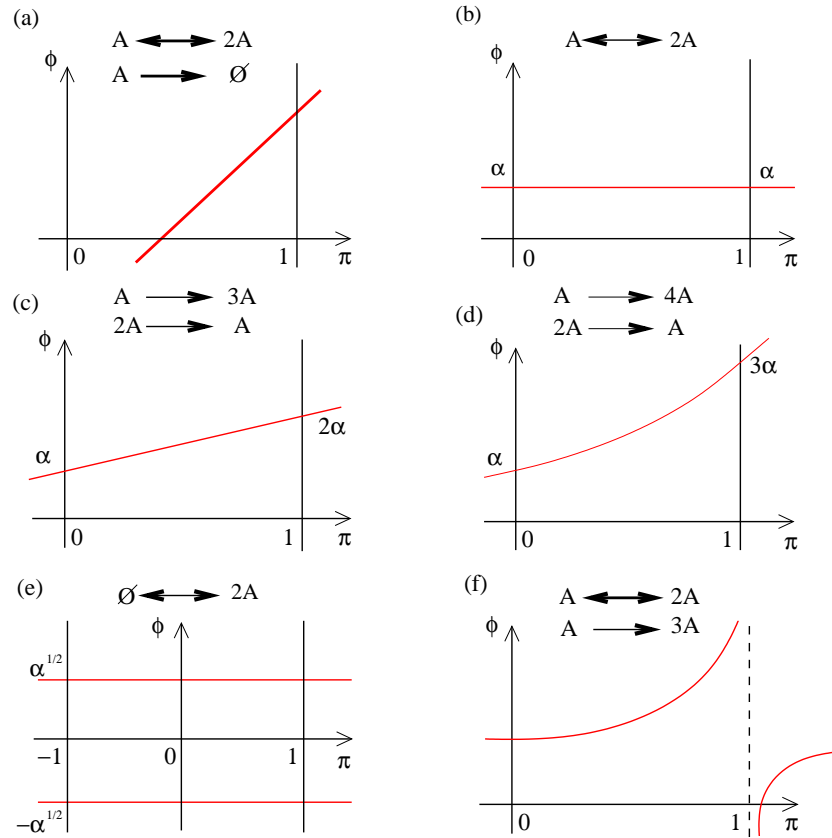
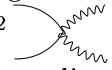
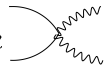
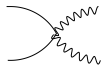
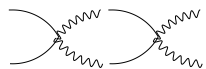
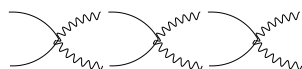
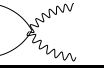



Figure 6.1: Schematic zero-energy manifolds (bold lines) for different reactions. The line marked in red (non-trivial manifold, depending on the control parameter μ) moves downward upon approaching the critical point in all cases: $\alpha = \mu/\sigma$. While directed percolation is characterized by a triangular structure as in (a), models without an accessible vacuum state have a different form, being rectangular (b), trapezoidal (c), or more complicated geometries (d), for different reactions. For reversible models with an unstable vacuum, $\phi = 0$ is not a zero-energy manifold (e). The structures in (c) and (d) are not robust under RG flow, but evolve to non-closed topologies as the one in figure (f).

bare-action symmetry, or associated topological structure, survives to the inclusion of fluctuations (i.e. it remains valid beyond mean-field [110]).

The basic elements for a complete perturbative expansion at a diagrammatic level are: the usual DP-noise vertex ($\pi^2\phi$) [95, 103, 106], the pair-coagulation ones ($\pi\phi^2$ and $\pi^2\phi^2$), as well as the propagator $(-i\omega + D\kappa^2 + \mu)^{-1}$ [105, 103, 106]. Diagrammatically, we represent response fields by wavy lines and the density fields by straight ones. For instance, the pair-coagulation noise vertex is depicted as σ^2  and analogous figures, with different numbers of straight and/or wavy lines are employed for the other vertices and the propagator.

In order to perform a sound perturbative expansion to all orders in perturbation theory, we choose to write separately diagrams with and without corrections proportional to μ . The second group includes only diagrams with vertices proportional to σ (i.e. expansions of Z-functions in powers of σ). Simple inspection reveals that such diagrammatic corrections are those of the pair-coagulation process, a theory well-known to be *super-renormalizable*, i.e., all these diagrams can be computed and resummed to all orders. Indeed, the only possible diagrammatic corrections to the pair-coagulation vertices, proportional to σ , have the typical “bubble” structure, leading to a geometric series

$$\begin{aligned}
 \sigma_R \text{  } &= \sigma \text{  } \\
 &- \sigma^2 \text{  } \\
 &+ \sigma^3 \text{  } + \dots \\
 &= \frac{\sigma \text{  }}{1 + \sigma \text{  }}
 \end{aligned}$$

where σ_R is the renormalized (or “dressed”) coagulation coefficient. Omitting external legs in Eq.(6.3), $\sigma_R = \frac{\sigma}{1+\sigma I} = \sigma(1 - \sigma\Sigma)$ with $\Sigma = \frac{I}{1+\sigma I}$, where I denotes the one-loop diagram evaluated at zero external frequency and arbitrary momentum scale Λ [107, 82, 103]:

$$I = \frac{1}{(2\pi)^{(d+1)}} \int d^d\kappa d\omega \frac{1}{i\omega + D\kappa^2} \frac{1}{-i\omega + D\kappa^2} \propto \frac{\Lambda^{-\epsilon}}{\epsilon} \quad (6.3)$$

with $\epsilon = 2 - d$. Similar expressions are obtained for all the renormalized coefficients by just changing the leftmost and/or the rightmost vertex of the series in Eq.(6.3). If these were the only corrections, (i.e. if the RG fixed point was at $\mu_c = 0$ so that diagrams including corrections proportional to μ would not give any non-vanishing contribution) then the renormalized parameters would be:

$$\begin{aligned}\mu_R &= Z_\mu \mu = \mu(1 - \sigma\Sigma) \\ \sigma_R &= Z_\sigma \sigma = \sigma(1 - \sigma\Sigma).\end{aligned}\tag{6.4}$$

for the two coefficients proportional to μ and the two proportional to σ respectively, showing that the subtle symmetry is not broken. The corresponding flow equations would be

$$\begin{aligned}\partial_l \mu_R &= \mu(2 - \sigma \partial_l \Sigma) \\ \partial_l \sigma_R &= \sigma(\epsilon - \sigma \partial_l \Sigma)\end{aligned}\tag{6.5}$$

where ∂_l stands for the logarithmic derivative with respect to the momentum scale at which integral are evaluated [107, 103, 82, 106]. For $\epsilon < 0$, i.e. $d > 2$, the trivial (mean field) solution $\sigma = \mu = 0$ is infrared stable, while for $\epsilon > 0$, the only infrared stable fixed point is $\sigma^* = \epsilon/(\partial_l \Sigma)$ with $\mu = 0$. Plugging this into the first equation in (6.5), we obtain the anomalous scaling dimension of μ_R , $[\mu_R] = 2 - \epsilon = d$, which coincides with the one-loop result obtained in [103, 91] (see also [104]).

The change in the scaling dimension of the “mass” term, from its naïve value $[\mu] = 2$ to the renormalized exact one, $[\mu_R] = d$, induces a change in all critical exponents corresponding to magnitudes measured away from the critical point with respect to their corresponding mean field values. Moreover, as happens in pair-coagulation, there is no further renormalization required for the fields nor the diffusion constant [105, 103, 111] and therefore all exponents can be exactly computed at any dimension. For instance, the scaling dimension of the field is Λ^d and, hence, scales as μ_R , implying $\beta = 1$ in any dimension. Using the same logic one obtains $\nu_{\parallel} = 2$, $\nu_{\perp} = 1$ for the correlation time and correlation length exponents, while right at the critical point $z = 2$. Using standard scaling relations, the density of particles as a function of time decays in one dimension with an exponent $\theta = 1/2$, while in $d = 2$ a similar calculation leads to logarithmic corrections and, in particular, to a decay $\ln(t)/t$, while β remains equal to 1 [103].

In order to prove that the fixed point with $\mu_c = 0$ is not just *a solution* but also the *only one* one should consider all the possible diagrams (even if this can be done only in a symbolic form [112]), write down the 4 Z-functions, analogous to eq.(6.4) for the 4 vertex functions (2 proportional to μ and 2 to σ in their bare form). Doing this, it is straightforward to check that 3 different and independent flow equations are obtained. The fourth one is not independent owing to the usual duality symmetry [95] but this is not important for the argumentation here. As there are only 2 independent bare parameters, there is no way to find a fixed point for this set of 3 independent equations except for the trivial one $\mu_c = 0$, which simultaneously satisfies in a trivial way the first 2 equations, and leads back to the preceding calculation, to the symmetry preserving Eq.(6.4), and to the same set of exponents.

Note that in models in the DP class, where the naïve power counting is different, with $d_c = 4$, only 2 independent parameters in the flow equations need to be fine tuned to zero. The third one (corresponding to the highest order noise coefficient) is irrelevant (flows to zero) already at mean field level and, therefore, does not require fine tuning to vanish asymptotically. Hence, contrarily to the previous case, a non-trivial solution, $\mu_c \neq 0$ exists leading to a DP fixed point.

As pointed out in [104], the reversible reaction studied here and $2A \leftrightarrow 0$ share the same type of critical behavior. Indeed, the Hamiltonian in this latter case is $(\pi^2 - 1)(\mu - \sigma\phi^2)$ where, as before, μ and σ are the creation and annihilation rate respectively. The zero-energy manifolds are: $\pi = \pm 1$ and $\phi = \pm\sqrt{\mu/\sigma}$ (fig. 1e). They define a quadrangular structure, as the one described above, but in this case $\phi = 0$ is not an invariant manifold: the vacuum state is accessible but it is not stable, so it is not properly an absorbing state phase transition. A perturbative analysis analogous to the one above can be done for the present case (indeed this is the model studied in [103, 104]) and leads to the same set of critical exponents; here the common factor $\pi^2 - 1$ plays the role of the subtle symmetry above.

Finally, for reversible coagulation reactions involving *triplets* instead of pairs, $A \leftrightarrow 3A$, we obtain similar results: vanishing critical point and exactly computable exponents, but the critical dimension is $d_c \leq 1$ in this case [91].

6.3 Extension to non-reversible reactions

A careful but simple inspection of the arguments in the preceding section leads to the conclusion that none of the reported results depends on the fact that the creation reaction is of the form $A \rightarrow 2A$. As will be argued in this section, most of them apply to more general *non-reversible* processes with creation reactions as $A \rightarrow nA$. For these, the creation part of the Hamiltonian is $\mu(\pi^n - \pi)\phi$, which together with the pair-coagulation terms $\sigma(\pi^2 - \pi)\phi^2$ guarantees that $(\pi^2 - \pi)$ can be extracted as a common factor for non-reversible bare Hamiltonians, and hence π is dimensionless and $\pi = 0$ and $\pi = 1$ are zero-energy solutions as in the $n = 2$ case. For example for $n = 3$, $H = \mu(\pi^3 - \pi)\phi - \sigma(\pi^2 - \pi)\phi^2 = (\pi^2 - \pi)[\mu(\pi + 1)\phi - \sigma\phi^2]$. The existence of such a common factor in the *bare* Hamiltonian is, as explained before, guaranteed if and only if the vacuum state is not accessible.

For the family of non-reversible models with $n > 2$, the geometry of the zero-energy manifolds of the bare Hamiltonian *is not a rectangular one* as occurs for the reversible set of reactions with $n = 2$ [91]. For instance, for $n = 3$ one obtains a *trapezoidal geometry* (zero-energy solutions: $\pi = 0$, $\pi = 1$, $\phi = 0$ and $\phi = (\pi+1)\mu/\sigma$, (see figure 1c), but the overall *topology* is not changed. Indeed, as the critical point is approached the difference between the rectangle and the trapezium becomes negligible, and at criticality this manifold merges with the $\phi = 0$ one. Analogously, for $n = 4$ one obtains a quadrangle with 3 straight lines and a curved one ($\phi = (\pi^2 + \pi + 1)\mu/\sigma$) (see fig. 1d), which also becomes closer and closer to the horizontal line upon approaching the critical point. In all cases, the non-trivial μ -dependent manifold merges with the absorbing-state one $\phi = 0$ at the critical point, and this constitutes the main trait of this class as will be illustrated here: in DP they intersect at criticality at a single point, in PC they intersect in one point in the active phase and merge at criticality [91], while in the class under scrutiny, they do not intersect in the active phase and merge at the critical point.

Note that, as π is dimensionless, all the different processes for different values of n are equally relevant at mean-field level (they just differ in powers of π). As a consequence, the naïve scaling dimensions for any $n > 2$ are as in the preceding section, leading to $d_c = 2$. It is also important to realize that *higher-order processes generate effectively lower-order ones* (in particular, $A \rightarrow 2A$ is always generated) and all of them share the same degree of *naïve* relevancy. The generation of lower-order processes induces changes in

the zero-energy manifolds, and leads to combinations of the previous “pure” topologies obtained for creation processes involving only one value of n . In order to render the theory renormalizable, lower order terms have to be included in the bare Hamiltonian, with coefficients proportional to μ (as they have to vanish as $\mu \rightarrow 0$) that we call μ_n . Indeed, from now on we study physical processes where various types of creation events with different values of n are simultaneously present (in particular $n = 2$ is always generated).

At a perturbative level, one can proceed as before, and separate corrections proportional and not proportional to μ . The first notorious difference with the reversible case is that upon renormalizing, the shape of some zero-energy manifolds is deformed if terms with $n \geq 3$ are present. Indeed, owing to the fact that the coefficients of π^n , with $n \geq 3$, in these generalized processes renormalize as

$$\mu'_{n,R} = \mu_n \left(1 - \frac{n(n-1)}{2} \sigma \Sigma \right) \quad (6.6)$$

up to one loop [113] while the corresponding “mass” coefficient renormalizes as in Eq.(6.4), different corrections are generated for these two coefficients equal at a bare level (therefore, the need to use different names, $\mu'_{n,R}$ and $\mu_{n,R} = \mu_R$, for the two of them, as a generalization of the single equation for μ_R in Eq.(6.4)). Eq.(6.6) shows that the scaling dimensions of the non-linear term coefficients, $\mu'_{n,R}$ varies with n : the lower the value of n , the more relevant the corresponding non-linear term.

Proceeding as before, it is straightforward to see by performing a perturbative expansion around $d_c = 2$ that the only way to find a solution of the RG flow equations at any arbitrary order in perturbation theory is by fixing $\mu = 0$. For instance, considering creation reactions with $n = 2$ and $n = 3$, one has 3 independent parameters: σ , μ_2 and μ_3 and 5 independent flow equations. Hence, at criticality all creation rates have to vanish, and one recovers the fixed point and exponents in the previous section, so *the universality class is preserved under the introduction of non-reversible reactions*. Note that, in order to extend the calculation in the preceding section, it has been enough to impose that all creation terms are proportional to μ . This ensures that all of them vanish at the critical point and generate no extra diagrammatic correction, but they do not need to be all equal as happens in the reversible case.

We should also emphasize that, as said before, the mass-like terms associated to each n -creation process are all equally relevant and they all renor-

malize as μ_2 , while the μ'_n renormalize differently for $n \geq 3$ (see Eq.(6.6)) and hence, $\pi^2 - \pi$ is not a common factor of the *renormalized* Hamiltonian, except at the critical point $\mu = 0$ where such a subtle symmetry is restored. The common factor or subtle symmetry invoked all along the calculation in the previous section, equivalent to the existence of reversibility or detailed balance, is not a necessary condition. As a consequence, the zero-energy manifold structure is affected: the topology shown in figures 1c and 1d is not stable under the RG flow, $\pi = 1$ is not a zero-energy manifold of the renormalized Hamiltonian, and the phase portrait structure becomes more complicated (see Fig. 1f).

Despite of this, we observe that from the phase-portrait point of view, *a key ingredient, not altered upon introducing non-reversible reactions, is the fact that the non-trivial μ -dependent manifold and the trivial one $\phi = 0$ do not intersect in the active phase and merge into a degenerate manifold at the critical point.* Therefore, the main ingredient of this universality class is *not* the reversibility nor the existence of a common factor in the renormalized Hamiltonian but the way in which the non-trivial manifold and the trivial one merge [114]. In summary, *reversibility is a sufficient but not a necessary requirement.*

For completeness' sake let us comment on another family of reactions without an accessible vacuum, including higher-order creation reactions as $kA \rightarrow (k+n)A$ with $k \geq 2$ which exhibit a different type of scaling behavior. These have to be complemented with higher order annihilation reactions as $jA \rightarrow lA$ with $j \geq k$ and $j > l \geq 1$ in order to ensure the existence of a bounded stationary state. For instance, taking $2A \rightarrow 3A$ (with rate μ) as a creation reaction together with $2A \rightarrow A$ (rate σ), we need another annihilation reaction, as $3A \rightarrow 2A$ (with rate $\lambda > \mu$) to have a well defined stationary state. For this case, even if $\pi = 0$ and $\pi = 1$ are constant energy solutions (at least at a bare level) the manifold $\phi = 0$ is degenerated, and the non-trivial zero-energy solution, $\phi = \mu/\lambda - \sigma/(\lambda\pi)$, intersects the line $\phi = 0$ at σ/μ and becomes singular at $\pi = 0$, originating a very different topology from the one above. This topology corresponds to the PCPD class [91, 98]. Therefore, *creation from pairs* in systems without an accessible vacuum leads to a different universality class.

Finally, for non-reversible *coagulation reactions involving triplets* ($3A \rightarrow A$ and $A \rightarrow nA$) we obtain again that the universality class remains unchanged with respect to the corresponding reversible reaction (see last paragraph of the previous section).

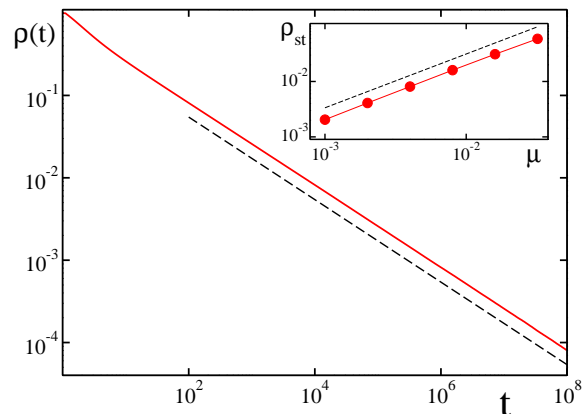


Figure 6.2: (Color online) Results of Monte-Carlo simulations for $2A \rightarrow A$ and $A \rightarrow 3A$ implemented in a bosonic way in one dimension. The decay of the order parameter at criticality ($\mu_c = 0$) is given by $t^{-0.5}$ (main plot). This result is well known as at $\mu = 0$ this model coincides with pair-coagulation. The order-parameter critical exponent is perfectly fitted by $\beta = 1.00$ (inset). Very similar results are obtained for the reversible case, $n = 2$, as well as for higher-order non-reversible cases, as $n = 4$ and $n = 5$.

6.4 Monte-Carlo simulations

In order to verify the above field theoretical predictions we have performed Monte-Carlo simulations of the reversible reactions (reproducing some existing results [101]) and, more relevantly, *non-reversible* set of reactions: $2A \rightarrow A$ together with $A \rightarrow nA$ with $n = 3, 4, 5$. We have considered two different implementations: a *bosonic* one in which the number of particles at every site in a lattice is unrestricted (which is the one directly related to the bosonic field theory presented here), and a *fermionic* one with number occupancy restricted to be 0 or 1. For both of them the same type of numerical experiments have been performed. Figure 2 shows our main results for $n = 3$ in the bosonic implementation. In the main body, we plot the time evolution of the order-parameter as a function of time for a one-dimensional lattice of size 2^{20} . A clean power-law decay is observed at $\mu_c = 0$ with slope $\theta = 0.500(1)$ in a log-log plot. This is not surprising as at $\mu = 0$ this model coincides with pair-coagulation. Direct measurements of the order-parameter as a function of the distance to the critical point (up-

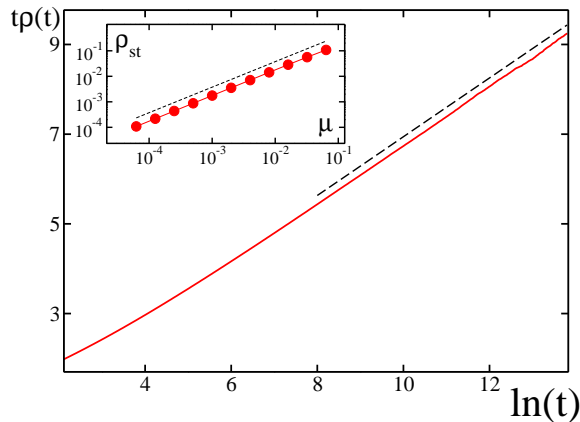


Figure 6.3: (Color online) Results of Monte-Carlo simulations for $2A \rightarrow A$ and $A \rightarrow 3A$ implemented in a bosonic way in two dimensions. The decay of the order parameter at criticality ($\mu_c = 0$) is proportional to $\ln(t)/t$ (main plot). At this critical point $\mu = 0$, this model coincides with pair-coagulation, for which this is a well known results. The order-parameter critical exponent is perfectly fitted by $\beta = 1.00$ (inset).

per inset) lead to $\beta = 1.00(1)$. Also, from measures of the mean-squared distance associated with two point correlation functions [104] one can easily measure $z = 2$ in all the cases under consideration. All the remaining exponents can be derived using standard scaling laws, providing a full check of the theoretical predictions for the bosonic model. For the fermionic model we obtain identical conclusions. In $d = 2$ mean-field exponents with logarithmic corrections have been measured confirming that $d_c = 2$ (see figure 3). In $d = 3$, Jack et al. [104] showed by means of Monte-Carlo simulations that the scaling is Gaussian as expected.

We have also verified that for the sets of non-reversible reactions with $n = 4$ and with 5 one obtains the same set of critical exponents, supporting again the theoretical conclusions.

6.5 Conclusion

We have shown using field theoretical arguments and verified by means of Monte-Carlo simulations that all reaction-diffusion processes including pair coagulation $2A \rightarrow A$ and creation in the form $A \rightarrow nA$ belong to the

same universality class, regardless of whether the reactions are reversible or not. The critical point is located at zero creation rate, and all critical exponents are controlled by the well-known pair-coagulation renormalization group fixed point and can be exactly computed. These conclusions are in agreement with exactly known results for the reversible model in one dimension [101]. The main ingredient of this class of absorbing-state transitions is that the vacuum state is not accessible and creation occurs from individual particles. If creation occurs only from pairs then scaling is as in the PCPD class while, as soon as a reaction making the vacuum accessible, as, for example, $2A \rightarrow 0$ is switched-on, the system recovers standard DP scaling. There are also models in this universality class as $2A \leftrightarrow 0$ where the vacuum state is accessible but in these cases it is not stable: $0 \rightarrow 2A, 3A, \dots$, so they are not properly absorbing-state transitions.

We have shown that the topology of the zero-energy manifolds is very important to unveil universality classes, but there could be many subtleties leading to surprises. We hope that this work fosters new studies to clarify some of the still-standing problems on universality in non-equilibrium critical phenomena.

Chapter 7

Resumen

7.1 Introducción

Este trabajo de tesis constituye un trabajo original desarrollado con el fin de aplicar las ecuaciones de Langevin a transiciones de fase de no-equilibrio. En primer lugar y a modo de comienzo, se presenta la motivación física y se introducen las técnicas y conceptos usados.

Muchos sistemas físicos pueden estar en varias fases: líquida, gaseosa o sólida. En cada una de estas fases, el sistema que estudiamos posee propiedades que varían en el espacio y en el tiempo. Típicamente, estas variaciones están caracterizadas por longitudes de correlaciones, tanto espaciales como temporales, cortas. Suelen decaer de forma exponencial, así que existe una distancia característica que aparece en la exponencial notada λ . De este modo, dos puntos del sistema espaciados por una distancia más grande que λ sufren fluctuaciones independientes. El promedio de fluctuaciones independientes es fácil de tratar y no crea dificultades.

La situación que nos atañe es bastante distinta. Nos concentraremos en transiciones de estado continuas, llamadas fenómenos críticos. En la cercanía de un punto crítico, la longitud de correlación diverge como una ley de potencia y dos puntos a cualquier distancia el uno del otro, siempre acaban apareciendo correlacionados, suficientemente cerca del punto crítico. En

esta situación, las fluctuaciones están correlacionadas y resultan mucho mas importantes para entender el comportamiento del sistema pero también son más difíciles de tratar.

Aprovechando el crecimiento de la longitud de correlación, podemos emplear descripciones efectivas que promedian espacialmente el parámetro de orden, variable que describe el estado sistema, y así obtener una descripción continua del sistema. Estas descripciones se llaman, ecuaciones de Langevin. Estas tienen como ventajas **i)** que se pueden tratar más fácilmente de forma analítica por medio de herramientas de teoría de campos, usando la equivalencia con el formalismo del funcional generador; **ii)** en este formalismo, las simetrías del sistema aparecen de forma trasparente, permitiendo usar la intuición física de forma fácil; **iii)** este formalismo, aunque delicado, puede ser estudiado por herramientas numéricas eficientes y de tal manera, comprobar o inferir las intuiciones, sirviendo de guía; **iv)** este formalismo puede ser obtenido desde los modelos microscopicos a los cuales es equivalente, siendo así es un representante especial y elegante de las clases de universalidad, y **v)** como punto final es equivalente a una ecuación de Fokker-Planck y permite así hacer calculos de campo medio de forma autoconsistente estándar. Todas estas características, constituyen el nodo central, subyacente a la mayoría de los razonamientos presentados en esta tesis.

7.2 Capítulo 2: Transiciones con dos Estados Absorbentes que compiten

El trabajo presentado en el capítulo 2 fue realizado en colaboración con Hugues Chaté, Ivan Dornic y Miguel Angel Muñoz [16].

La forma en la que se divide este capítulo es la siguiente:

- 2.1, es una introducción a la problemática.
- 2.2, presenta la descripción del modelo que vamos a estudiar y la metodología numérica que hemos empleado.
- 2.3, presenta los resultados que hemos obtenido en campo medio, en dos y una dimensiones.
- 2.4, presenta resultados de un modelo generalizado de los precedentes, investigando cuáles son las simetrías imprescindibles para la clase de universalidad del Votante Generalizado (GV).
- 2.5, presenta una discusión de las limitaciones de nuestros resultados, sugiriendo posibles nuevos estudios.
- 2.6, es la conclusión de este capítulo.

El campo de investigación de los cambios de fase fuera del equilibrio ha sido muy activo durante las últimas décadas. Un caso particular de cambio de fase fuera del equilibrio es el de los cambios de fase a uno o varios estados absorbentes. Un estado absorbente es uno tal que el sistema no pueda salir de él. Así, es una manera drástica de imponer irreversibilidad y de forzar el sistema a encontrarse fuera del equilibrio. Este es un tema de mucho interés y para un estudio detallado se pueden ver [1, 2]. Las transiciones de fase a dos estados absorbentes se han estudiado empleando modelos reticulares. Algunos modelos dieron resultados que pueden parecer discrepar [5, 6] en dimensión dos. Los autores de [5] sugieren que la presencia de dos estados absorbentes simétricos lleva a una transición de fase que caracterizan con precisión y llaman votante generalizado (GV) mientras que los autores de [6] demuestran que en algunos casos se pueden ver dos transiciones: Ising y Percolación Dirigida (DP). En este trabajo queremos estudiar estas transiciones

con una descripción continua, proponemos una ecuación de Langevin,

$$\frac{\partial \phi(r, t)}{\partial t} = (a\phi - b\phi^3)(1 - \phi^2) + D\nabla^2 \phi(r, t) + \sigma \sqrt{(1 - \phi^2(r, t))} \eta, \quad (7.1)$$

con dos estados absorbentes simétricos. Las ecuaciones de Langevin suelen tener como ventaja sobre los modelos reticulares que permiten ver más fácilmente las simetrías y además, permiten un tratamiento analítico [21]. Estudiando (7.1) numéricamente, vemos que conseguimos reproducir los escenarios presentados en [5] y [6]. Con una metodología ya establecida [1, 2] podemos caracterizar los cambios de fase. En el caso de que se den dos transiciones, se ve que una es del tipo Ising, por lo que se rompe la simetría, aparece una magnetización; la otra transición es de tipo DP (2.7.b y d). En el caso de que haya sólo una transición, esta transición presenta simultáneamente una ruptura de simetría y una transición absorbente y pertenece a la clase del GV (2.7.c). Bajo el punto de vista que aportamos, quedan claros y naturales los resultados presentados por [5, 6] y recordados en 2.1.2.

Es bien sabido que el comportamiento crítico de un modelo depende de la dimensión en la que se estudia. A medida que la dimensión del sistema estudiado baja, este se aleja del posible campo medio en dimensión alta, y las fluctuaciones en el sistema aumentan, haciendo que su comportamiento sea generalmente más interesante. Las propiedades de (7.1) también resultan ser interesantes en una dimensión. Tanto en este caso como en dimensión dos, se han estudiado muchos modelos reticulares con dos estados absorbentes simétricos que comparten las mismas propiedades críticas que nuestra ecuación y por lo tanto parecen definir una clase de universalidad, DP2, Parity-conserving (2.1), Votante o Ising cinético. En una dimensión, Ec. (7.1) presenta un comportamiento crítico común al de DP2 o Parity-conserving y permite ilustrar claramente la equivalencia de estas dos clases de universalidad en una dimensión. Esta equivalencia reside en la dinámica que lleva a la transición del GV. La transición del GV separa dos fases: una ordenada en la que todo el sistema se encuentra en el mismo estado (+1 o -1), y otra desordenada en la que hay interfaces que separan dominios de signos opuestos. En el GV no hay ruido de 'bulk' y sólo interesa la dinámica de las interfaces. Un número impar de interfaces separa siempre dos dominios de signos opuestos y un número par separa dos dominios del mismo signo. Esto da lugar a una ley de conservación 'geométrica' o 'topológica' que se expresa de la siguiente manera: 'Se pueden crear interfaces o se pueden aniquilar,

pero se conserva la paridad del número de interfaces.'. Así tenemos una descripción en la que asociando a cada interfaz una partícula, se ve muy fácilmente la analogía entre DP2 y Parity-conserving en una dimensión. En la parte 2.5, damos una explicación de esto; también se puede ver [2] (p.94). Esto explica por qué estas dos clases de universalidad coinciden sólo en una dimensión.

7.3 Capítulo 3 : Fenómenos de mojado fuera del equilibrio

En este capítulo, se describe nuestra aportación al entendimiento de los fenómenos de mojado fuera del equilibrio. El modelo que hemos considerado es una interfaz de tipo Kardar-Parisi-Zhang (KPZ) en interacción, de corto alcance, con una pared. Según su posición, la pared limita las fluctuaciones de la interfaz a valores inferiores o superiores de un determinado valor. La ecuación de KPZ describe una interfaz univaluada, con una no-linealidad, que hace que las caras superiores y inferiores de las interfaces sean distinguibles. Un parámetro de control permite controlar la distancia media entre la interfaz y la pared. Para paredes repulsivas, existe un valor del parámetro de control para el que la velocidad de una interfaz a una distancia infinita de la pared se anula. Para este valor del parámetro de control, se observa una transición de segundo orden para parámetros de orden como la distancia media entre interfaz y pared o el número de puntos de contactos entre interfaz y pared. Según el signo de la no-linealidad de la KPZ, el cambio de estado es distinto. Nos hemos centrado en el caso de una pared inferior y de una no-linealidad positiva. Para este caso hemos demostrado que un cambio de variable apropiado tipo “Cole-Hopf”, permitía conseguir una ecuación de Langevin, para la variable inversa del parámetro de orden,

$$\frac{\partial n(r, t)}{\partial t} = D\nabla^2 n + an + bn^{1-q} + \sigma n\eta(r, t). \quad (7.2)$$

Esta ecuación da resultados completamente compatibles con los modelos microscópicos.

La forma en la que se divide este capítulo es la siguiente:

- 3.1, es una introducción a la problemática.
- 3.2, descripción de modelos microscópicos describiendo una interfaz libre.
- 3.3, descripción de modelos microscópicos describiendo una interfaz limitada por una pared de corto alcance.
- 3.4, se recuerdan la teorías Edwards-Wilkinson y Kardar-Parisi-Zhang para interfaces libres, de equilibrio tanto como de no-equilibrio.

- 3.5, se presenta el formalismo estudiado y los resultados obtenidos.
- 3.6, discutimos posibles realizaciones experimentales de nuestros resultados teóricos.
- 3.7, es la conclusión de este capítulo.

Detallamos el contenido de este capítulo, se propone un recordatorio de modelos de interfaces, tanto de equilibrio como de no-equilibrio. Se describen los modelos microscópicos como los modelos continuos mas relevantes para entender nuestro trabajo. El modelo microscópico de equilibrio descrito es: la deposición aleatoria con relajación en la superficie (ver Fig. 3.2). Modificando este modelo de manera que las partículas que caen sobre la interfaz se peguen a la primera partícula que se encuentran en contacto, nos lleva a una interfaz fuera del equilibrio. Este modelo modificado en una dimensión, pertenece a la clase de universalidad de KPZ. La situación física que nos interesa es la del mojado en la que la interfaz interacciona con una pared. Describiendo esto en una situación de equilibrio presentamos un modelo estudiado en la referencia [34] en detalle. Este modelo tiene el interés de ser muy ilustrativo, cambiar el valor de un parametro permite modificarle de forma a que describa la situación de no-equilibrio, o la situación de equilibrio. Permite también modificar la pared, dandole un caracter atractivo o repulsivo, siempre de corto alcance en la forma presentada.

Nuestros resultados más relevantes son las estimaciones de los exponentes críticos vía calculo de campo medio y simulaciones numéricas. El calculo de campo medio se lleva a cabo buscando soluciones autoconsistentes del formalismo de Fokker-Planck asociado a nuestra ecuación de Langevin. Esto había sido hecho en el caso de una ecuación KPZ con no-linealidad negativa y pared inferior referido como ruido multiplicativo 1 (MN1) en el que da lugar a dos regímenes llamado respectivamente de ruido débil y ruido fuerte. En nuestro caso llamado MN2 solo permite obtener un régimen de ruido débil, aunque un régimen de ruido fuerte también es de esperar en el sistema real. Las simulaciones numéricas de la ecuación (4.10) dan resultados completamente compatible con resultado obtenidos con modelos microscópicos, mejorando su precisión. Hemos demostrado que una ecuación de Langevin puede describir con fidelidad este problema permitiendo usar este formalismo para otros estudios tanto numéricos como analíticos.

7.4 Capítulo 4 : Fenómenos de Mojado con potenciales de largo alcance

El trabajo contenido en este capítulo es fruto de una colaboración con F. de los Santos, M. A. Muñoz y M. M. Telo da Gama.

Estudiamos la transición de fase que presenta una interfaz de tipo KPZ en interacción con una pared rígida impenetrable de largo alcance. Precedentemente, se había considerado paredes de corto alcance. Las interacciones físicas entre la pared y la interfaz son de tipo electromagnético, que en el vacío decaen como una ley de potencia. En un medio con cargas móviles, se espera un efecto pantalla debido a la movilidad de las cargas, pudiendo hacer que el potencial resultante decaiga de forma exponencial. Con lo cual, tiene sentido considerar tanto potenciales con forma funcional exponencial como leyes de potencia. Este capítulo tiene como objetivo evaluar las consecuencias, que se producen a cambiar de un potencial de corto alcance a otro de largo alcance. El formalismo que usamos es el de las ecuaciones de Langevin. Nos permite obtener resultados intuitivos a través de aproximaciones de campo medio y resultados numéricos. Para verificar nuestros resultados también hemos realizado el estudio de un modelo microscópico.

La forma en la que se divide este capítulo es la siguiente:

- -, se hace una breve introducción al trabajo presentado
- 4.3, presenta el modelo que estudiaremos.
- 4.4, es un repaso de los resultados conocidos para el problema del mojado en equilibrio.
- 4.5, presenta los resultados conocidos para el wetting de no-equilibrio con fuerzas de corto alcance.
- 4.6, presenta nuestros resultados.
- 4.7, presenta las conclusiones de este capítulo.

Para poder explicarnos con claridad, detallaremos el problema que hemos tratado. La forma funcional del potencial de interacción entre pared e interfaz

que hemos considerado es la siguiente:

$$V(h) = \frac{b}{ph^p} + \frac{c}{qh^q}, \quad (7.3)$$

donde, $b, c > 0$, y $p < q$ son los parámetros que haremos variar. Queremos una interfaz que describa un sistema fuera del equilibrio, con lo cual, juntamos una ecuación de tipo KPZ con el potencial 7.3. Nuestra ecuación se puede escribir de la siguiente forma,

$$\partial_t h = \nabla^2 h + \lambda(\nabla h)^2 + a + \frac{b}{h^{p+1}} + \frac{c}{h^{q+1}} + \sigma\eta(\mathbf{x}, t). \quad (7.4)$$

Los detalles de esta ecuación aparecen descritos en la tesis. Sólo diremos que para poder estudiarla numéricamente de forma eficiente, hicimos un cambio de variable dependiente del signo de λ (ver capítulo 3). Esto lleva a una ecuación para el parámetro de orden o para la variable inversa. Según el valor que tome a , la media de h , es finita (para $a < a_c$ con a_c el punto de transición) o tiende al infinito (para $a > a_c$). Justo en $a = a_c$, tenemos una transición que puede ser tanto continua, o discontinua. Separamos el problema en dos casos: el de una pared repulsiva, $b > 0$, y el de una pared atractiva, $b < 0$.

Podemos separar dos contribuciones al desplazamiento de la interfaz: la del término KPZ que da lugar a un crecimiento de la rugosidad en $\bar{h} \propto t^{1/3}$, y la del potencial determinista que implica $\bar{h} \propto t^{1/(p+2)}$. El punto $p = 1$ aparece naturalmente como el punto límite que separa dos regímenes. En el caso que $p > 1$, la transición es idéntica a la del caso con interacciones de corto alcance. Cuando $\lambda > 0$, tenemos una transición del tipo MN2. Si $\lambda < 0$, la transición es del tipo MN1. Para el largo alcance con $p > 1$, todos los exponentes coinciden con el corto alcance. Significa que estos dos casos pertenecen a la misma clase de universalidad. En cambio, cuando $p < 1$, la transición es distinta. Los exponentes nu y z siguen siendo los de KPZ, respectivamente $2/3$ y 2 pero los demás exponentes se modifican de forma que el problema se parezca a un campo medio. Las fluctuaciones de la variable h , son pequeñas implicando que, $\langle (h - \bar{h})^2 \rangle \ll \bar{h}^2$, con lo cual, los exponentes se obtienen directamente a partir de argumentos sencillos de campo medio y predecimos $\bar{h} \propto t^{1/(p+2)}$. Esto significa que el potencial decae lo suficientemente rápido cuando $p > 1$ para que la interfaz tenga interacciones casi inexistentes con la pared cuando h tiende al infinito. En cambio, cuando

$p < 1$, el potencial determina el valor medio de h . Este razonamiento es válido tanto para $\lambda > 0$ como para $\lambda < 0$. Esto se compara interesantemente con el caso del problema del mojado de equilibrio. En el caso del equilibrio, el exponente de la rugosidad que se compara con el exponente $1/(p+2)$ es $1/4$ así el punto de transición entre un régimen de fluctuaciones fuertes con un régimen de fluctuaciones débiles es $p = 2$.

En el caso de una pared atractiva, nuestros resultados coinciden con el problema del corto alcance. Si $\lambda > 0$, tenemos una transición discontinua. Para $\lambda < 0$, se observan dos transiciones: una de primer orden y otra de tipo Percolación Dirigida. Entre las dos líneas de transición, una parte extendida del diagrama presentando coexistencia de fase genérica. Este hecho es posible sólo en equilibrio. Esta fenomenología es insensible al valor de p .

En el caso de un sistema bi-dimensional, se espera que toda la fenomenología descrita arriba se conserve reemplazando las clases de universalidades por las correspondientes en dimensión dos. Nuestro trabajo tiene también como objetivo motivar a experimentalistas a intentar reproducir toda esta fenomenología. Hemos demostrado que cualquier fuerza de interacción física, que decae a cero en infinito y cuya energía correspondiente es finita, sin presencia de ruido quench en el potencial, debe de permitir observar resultados apasionantes. Se espera ser posible observar las transiciones MN1, MN2 y DP. Estos experimentos, si fuesen conclusivos, serían verdaderamente un acontecimiento de gran importancia para la mecánica estadística de no-equilibrio. Así, esperamos que este trabajo pueda motivar experimentalistas a seguir este camino de investigación.

7.5 Capítulo 5 : Substratos desordenados y modelos de ADN estocásticos

Los resultados presentados en este capítulo se obtuvieron en una colaboración con F. de los Santos, M. A. Muñoz. El punto de partida del trabajo es el estudio de un modelo introducido en varios trabajos por Peyrard, Bishop y Dauxois (PBD) [87, 88]. Este modelo describe de manera continua la distancia entre bases del ADN. De esta forma constituye un refinamiento de modelos estudiado antes como el de Poland-Sheraga [89] que considera variable discretas. La naturaleza continua de la descripción permite incluir mecanismos no-lineales variados. Nuestro objetivo es describir la transición de desnaturalización, apertura de la molécula, que padece la molécula de ADN cuando se aumenta la temperatura del medio. Recientemente, estudios experimentales se concentraron en el estudio de la desnaturalización causada por esfuerzo mecánico sobre la molécula.

La forma en la que se divide este capítulo es la siguiente:

- 5.1, se hace una introducción al trabajo presentado
- 5.2, resultados obtenidos para la Teoría de campos Reggeon (RFT) con ruido quenched.
- 5.3, ecuación de Langevin para el modelo de Peyrard-Bishop-Dauxois.
- 5.4, resultados del estudio de la transición de desnaturalización del ADN.
- 5.5.1, las conclusiones del trabajo

El modelo de PBD considerado se escribe de la siguiente forma,

$$\frac{\partial h_n(r, t)}{\partial t} = -\frac{\partial V(h_n)}{\partial h_n} + \sigma \eta(r, t), \quad (7.5)$$

con el potencial incluyendo los siguientes terminos,

$$V(h_n) = D_n(e^{-a_n h_n} - 1)^2 + \frac{k}{2}(1 + \rho e^{-\beta(h_{n+1} + h_n)})(h_{n+1} - h_n)^2 + \text{symmetric}. \quad (7.6)$$

El primer término de la derecha es un potencial de Morse que se eligió originalmente en los trabajos [87, 88] porque facilitaba los cálculos analíticos. El segundo término acopla las distancias entre distintas bases para describir las interacciones que hay entre ellas. El origen de estas interacciones y su forma exacta no son conocidas. Lo que se sabe es que la intensidad de esta interacción es mayor cuando las bases están cerca. Cuando se alejan las bases, el volumen disponible para su desplazamiento es muy grande. La dependencia de la intensidad de la interacción en función de la distancia aparece como un efecto de entrópico. Cuando $\rho = 0$, la transición de fase es continua y se hace discontinua cuando $\rho > 0$. Hemos verificado que nuestro formalismo es capaz de reproducir estos resultados. Después, nos centramos en el caso más realista de $\rho > 0$ y estudiamos el carácter local del efecto de las mutaciones. Estudios teóricos recientes predicen que el efecto de las mutaciones es local. Nuestros resultados, obtenidos para el caso de un desorden estructurado, demuestran que también se pueden ver efectos no-locales. Esto conduce a pensar que en el caso de una cadena real se pueden llegar a observar efectos no-locales. Nuestros resultados pueden aportar una interpretación de las causas de ciertas enfermedades genéticas.

7.6 Capítulo 6 : Sistemas de reacción-difusión y ecuaciones de Langevin

Este capítulo presenta un trabajo realizado en colaboración con J. A. Bonachela y M. A. Muñoz. Hemos realizado un estudio de sistemas de reacción-difusión. Usando métodos de teoría de perturbaciones estándar y simulaciones Monte-Carlo, hemos estudiado un modelo ya resuelto exactamente, $2A \leftrightarrow A$. Hemos generalizado nuestros resultados a otros modelos no resueltos, como la reacción de coagulación, $2A \rightarrow A$ acoplada a procesos de creación $A \rightarrow nA$ con $n \geq 2$, demostrando que poseían un punto crítico con las mismas propiedades. Hemos determinado las restricciones y los ingredientes relevantes, para que un modelo exhiba estas propiedades críticas. Así, demostramos la existencia de una nueva clase de universalidad que hemos caracterizada.

La forma en la que se divide este capítulo es la siguiente:

- 6.1, se hace una introducción al trabajo presentado
- 6.2, se estudia la teoría de campos para el proceso $A \leftrightarrow 2A$.
- 6.3, se extiende el estudio al caso no-reversible de coagulación acoplada con $A \rightarrow nA$
- 6.4, resultados de simulaciones Monte-Carlo de los modelos de reacción-difusión considerados
- 6.5, las conclusiones del trabajo

Usando el formalismo de Doi-Peliti, la ecuación de Langevin correspondiente al modelo reversible es,

$$\partial_t \phi(\mathbf{x}, t) = D \nabla^2 \phi + \mu \phi - \sigma \phi^2 + \sqrt{\mu \phi - \sigma \phi^2} \eta(\mathbf{x}, t). \quad (7.7)$$

Esta ecuación no es fácil de estudiar. Permanecen problemas a la hora de interpretarla porque desarrolla una parte imaginaria por lo cual seguiremos usando modelos microscópicos y el funcional generador equivalente a esta ecuación,

$$\begin{aligned} \mathcal{S}[\phi, \pi] &= \int dt \int d^d x [\pi (\partial_t \phi - D \nabla^2 \phi) - H[\phi, \pi]], \quad \text{con} \\ H[\phi, \pi] &= (\pi^2 - \pi)(\mu \phi - \sigma \phi^2), \end{aligned} \quad (7.8)$$

donde $\phi(\mathbf{x}, t)$ and $\pi(\mathbf{x}, t)$ son los campos de densidad y de respuestas. De estas ecuaciones, se obtienen los resultados analíticos vía teoría de perturbaciones.

7.7 Conclusiones

Las transiciones de fase son muy ubicuas en la naturaleza y la mayor parte de aquellos sistemas se encuentran fuera del equilibrio. Al contrario de lo que pasa en el caso del equilibrio, no existe ningún formalismo que permita describir los sistemas fuera del equilibrio. Esto implica que haya que estudiar los problemas uno a uno con herramientas adaptadas. Este trabajo se empea en determinar las posibilidades y las limitaciones del formalismo de las ecuaciones de Langevin aplicandolo a algunos ejemplos practicos. De esta forma, constituye un avance en el entendimiento de transiciones de fases fuera del equilibrio. Gracias a la metodología usada, las ecuaciones de Langevin y las herramientas asociadas al formalismo de Langevin, hemos resueltos problemas sin resolver. Aportando también al entendimiento de descripción efectiva de un problema físico.

Bibliography

- [1] J. Marro and R. Dickman, *Nonequilibrium Phase Transitions in Lattice Models*, Cambridge University Press, Cambridge (1999).
- [2] H. Hinrichsen *Critical phenomena in Nonequilibrium systems*, Adv. Phys. **49**, 815 (2000).
- [3] E. V. Albano, J. Phys. **A 27**, L881–L886 (1994).
- [4] D. Mollison, J. Roy. Stat. Soc. **B 39**, 283 (1977).
- [5] I. Dornic, H. Chaté, J. Chave, and H. Hinrichsen, Phys. Rev. Lett. **87**, 045701 (2001)
- [6] M. Droz, A. L. Ferreira, and A. Lipowski, Phys. Rev. E **67**, 056108 (2003)
- [7] L. Devroye, *Non-Uniform Random Variate Generation* Springer(New York), (1986)
- [8] I. Dornic, H. Chaté, and M. A. Muñoz, Phys. Rev. Lett **94**, 100601 (2005).
- [9] L. Pechenik and H. Levine, Phys. Rev. E **59**, 3893 (1999).
- [10] E. Moro, Phys. Rev. E **70**, 045102(R) (2004)
- [11] R. Dickman, Phys. Rev. E **50**, 4404 (1994)
- [12] P. Grassberger, F. Krause, and T. von der Twer, J. Phys. **A 17**, L105–L109 (1984).
- [13] P. Grassberger, J. Phys. **A 22**, L1103–L1107 (1989).

-
- [14] N. Menyhárd, J. Phys. **A 27**, 6139–6146 (1994).
- [15] N. Menyhárd and G. Ódor, J. Phys. **A 29**, 7739–7755 (1996).
- [16] O. Al Hammal, H. Chaté, I. Dornic and M.A. Muñoz, Phys. Rev. Lett. **94**, 230601 (2005).
- [17] M. Scheucher and H. Spohn, J. Stat. Phys. **53**, 279 (1988).
- [18] P. L. Krapivsky, Phys. Rev. A **45**, 1067 (1992); L. Frachebourg and P. L. Krapivsky, Phys. Rev. E **53**, R 3009 (1996).
- [19] H. Hinrichsen, cond-mat/0006212, “First-order transitions in fluctuating 1+1-dimensional nonequilibrium systems”. (2000)
- [20] M. A. Muñoz, Phys. Rev. E **57**, 1377 (1998).
- [21] L. Canet, H. Chaté, B. Delamotte, I. Dornic, M.A. Muñoz, Phys. Rev. Lett. **95**, 100601 (2005)
- [22] J. W. Cahn, J. Chem. Phys. **66** (1977) 3667.
- [23] D. Bonn and D. Ross, Rep. Prog. Phys. **64**, 1085-1163 (2001).
- [24] M. Schick, *Liquids at interfaces: Les Houches, Session XLVIII* ed. J. Charvolin, J.F. Joanny and J. Zinn-Justin (Amsterdam: Elsevier) p415 (1990).
- [25] U. Alon, M. R. Evans, H. Hinrichsen, and D. Mukamel, Phys. Rev. Lett. **76**, 2746 (1996); Phys. Rev E **57**, 4997 (1998).
- [26] H.K. Janssen, Z. Phys. B **42**, 151 (1981). P. Grassberger, Z. Phys. B **47**, 365 (1982).
- [27] *Influence of diffusion on models for non-equilibrium wetting* S. Rossner, H. Hinrichsen Preprint (2006)
- [28] J. Hooyberghs, F. Igloi, and C. Vanderzande, Phys. Rev. Lett. **90**, 100601 (2000). Phys. Rev. E **69**, 066140 (2004).
- [29] T. Vojta and M. Dickison, Phys. Rev. E **72**, 036126 (2005).

-
- [30] S. F. Edwards and D. R. Wilkinson, Proc. R. Soc. London A 381, 17 (1982)
- [31] M. Kardar, G. Parisi and Y.C. Zhang Phys. Rev. Lett. **56**, 889 (1986)
- [32] I.E Dzyaloshinskii, E.M. Lifshitz, and L.P. Pitaevskii, Adv. Phys., **10**, 165 (1961).
- [33] O. Al Hammal, F. De los Santos, M. A. Muñoz and M. M. Telo da Gama. Accepted for publication in PRE (2006).
- [34] H. Hinrichsen, R. Livi, D. Mukamel, and A. Politi, Phys. Rev. Lett. **79**, 2710 (1997); Phys. Rev. E **61**, R1032 (2000); Phys. Rev. E **68**, 041606 (2003).
- [35] F. Family, J. Phys. A, **19**, L441-446 (1986).
- [36] A. -L. Barabási and H. E. Stanley, *Fractal Concepts in Surface Growth*, Cambridge University Press, Cambridge (1995).
- [37] Halpin-Healy T and Zhang Y C 1995 *Phys. Rep.* **254** 215
- [38] M.A. Muñoz, in *Advances in Condensed Matter and Statistical Mechanics*, Ed. E. Korutcheva and R. Cuerno, pg. 37, Nova Science Publishers (2004).
- [39] O. Al Hammal, F. de los Santos, and M. A. Muñoz, J. Stat. Mech.: Theor. Exp. P10013. (2005).
- [40] M. A. Muñoz, F. de los Santos, and A. Achahbar, Braz. J. Phys. **33**, 443 (2003).
- [41] Muñoz M A and Pastor Satorras R 2003 *Phys. Rev. Lett.* **90** 204101
- [42] G. Grinstein, M.A. Muñoz, and Y. Tu Phys. Rev. Lett. **76**, 4376 (1996).
- [43] Y. Tu, G. Grinstein and M.A. Muñoz, Phys. Rev. Lett. **78**, 274 (1997).
- [44] M.A. Muñoz and T. Hwa, Europhys. Lett. **41**, 147 (1998).
- [45] W. Genovese and M.A. Muñoz, Phys. Rev. E **60**, 69 (1999).

-
- [46] F. Ginelli et al 2004 J. Phys. A: Math. Gen. **37** 11085-11100 (Mean field theory for skewed height profiles in KPZ growth processes.).
- [47] F. Family and T. Vicsek, J. Phys. A **18**,L75 (1985) (Scaling of the active zone in the Eden process on percolation networks and the ballistic deposition model.).
- [48] Kissinger T, Kotowitz A, Kurz O, Ginelli F, and Hinrichsen H 2005 *J. Stat. Mech.* P06002 (*Preprint cond-mat/0503582*)
- [49] San Miguel M and Toral R 1997 *Stochastic Effects in Physical Systems* (Instabilities and Nonequilibrium Structures VI) ed Tirapegui E and Zeller W (Kluwer Academic Publishers) pp 35-130 (*Preprint cond-mat/9707147*)
- [50] Le Doussal P., and Wiese K.J. 2003, Phys. Rev. E, **67**, 016121.
- [51] Dietrich, S. 1983, in Phase Transitions and Critical Phenomena, vol. 12, C. Domb and J. Lebowitz (Eds.), Academic Press; Sullivan, D.E., and Telo da Gama, M.M. 1986, in Fluid Interfacial Phenomena, C.A. Croxton (Ed.), Wiley, New York. H. Nakanishi and M. E. Fisher, Phys. Rev. Lett. **49**, 1565 (1982).
- [52] D. M. Kroll, R. Lipowsky, and R. K. P. Zia, Phys. Rev. B **32**, R1862 (1985).
- [53] U. Alon, M. R. Evans, H. Hinrichsen, and D. Mukamel, Phys. Rev. Lett. **76**, 2746 (1996); Phys. Rev E **57**, 4997 (1998). H. Hinrichsen, R. Livi, D. Mukamel, and A. Politi, Phys. Rev. Lett. **79**, 2710 (1997); Phys. Rev. E **61**, R1032 (2000); Phys. Rev. E **68**, 041606 (2003) J. Candia and E.V. Albano, Phys.Rev.Lett. **88**, 016103 (2002);
- [54] F. de los Santos, M.M. Telo da Gama, and M.A. Muñoz, Europhys. Lett. **57**, 803 (2002); Phys. Rev. E. **67**, 021607 (2003).
- [55] M.A. Muñoz, in *Advances in Condensed Matter and Statistical Mechanics*, Ed. E. Korutcheva and R. Cuerno, pg. 37, Nova Science Publishers (2004). F. de los Santos and M.M. Telo da Gama Trends in Statistical Physics Vol. 4 pp. 61 (2004).

- [56] M.I. Boamfa, M. W. Kim, J.C. Maan, and Th. Rasing, *Nature*, **421**, 149 (2003).
- [57] A. Ballestad, et al. *Phys. Rev. Lett.* **86**, 2377 (2001). H.-C. Kan, et al. *Phys. Rev. Lett.* **92**, 146101 (2001).
- [58] V. A. Shchukin and D. Bimberg, *Rev. Mod. Phys.* **71**, 1125 (1999).
- [59] T. Halpin-Healy and Y. C. Zhang, *Phys. Rep.* **254**, 215 (1995). Barabási A L and Stanley H E 1995 *Fractal Concepts in Surface Growth* (Cambridge: University Press Cambridge) and references therein.
- [60] R. Lipowsky, *J. Phys. A* **18**, L585 (1985).
- [61] I. E. Dzyaloshinskii, E. M. Lifshitz, and L. P. Pitaevskii, *Adv. Phys.* **10**, 165 (1961).
- [62] Note that for higher dimensional interfaces, the mean field regime dominates for any p , $1/(p+2) > 0$, as the free fluctuations are flat, being characterized by a zero roughness exponent and a logarithmic growth in $d = 2$.
- [63] M. Kardar, G. Parisi, and Y. C. Zhang, *Phys. Rev. Lett.* **56**, 889 (1986).
- [64] Another possibility (presently under study) is to analyze molecular beam epitaxy (MBE) Langevin equations (known to represent a broad family of non-equilibrium interfacial growth [59]) in the presence of bounding potentials.
- [65] T. J. Newman and A. J. Bray, *J. Phys. A* **29**, 7917 (1996). See also, C. H. Lam and F. G. Shin, *Phys. Rev. E* **58**, 5592 (1998).
- [66] G. Grinstein, M.A. Muñoz, and Y. Tu, *Phys. Rev. Lett.* **76**, 4376 (1996); Y. Tu, G. Grinstein, and M.A. Muñoz, *Phys. Rev. Lett.* **78**, 274 (1997); M.A. Muñoz and T. Hwa, *Europhys. Lett.* **41**, 147 (1998); W. Genovese and M.A. Muñoz, *Phys. Rev. E* **60**, 69 (1999).
- [67] M. Lässig and R. Lipowsky, in *Fundamental Problems in Statistical Mechanics VIII*, H. van Beijeren and M.H. Ernst editors, (Elsevier Science, 1984); *Phys. Rev. Lett.* **70**, 1131 (1993).
- [68] R. Lipowsky, *Ferroelectrics* **73**, 69 (1987).

- [69] M. A. Muñoz, F. de los Santos, and A. Achahbar, *Braz. J. Phys.* **33**, 443 (2003).
- [70] M. A. Muñoz and R. Pastor-Satorras, *Phys. Rev. Lett.* **90**, 204101 (2003).
- [71] M. A. Muñoz, F. de los Santos, and M.M. Telo da Gama, *Eur. Phys. Jour.* **43**, 73-79 (2005). C. H. Bennett and G. Grinstein, *Phys. Rev. Lett* **55**, 657 (1985). G. Grinstein, *IBM J. Res. & Dev.* **48**, 5 (2004); www.research.ibm.com/journal/rd/481/grinstein.pdf.
- [72] R. Lipowsky, in *Random Fluctuations and Pattern Growth*, edited by H. Stanley and N. Ostrowsky, Nato ASI Series E, vol 157, Kluwer Akad. Publ., Dordrech (1988).
- [73] R. Lipowsky, *Phys. Rev. Lett.* **52**, 1429 (1984).
- [74] C. J. DeDominicis, *J. Physique* **37**, 247 (1976); H.K. Janssen, *Z. Phys. B* **23**, 377 (1976); P. C. Martin, E. D. Siggia and H. A. Rose, *Phys. Rev. A* **8**, 423 (1973); L. Peliti, *J. Physique*, **46**, 1469 (1985).
- [75] M. San Miguel and R. Toral, *Stochastic Effects in Physical Systems, in Instabilities and Nonequilibrium Structures*, VI, E. Tirapegui and W. Zeller, eds. Kluwer Academic Pub. (1997). (Cond-mat/9707147).
- [76] The part of the Langevin equation to be integrated is written as $dn_t = an_t dt + \sigma n_t dW_t$ where dW is a Wiener process. Since this is interpreted in the Stratonovich sense, we can perform the change of variables $Y_t = \ln n_t$ and obtain $dY_t = a dt + \sigma dW_t$. This is a drifted Brownian motion equation whose solution is given by a normal distribution of mean $y_0 + a dt$ and variance $\sigma^2 dt$: $Prob(Y_{t+dt} = y | Y_t = y_0) = N(y_0 + a dt, \sigma^2 dt)$. Reverting the change of variables, we obtain a log-normal form, which can be sampled in an exact way by taking: $n[t + dt | n(t) = n_0] = n_0 \exp(a dt + \sigma \sqrt{dt} \eta)$. This expression can also be derived by changing variables in the Langevin equation, performing one time-step evolution, and changing back variables.
- [77] T. Kissinger, A. Kotowicz, O. Kurz, F. Ginelli, and H. Hinrichsen, *J. Stat. Mech.* **0605** (2005) P06002.

- [78] F. Ginelli, H. Hinrichsen, R. Livi, D. Mukamel, and A. Politi, Phys. Rev. E **71**, 026121 (2005).
- [79] The true straight-line boundary may be easily mistaken for a temperature-dependent curve. This is due to a roughness suppression effect that effectively switches off the KPZ nonlinear term when the interfaces are initially placed close to the substrate and within the potential well. In this case, a transient renormalized $\lambda_R(b)$ may be observed that leads to an apparent temperature-dependent transition $a + \lambda_R(b)\langle(\nabla h)^2\rangle = 0$.
- [80] I. Jensen, J. Phys. A: Math. Gen. **32**, 5233 (1999).
- [81] H. Hinrichsen, Braz. J. of Phys. **30**, 69 (2000).
- [82] J. Zinn-Justin, *Quantum Field Theory and Critical Phenomena* (Oxford University Press, 4th edition, 2002).
- [83] R. Lipowsky and M. E. Fisher, Phys. Rev. B **36**, 2126 (1987).
- [84] M. E. Fisher and D. S. Fisher, Phys. Rev. B **25**, 3192 (1982).
- [85] D.S. Fisher and D. A. Huse, Phys. Rev. B **32**, 247 (1985).
- [86] F. Ginelli and H. Hinrichsen, J. Phys. A **37**, 11085 (2004).
- [87] M. Peyrard M. and A. R. Bishop, Phys. Rev. Lett., **62**, 2755 (1989)
- [88] Dauxois T., Peyrard M. and Bishop A. R., Phys. Rev. E, **47**, R44 (1993)
- [89] D. Poland and H. A. Scheraga, J. Chem. Phys., **45**, 1456 (1966)
- [90] A. Campa, and A. Giansanti, Phys. Rev. E. **58**, 3585 (1998)
- [91] V. Elgart and A. Kamenev, Phys. Rev. E **74**, 041101 (2006).
- [92] G. Ódor, Rev. Mod. Phys. **76**, 663 (2004). G. Grinstein and M. A. Muñoz, in *Fourth Granada Lectures on Computational Physics* edited by P. L. Garrido and J. Marro, Lecture Notes in Physics Vol 493 (Springer, Berlin), p. 223.

- [93] Additionally, they also identify some other classes (not enumerated here) marginal in one dimension.
- [94] Some of these universality classes might have a better representation in terms of two species [98]. Also, some other classes with absorbing states as, for example, the one of stochastic sandpiles [R. Dickman, M. A. Muñoz, A. Vespignani, and S. Zapperi, *Braz. J. of Physics* **30**, 27 (2000)] usually represented by two density fields, admit a one-species non-Markovian description. Hence, saying that there are 5 non-trivial one-species absorbing-state universality classes is somehow ambiguous.
- [95] J.L. Cardy and R.L. Sugar, *J. Phys. A* **13**, L423 (1980). H.K. Janssen, *Z. Phys. B* **42**, 151 (1981). P. Grassberger, *Z. Phys. B* **47**, 365 (1982).
- [96] P. Grassberger, F. Krause, and T. von der Twer, *J. Phys. A* **17**, L105 (1984). See also [92] for reviews on this.
- [97] O. Al Hammal, H. Chaté, I. Dornic, and M. A. Muñoz, *Phys. Rev. Lett.* **94**, 230601 (2005).
- [98] For an overview, see M. Henkel and H. Hinrichsen, *J. Phys. A* **37**, R117 (2004).
- [99] Indeed, the results in [91] can be taken as a new evidence supporting the conclusion that PCPD differs from DP.
- [100] G. Ódor, *Phys. Rev. E* **73**, 047103 (2006).
- [101] M. Burschka, C. R Doering, and D. ben-Avraham, *Phys. Rev. Lett.* **63**, 700 (1989). D. ben-Avraham, M. Burschka, and C. R Doering, *J. Stat. Phys.* **60**, 695 (1990). See also, K. Krebs, M. Pfanmueller, B. Wehefritz, and H. Hinrichsen *J. Stat. Phys.* **78**, 1429 (1995). H. Hinrichsen, S. Sandow, and I. Peschel, *J. Phys. A.* **29**, 2643 (1996). H. Hinrichsen, K. Krebs, and I. Peschel, *Z. Phys. B* **100**, 105 (1996). H. Hinrichsen, V. Rittenberg, and H. Simon, *J. Stat. Phys.* **86**, 1203 (1997).
- [102] D. ben-Avraham, *Mod. Phys. Lett. B* **9**, 895 (1995). D. ben-Avraham, in *Statistical Mechanics in one-dimension*, Ed. V. Privman, pg. 29, Cambridge University Press, Cambridge 1997.

- [103] J. Cardy and U. C. Täuber, *Stat. Phys.* **90**, 1 (1998).
- [104] In R. Jack, P. Mayer, and P. Sollich, *J. Stat. Mech.* (2006) P03006, conclusions identical to ours are obtained for the *reversible case* by exploiting the existence of *detailed balance*.
- [105] L. Peliti, *J. Phys. A* **19**, L365 (1986). M. Droz and L. Sasvari, *Phys. Rev. E* **48**, R2343 (1993). See also, B. P. Lee, *J. Phys. A* **27**, 2633 (1994). B. P. Lee and J. Cardy, *J. Stat. Phys.* **80**, 971 (1995). J. Cardy, *Field Theory and Nonequilibrium Statistical Mechanics*, (Troisième cycle de la Physique en Suisse Romande, 1998-1999, semestre d'été). <http://www-thphys.physics.ox.ac.uk/users/JohnCardy/home.html>
- [106] For a recent and nice review see, U. C. Täuber, M. Howard, and B. P. Vollmayr-Lee, *J. Phys. A* **38**, R79 (2005). For non-perturbative calculations see L. Canet, H. Chaté, and B. Delamotte, *Phys. Rev. Lett.* **92**, 255703 (2004). See also [103].
- [107] M. Doi, *J. Phys. A* **9**, 1479 (1976). L. Peliti, *J. Physique*, **46**, 1469 (1985). P. Grassberger and M. Scheunert, *Fortschr. Phys.* **28**, 547 (1980). C. J. DeDominicis, *J. Physique* **37**, 247 (1976). H. K. Janssen, *Z. Phys. B* **23**, 377 (1976). P. C. Martin, E. D. Siggia, and H. A. Rose, *Phys. Rev. A* **8**, 423 (1978).
- [108] Alternatively, Eq. (6.1) can also be obtained by employing the Poissonian transformation method [109]. It has been proved that both formalisms are completely equivalent: M. Droz and A. McKane, *A* **27**, L467 (1994).
- [109] C. W. Gardiner, *Handbook of Stochastic Methods*, Springer-Verlag, Berlin and Heidelberg, 1985. M. A. Muñoz, *Phys. Rev. E* **57**, 1377 (1998).
- [110] By imposing the first derivatives of the Hamiltonian, H , with respect to ϕ and π to vanish, one can identify the homogeneous classical (mean-field) stationary solution. The non-trivial expectation value of ϕ is $\langle\phi\rangle = \mu/\sigma$ and hence, at mean-field level, the critical point is located at $\mu_c = 0$ and the order-parameter critical exponent is $\beta = 1$. At this critical point the coefficients of both the linear-deterministic and the leading noise terms vanish.

-
- [111] As the diagrams in eq.(6.3) are marginally divergent in $d = 2$, their derivatives do not require extra renormalization, and therefore the fields do not have anomalous dimensions [105].
- [112] Simple inspection of diagrams for different vertices, even those having the same topology (for example, the one-loop diagrams contributing to DP [95]), readily leads to the conclusion that combinatorial factors are different, and therefore, each bare constant would have distinct corrections.
- [113] More complicated two-loop diagrams are generated when higher order vertices are generated, breaking the super-renormalizability of the theory (see, for instance, fig. 3b in [103]).
- [114] Analogously, non-reversibility can also be included in models without a proper absorbing state as $2A \leftrightarrow 0$ by switching on reactions as $0 \rightarrow 3A, 4A, \dots$, without affecting their critical behavior.
- [115] J.J. Binney, N.J. Dowrick, A.J. Fisher and M.E.J. Newman, *The Theory of Critical Phenomena: An Introduction to the Renormalization Group*, Oxford University Press (1993).
- [116] J. Cardy, *Scaling and Renormalization in Statistical Physics*, Cambridge Lecture Notes in Physics, Cambridge University Press (1996).
- [117] T. M. Liggett, *Interacting Particle Systems*, Springer Verlag, New York, (1985).